UNIVERSITY OF CALIFORNIA

Santa Barbara

Biochemistry and Structure-Function Relationships in the Proteinaceous Egg Capsules of *Busycotypus canaliculatus*

A Dissertation submitted in partial satisfaction of the

requirements for the degree

Doctor of Philosophy in Biochemistry and Molecular Biology

by

Stephen Scott Wasko

Committee in charge:

Professor J. Herbert Waite, Chair

Professor James Cooper

Professor Christopher Hayes

Professor Frank Zok

June 2010

Biochemistry and Structure-Function Relationships in the Proteinaceous Egg Capsules of *Busycotypus canaliculatus*

ACKNOWLEDGEMENTS

I would like to first thank my father, Stephen, for instilling in me from a young age a profound curiosity for how the natural world around me operates, from the tiniest minutia up through the largest overall picture. My mother, Lee, for keeping me grounded and focused so that I never lost track of the value of my work. And to both of them, as well as my sister, Laura, for their loving encouragement throughout the entire process of my life to date. To my advisor, Herb, for guiding me along not only the finer points of biochemistry and biophysics, but for guiding me along the path to being a better scientist overall and better person with his eccentric style and allowing me the freedom to learn from my own mistakes and direct my own project. These were the primary reasons I had for joining his group, and I was certainly not disappointed with that decision. To members, past and present, of the Waite lab, and everyone else in the Marine Biotech Building for assistance both technical and philosophical, especially Ali who worked so hard to turn me into a materials scientist while I worked so hard to turn him into a biologist. To my committee for keeping me on track and providing valuable insights. And last, but certainly not least, to all of my wonderful friends, both those I've met since coming to Santa Barbara, and those who've kept in touch from previous times. You are too numerous to list here.

All of the intellectual stimulation in the world could not replace the joy that you bring me on a regular basis. I love you all.

Curriculum Vita, Stephen Scott Wasko

April 2010

Education:

2004-2010	PhD in Biomolecular Sciences and Engineering, 2010 (expected) Univeristy of California, Santa Barbara, CA. Advanced to candidacy May, 2007 Research advisor: J. Herbert Waite
1997-2001	BA in Biological Sciences, emphasis in Molecular and Cell Biology Cornell University, College of Arts and Science, Ithaca, NY.

Research experience:

2005-2010	Graduate Student Researcher, UC Santa Barbara Biomolecular Sciences and Engineering Program Advisor: J. Herbert Waite
2002	Field Research Technician, Cornell University Department of Plant Breeding Mentor: Julia Hansen
2000	Undergraduate Student Researcher, Cornell Univeristy Department of Microbiology Mentor: Anthony Hay

Teaching Experience:

2009	Teaching Assistant, UC Santa Barbara MCDB 1AL: Intro Biology Lab
2009	Mentor, UC Santa Barbara California Nanosystems Institute, Apprentice Researchers (AR) Mentee: Gabriel Li
2008	Mentor, UC Santa Barbara Materials Research Lab, Research Internships in Science and Engineering (RISE) Mentee: Christine F Carpenter
2005	Teaching Assistant, UC Santa Barbara MCDB 109L: Biochemistry Lab
2001	Teaching Assistant, Cornell Univeristy BIOG 206 (now BIOG 1106): Introductory Biology

Fellowships/Scholarships:

2007-2009 University of California Biotechnology Research and Education Program (BREP) Graduate Research and Education in Adaptive Bio-Technology (GREAT) Grant: Two years $100,000

1998-2000 Raytheon Incentive Scholars Award (undergraduate)

Awards:

• Chang Distinguished Alumni Award for Audience Participation at Friday Noon Seminar Series, 2009

• Chang Distinguished Alumni Award for Outstanding Talk at Friday Noon Seminar Series, 2008

Presentations:

• S. Scott Wasko and J. Herbert Waite Recoverable yield in an extensible, proteinaceous material found in gastropod egg capsules, 2008

Oral presentation at the Materials Research Society spring meeting in San Francisco.

• S. Scott Wasko and J. Herbert Waite Recoverable-Yield in a Poteinaceous Elastomer From Marine Whelks, 2007

Poster presented at the International Conference on Self-healing Materials in Noordwijk, NL.

Publications:

Ali Miserez, S. Scott Wasko, Christine F. Carpenter and J. Herbert Waite. "Non-entropic and Reversible Long-Range Deformation of an Encapsulating Bioelastomer." *Nature Materials*, **8** (11): 910-916 (2009).

(AM and SSW contributed equally to the manuscript)

S. Scott Wasko, J. Herbert Waite. Structural proteins from an egg capsule with nonentropic reversible extensibility," *Biomacromolecules*. (submitted/under review).

S. Scott Wasko, Matthew J. Harrington, Himadri S. Gupta, Peter Fratzl, J. Herbert Waite. "Characterizing the reversible α-helix β-sheet transition in a shape-memory biological material," (manuscript in preparation).

S. Scott Wasko, Matthew J. Harrington, Himadri S. Gupta, Peter Fratzl, J. Herbert Waite. "Supramolecular structure and nanoscale tensile behavior of a shape-memory biological material," (manuscript in preparation).

ABSTRACT

Biochemistry and Structure-Function Relationships in the Proteinaceous Egg Capsules of *Busycotypus canaliculatus*

by

Stephen Scott Wasko

The designs of highly extensible soft materials in nature are of a fundamental interest to engineers so that insights into the production of modern, synthetic materials can be gleaned. Marine gastropods of the genus *Busycotypus* produce a protein based elastomer which possesses a unique combination of stiffness and extensibility. Furthermore, this material displays shape-memory/self-healing properties that are unmatched in synthetic engineering systems. Four variants of the precursor protein components of the egg capsules are highly unique in their amino acid sequences, showing no homology to any known protein families. These proteins are strongly α-helical in nature, and can self-assemble into nanometer scaled fibers *in vitro*. The remarkable reversibly extensibility of

the bulk material is dictated not by entropic forces, but rather by a crystalline phase transition within the protein components when the material is put under tension. Proteins shift from α-helix to β-sheet, and it is this uncoiling of helices within the polymer backbone that allows for the extensibility of the egg capsules. This transition is reversible, as when loads are removed and the material is allowed to relax, it returns to its original α-helical conformation. When examined more closely, it is shown that this $\alpha \leftrightarrow \beta$ transition is a multi-step transformation which involves first the uncoiling of crystalline α-helices into non-crystalline random coils before these then lock into β-sheets. These different steps dictate changes in the mechanical properties of the material as this transition is occurring. Furthermore, the supramolecular structure of how the individual proteins interact in the intact material also changes throughout tension/relaxation cycles. These structural changes also have effects on the bulk mechanical properties of the material. This work explores in detail the structure-function relationships of *Busycotypus* egg capsule material mentioned above.

Table of contents

1. Introduction.....1

A. Overview.....1

B. Elastomeric Materials: Properties, Theories, and Applications.....2

C. Biomimetics: Taking Inspiration from Nature.....8

D. Fibrous Biological Materials.....10

E. Whelk Egg Capsules as a Model System.....15

F. Research in this Dissertation.....21

G. References.....22

2. Characterization of precursor proteins from *Busycotypus canaliculatus*..25

A. Abstract.....25

B. Introduction.....26

C. Materials and Methods.....30

D. Results.....34

E. Discussion.....42

F. Conclusions.....50

G. Accession Numbers.....52

H. Acknowledgments.....52

I. References.....54

3. Thermomechanical properties of *Busycotypus canaliculatus* egg capsules: entropic vs non-entropic....56

A. Abstract....56

B. Introduction....57

C. Materials and Methods....59

D. Results and Discussion....62

E. Conclusions....78

F. Acknowledgments....79

G. References....80

4. Using wide angle x-ray scattering to characterize the phase transition from α-helix to β-sheet as a result of uniaxial tension....82

A. Abstract....82

B. Introduction....82

C. Materials and Methods....85

D. Results....86

E. Discussion....91

F. Conclusions....97

G. Acknowledgments....98

H. References....99

5. The supramolecular hierarchical ordering of *Busocotypus canaliculatus* egg capsules and its role in tensile mechanics....102

A. Abstract....102

B. Introduction....103

C. Materials and Methods....104

D. Results....106

E. Discussion....113

F. Conclusions....120

G. Acknowledgments....121

H. References....122

6. Conclusions and future directions....124

A. Abstract....124

B. Conclusions from this Work....125

C. Future Directions....129

D. Materials and Methods for Preliminary Studies....131

E. Preliminary Results....133

F. Acknowledgments....139

H. References....140

Chapter 1. Introduction

A. Overview

Research into soft elastomeric materials has been ongoing and active for a considerable amount of time. With a broad range of functionalities and mechanical properties, these materials can be utilized in a wide variety of applications. Fibrous composite materials can, and often do add a level of anisotropic structure which can further tune these functionalities and hence applications.

In biologic systems, elastomers are frequently formed from naturally occurring fibers such as protein or carbohydrate. The somewhat recent notion of studying these kinds of natural materials and systems with the intent of applying what is learned to manmade engineering strategies has been dubbed biomimetics, and this field has gained considerable momentum over the past few years. Research into biological fibers has increased dramatically as a result.

One such biologic elastomer is the egg capsule that marine prosobranch gastropods, commonly known as whelks, use to protect embryos during development. This material has shown to not only have strong biomimetic potential, but to also serve as a model system to further elucidate theory regarding the thermodynamics of reversible extensibility, and phase transition in materials. The characterization of the biochemistry

and structure-function relationships in this egg capsule material is the topic of this dissertation.

B. Elastomeric Materials: Properties, Theories, and Applications

An elastomer has been defined as "a macromolecular material that returns rapidly to approximately the initial dimensions and shape after substantial deformation by a weak stress and release of the stress."[1] Some choose to establish more detailed conditions that the material must meet in order to be classified an elastomer: it must be capable of being stretched at least 100% of it's original length[2], and that after being stretched to 100%, held for five minutes, and then released, it must retract to within 10% of its original length within five minutes after release[3]. Regardless of specifics, elastomers are materials which exhibit little plastic flow and demonstrate a quick and nearly complete recovery from an extending force.

Such materials have countless applications in both manmade as well as natural systems. In synthetic applications, elastomers are employed as protective coatings, adhesives, composite components to increase extensibility and durability, insulators (both thermal and electrical), textiles, implants, foams, the list goes on and on[2,5]. Numerous fields employ elastomeric materials in their respective systems, from construction to automotive to biomedical and beyond. Natural systems have also developed elastomeric polymers which serve roles equally as diverse as their

manmade counterparts: as shock absorbers in, for example, hydrated dragline spider silks[6], for elastic energy storage capacity in the resilin of jumping and flying insects[7] and to ensure adequate elasticity in the integument and arteries of various organisms[8-10]. With such varied uses and functional environments, these materials, both manmade and natural, are also varied in the properties that they possess.

The properties that must be considered when selecting an appropriate elastomer for a given system include mechanical properties (extensibility, hardness, strength, stiffness, resilience, scratch and abrasion resistance, creep, compressibility, etc) as well as environmental compatibility (temperature performance at both low and high temps, resistance to solvents and oils, behavior in aqueous environments, biocompatibility, flame resistance, UV resistance, age related degradation, etc)[2]. All of these must be examined to find the perfect match for a specific application.

Many of the mechanical properties are dictated by the thermodynamic nature of extensibility in each material. The primary forces that contribute to this can be grouped as either entropic or internal. Entropic force is dictated by the second law of thermodynamics which states that systems have a tendency to maximize entropy (disorder) within that system. Internal force, or bond energy, is the sum of energy in the chemical bonds as well as the weak force interaction between atoms within a system. Simply put, while a system may seek to maximize disorder, the forces associated

with bond energies in that system resist that tendency. The interplay of these forces is represented by the Hemholtz free energy relationship[2,4].

$$A \equiv U - TS \tag{1.1}$$

Wherein A is the Hemholtz free energy, U is the internal energy, T is absolute temperature and S is entropy. The differential of the maximum work function dA can be written to include the work done on an elastomer by the application of a force, f, over the change in length, dL.

$$dA = -PdV - SdT + fdL \tag{1.2}$$

Where P is pressure and V is volume. Accordingly, the force is comprised of two components, and internal energy component, f_U, and an entropy component, f_S.

$$f = f_U + f_S \tag{1.3}$$

The partial differential of A with respect to length at constant V, T, and composition, n, can be rewritten as

$$f_U/f = -T(\partial \ln[f/T]/\partial T)_{V,L,n} \tag{1.4}$$

which allows for an experimental estimate of the f_U/f ratio from the slope of a plot of $\ln(f/T)$ versus temperature under conditions of constant V, L, and composition, n, so long as appropriate correction terms are applied.

Many elastomers, both synthetic and natural rubbers[2,5,11,12] as well as some biological materials such as elastin[9] and resilin[7], exhibit classic entropic elasticity wherein f_S is far greater than f_U. In this model, an elastomeric material in a relaxed state is composed of a network of random chains which with a low crosslink density. The extension of this material from the relaxed state by an external force causes a decrease in entropy, governed by the Boltzmann relationship[2,4], as chains become aligned in an anisotropic manner.

$$\Delta S = (S^e - S^r) = R \ln(W^e/W^r) \qquad (1.5)$$

Wherein R is the Boltzmann constant. This decrease in entropy largely overshadows any internal energy component and, and once the external force is removed, the system seeks to reestablish the thermodynamic equilibrium of the relaxed state by the polymer chains randomly orienting themselves again, causing a contraction of the material (Fig 1.1)

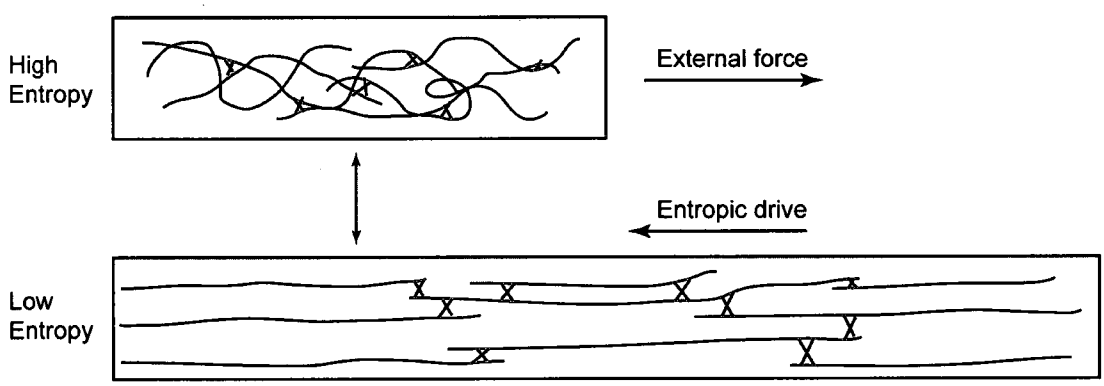

Figure 1.1. Schematic of classic entropically driven elastomeric behavior

The flip side of this thermodynamic relationship has internal forces dominating reversible extensibility. The sequential rupturing of weak chemical bonds in a material without compromising the polymer backbone can allow for an increase in overall length of the material. Furthermore, if the ruptured bonds are both capable of, and are allowed to reform, the material may recover initial dimensions and shape after deformation, thereby qualifying it as an elastomer. This paradigm has been dubbed "sacrificial bonds and hidden length," and allows for reversible, long range extensibility that is governed by internal rather than entropic energy[13] (Fig 1.2).

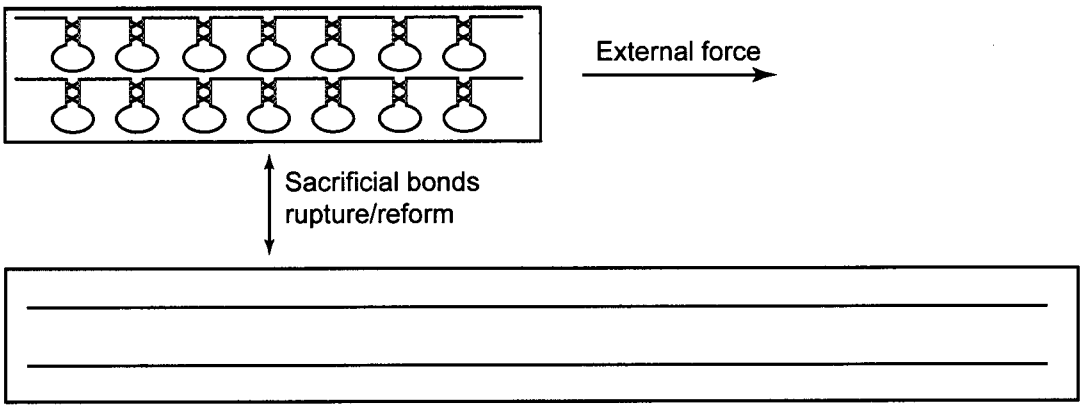

Figure 1.2. Schematic of sacrificial bond and hidden length internal energy driven elastomeric behavior

Well before sacrificial bond terminology was coined, this concept of non-entropic elasticity was explored in crystalline phase transitions. The weak interactions holding the polymer material in one crystalline phase would serve as the sacrificial bonds. Under no external forces, this phase represents the most stable conformation, but under an exerted load these weak bonds rupture and the material adopts a different crystalline structure. Once the load is removed, the material returns to the original thermodynamically stable structure. This model has been proven in shape memory alloys since 1972[14] (while not technically elastomers by the strictest definition, the two do share a great number of properties), and had been proposed in 1956 for proteinaceous materials[15]. While it has been demonstrated that numerous protein fibers undergo phase transitions as the

result of an applied physical load, no dedicated studies into the thermodynamics of those protein fibers' elasticity have been performed.

C. Biomimetics: Taking Inspiration from Nature

Every biological organism employs a variety of systems and materials to successfully fill its ecological niche. Ultimately these material designs are geared towards maximizing functionality, and frequently these functions include a form of load or impact bearing material that is designed to meet an organism's unique demands. However, it is not uncommon that the specific functions that these naturally occurring materials are designed for are also desired in manmade synthetic systems. As such, these materials can be studied and the lessons learned can be applied to modern engineering problems.

There are many intuitive advantages in taking inspiration from nature. Natural materials are invariably built under ambient conditions (temperature, pressure, pH, etc) using non-toxic, biologically friendly components. In the natural world, the overarching functionality of any system is to increase the individuals' evolutionary fitness, and materials systems are no different. The result of this is two-fold. Firstly, these biomaterials have been honed by generations upon generations of evolutionary pressure to perform its specific function very well. Secondly, as high energy consumption is an evolutionary liability, biomaterials are synthesized in an energetically efficient

manner. Nature rarely over-engineers its systems. Biomimetics can offer insights not only into designing systems and materials with desired functionalities, but also provide a fabrication process that is more environmentally friendly, with low energy costs, furthering "green" technologies.

In addition to load and impact bearing materials, biomimetic research has resulted in advances in numerous specific fields. Some of these include energy production and storage[16], adaptive materials[17], adhesives[18], self-healing/shape-memory materials[19], and biomedical systems[20]. It is a proven truth that by studying the structure function relationships of these kinds of systems, humans can apply the same principles that nature does to developing modern high-performance material systems.

However, it must also be stated that there are inherent limitations in this process. As mentioned before, evolutionary pressures direct the progression and functionality of these natural systems, but that does not mean that these systems are optimized. Instead they merely perform their intended functions at a satisfactory level for the evolutionary pressures applied, given the limited resources available to the organism (building components, synthesis conditions, energy allocation, etc). Furthermore, the demands that human engineered systems have may be greater than those that natural systems are adapted to perform. Another challenge is the fact that many biological systems are multifunctional and, as such, contain many

components, each designed to perform its own task in a synergistic manner with the other components. This makes deciphering exact structure-function relationships very difficult. Evolution has spent hundreds of millions of years designing a specific material, yet biomimeticists will attempt to elucidate their secrets and fabricate a suitable mimic in a few short years. This can be a daunting task indeed.

Despite these potential setbacks, the exploration of natural systems is still worthwhile. As mentioned above, great strides have already been made in numerous systems, and the adaptation of design strategies from natural to engineered materials continues to show more and more promise.

D. Fibrous Biological Materials

Natural fibers are typically made up of either carbohydrate or protein building blocks. The most prevalent of these are the plant-based structural polysaccharide fibers cellulose and lignin[21,22]. As plants, both aquatic and terrestrial, make up the vast majority of biomass on this planet, it is no wonder that these are so abundant[23]. Chitin, another carbohydrate, found in the cell walls of fungi and in the exoskeletons of arthropods, is also found in high abundance in the natural world and is arguably just as prevalent if not more so than lignin[21]. Proteins, by comparison, make up a very small proportion of fibrous biomass[21,24]. But while they may lack in bulk quantity,

the variety of different functionalities that protein materials possess is staggering.

Protein fibers are found in all kingdoms of life. They are located intracellularly, extracellularly, and extraorganismally and are involved in load bearing scaffolds such as the skeleton and cytoskeleton[25,26]; in cellular transport and cellular division[27]; in wear resistant tools such as teeth, mandibles, and radulae[25,28,29]; in locomotion of all kinds[24]; in tissue encapsulation, both internal[30] and external[31-33]; in shelter and protection[34,35]; in wound healing and response[36]; in holdfasts and prey capture[6,37]; and in a variety of other functions. As there is such a broad range of demands, the fibers themselves must also be highly varied as they are tuned to perform each specific task. Keratins in horns and nails primarily function in dry environments and must be stiff and wear resistant, whereas the fibrins involved in wound healing must allow for flexibility around the damaged area to maintain a tight seal while functioning in aqueous conditions. Microtubules must be programmable highways with controlled destinations so that transporters can guide their molecular cargo to specific targets, while spider silks must be able to withstand the forces of an entire organism impacting a web. As all proteins are composed of the same amino acid building blocks, differences in sequence and structure are responsible for the differences in functionality.

The majority of protein sequences involved in fiber formation are typically dominated by secondary structural domains. Collagens form a polyproline type-2 helix as a result of the G-X-Y (wherein X and Y are frequently proline or hydroxyproline) tandem repeats[38]. Silks have a high quantity of β-sheets β-turns throughout the protein sequences[39]. The keratin family has some members that are rich in β-sheets[40] (the appropriately named beta-keratins found in feathers, claws, and scales) and other members that are rich in α-helices[41] (the intermediate filament alpha-keratins found in hair, horns, and quills). These secondary structures contribute heavily to the mechanical properties of these protein fibers and help dictate the strength, toughness, and resilience of the material in addition to whether or not it be compliant or stiff, extensible or brittle, elastomeric or plastic[12,21,24].

The hierarchical structure of fibers also plays a critical role in these mechanical properties. Protein based fibers, unlike metals or ceramics, are typically not uniform throughout the entire structure and are frequently composites of multiple different proteins, or even non-protein biomacro-molecules, coming together in assembly[21,24,41,42]. Figure 1.3 illustrates the hierarchical organization of both tendon, built primarily from collagen, and of hair, built primarily from alpha-keratin intermediate filaments. The manners in which these fibers are arranged from single protein, up through bulk

material must also be studied thoroughly to gain a solid structure-function relationship for any protein fiber based material.

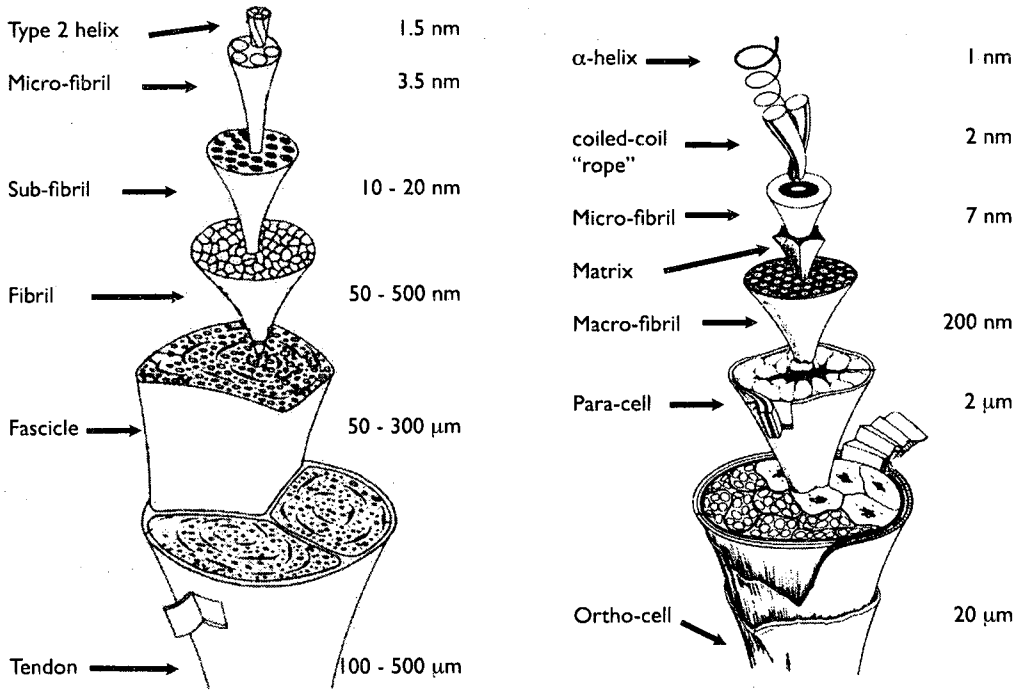

Figure 1.3. Hierarchical structural organization for a) tendon collagen[42], and b) hair keratin[41]

The hierarchical structure is dictated by the assembly of the fibers, be it self-assembly or directed assembly, as well as by crosslinking[21,24]. Protein building blocks need to leave the cell either before or during assembly. This exit can occur either by a controlled secretion pathway[27], or by programmed cell death[43,44]. Some constituent proteins will form intermediate multimers with each other before joining to form the fibers[45,46], while others will simply

add on single proteins to the structure[47]. Some materials will spontaneously self-assemble under the proper conditions (pH, ionic strength, etc)[43,44], others must be modified (frequently by protein cleavage) before assembly[48], still others require additional assistance from molecular chaperones[47,49]. Such variety in assembly processes leads to a variety of structures. Additionally the methods for crosslinking are just as varied. Crosslinks can come in the form of covalent bonds (disulfide bonds, desmosine, and glutamyl-lysine linkages are some of the more prevalent)[38], or in the form of weak interactions such as metal coordination complexes and hydrogen bonding[50-53]. The location of crosslinks throughout the fiber, whether they join the proteins end to end, end to middle, or middle to middle, also critically affects mechanical properties[54].

Many of the more extensible protein materials such as elastin[9] and resilin[7] have been shown to behave like classic rubbers from both a structural and a thermodynamic standpoint. That is the protein constituents are seemingly randomly oriented with a low level of crosslinks, and the extensibility and recovery of the material is dictated by entropic forces rather than internal bond energies. It had been proposed that a crystaline transformation can be responsible for long-range, reversible deformation in protein materials[15], greater than in the shape memory alloys. However, as mentioned above, while there have been numerous theoretical candidates for this non-entropic elasticity, either due to the complex nature of protein

materials or possibly a perceived lack of interest in the field, there has been no experimental conformation of the theory.

E. Whelk Egg Capsules as a Model System

Busycotypus canaliculatus (formerly known as *Busycon canaliculatum*) is a marine prosobranch gastropod that is endemic to the mid to northern regions of the North American Atlantic coast, and has been introduced to San Francisco Bay. Commonly known as the "channeled whelk", this organism is valued as a food resource. The species has male and female individuals and fertilization is internal as opposed to external spawning like some other aqueous organisms. Once fertilization is complete, the female will lay long strings of interconnected disk-shaped egg cases, colloquially known as "mermaids necklaces" (Fig 1.4), in shallow ocean waters, anchored by burying one end in the sand. These strings may be in excess of 1 meter in length, and can contain hundreds of individual egg cases, each case containing up to 25 developing embryos. After a incubation period of as many as 10 months, the embryos come to term as completely developed whelks and exit the egg cases[55].

Figure 1.4. Channeled whelk with a string of egg capsules, "mermaid's necklace"

During this time period, the egg cases are subjected to hazards such as extreme hydrodynamic forces generated by water velocities in excess of 10 $msec^{-1}$ [56], abrasion from sand and other particulates in the surrounding water, as well as predation[57]. In addition to physical protection, the diffusion of certain molecules, such as metabolic waste products, is also necessary[57]. As such, the organism has been forced to develop a very robust, yet permeable material to use as the egg capsule wall.

An acellular material composed of >90% protein, the egg capsule wall is highly ordered and possesses unique tensile properties. It has been previously established that multiple processing steps are required to produce the mature form of the material. Each one of these steps alters the tensile properties, physical appearance, and biochemical composition of the material[58-61]. The precursor proteins are produced in the nidamental gland (also known as egg capsule gland). Here, they are stored in secretory

granules for use during the reproductive cycle[62]. These precursors are soluble, and there is evidence that they are stored in a liquid crystalline array[58,62]. During egg capsule deposition, the proteins are secreted into the reproductive tract where they self-assemble into fibers and sheets to surround the embryos. At this stage, the egg capsule has a white appearance, no definitive shape, and limited structural stability. This "immature" capsule is soluble in detergents and denaturing agents, and is susceptible to enzyme-mediated proteolytic cleavage[63]. The unfinished product is then passed along the reproductive duct to the ventral pedal gland located on the ventral surface of the foot. Here, the capsule undergoes a sclerotization process for approximately 1-2 hours during which the capsule gains a yellowish tint, is molded into the disk-like shape, and develops the mechanical robustness necessary for protecting the embryos during development[55,57,59]. The material is now insoluble in even the harshest denaturants, and resists enzymatic cleavage[58,63]. This "mature" capsule is incorporated onto the string of capsules that came before it and is now anchored to the seabed.

While observed and described since the late 1800's [64], research into the material itself did not begin until the 1960s, when researchers at the University of Leeds, England, performed the first structural studies. Using wide-angle x-ray scattering it was determined that whelk egg case proteins resides primarily in a coiled-coil α-helix conformation. The same group used

TEM work to show that multiple laminate sheets make up the biaxial material, and that fibers are highly ordered in these sheets with a visible periodicity 50 nm[60,65].

In the 70s, work on the egg cases shifted to biochemical characterization of bulk material, as well as the protein precursors. Amino acid analysis of intact capsule wall indicated levels of the key structural residues glycine, proline, alanine, and valine in much lower proportions than those of collagens and elastins, suggesting that this material has a different structural composition. Charged residues (aspartate, glutamate, lysine, and arginine) dominate the amino acid content, making up >40% of the protein. Helix formers comprise 50% of the content with 25% helix indifferent and 25% helix breakers, which corroborates the x-ray studies of the 60s [62,66,67]. Over all, the amino acid composition of the capsule wall is very similar to that of α-keratin intermediate filaments (IF), with one notable difference: IFs have a high disulfide cystine content, where as the capsules have none. Therefore, a different crosslinking mechanism is probable in the latter system[21].

By comparing analyses of capsule wall and precursor proteins, it was shown that the lysine content drops significantly during processing. So it is thought that lysine based crosslinks could be involved[62]. Furthering this theory was the fact that borohydride reducible compounds were found in the bulk material[61]. Using tritium labeled borohydride, it was possible to isolate

these compounds for further study and evidence suggested that lysinonorleucine crosslinks were involved[61,62]. However, the results were never conclusively proven, and research on that topic stopped abruptly.

It was not until the late 90s and into the 00s that research on the material started again. Scientists at the Scripps Research Institute at UC San Diego examined tensile mechanical properties. Their stress-strain studies (using engineering stress and strain) indicate three regions with distinctly different elastic moduli[58,59]. At low strain there is high modulus in the range of 160 MPa. However, after being extended past ~3% strain, there is a sudden and dramatic drop in flow modulus, down to the 2 MPa range, which is maintained until ~80% strain. At this point it increases again to 11 MPa and is maintained until the breaking strain of ~170% . When the material is cyclically strained to a point below its breaking strain, it undergoes an energy absorbing hysteresis of 50% at 100% extension (Fig 1.5). Upon subsequent strain, recovers the initial high modulus

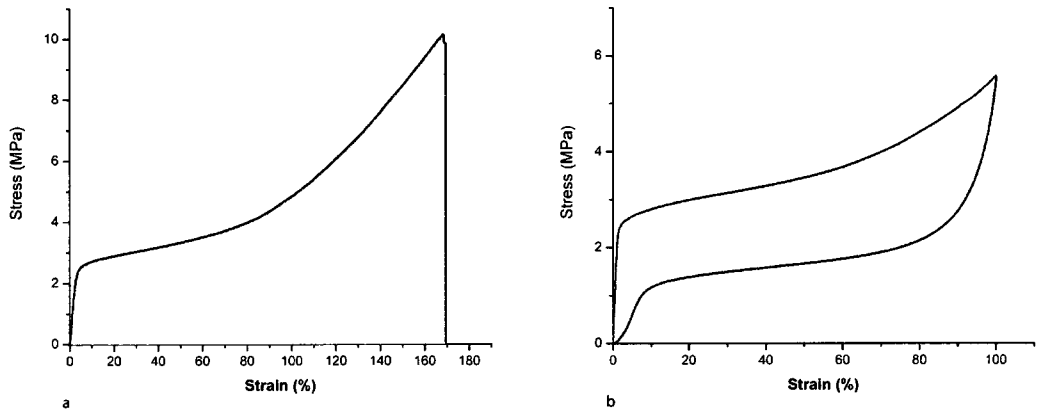

Figure 1.5. Stress strain curves of egg capsule material. a) shows extension to breaking. b) shows extension to 100% strain followed by relaxation back to 0%.

that was present in the first pulling of the material (Fig 1.6). Termed "recoverable-yield," this shape-memory recovery is near instantaneous and fully repeatable for a seemingly infinite number of cycles on the same sample[59].

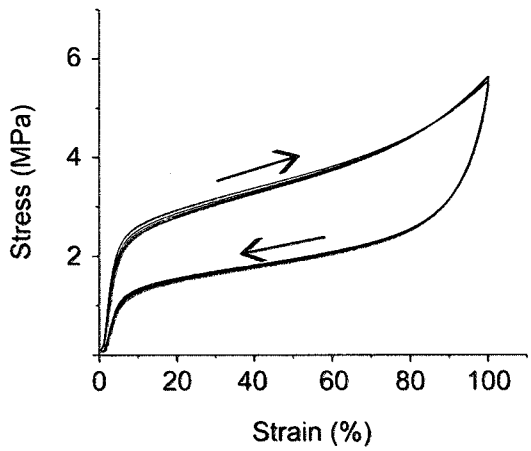

Figure 1.6. Stress strain curve of egg capsule material cyclically strained to 100% multiple times with no recovery time between cycles

G. Research in this Dissertation

The overarching goal of this research is to further elucidate the structure-function relationships in whelk egg capsule material in terms of biochemistry, molecular ordering, and mechanical properties. This necessitates work that crosses multiple disciplines. Firstly, characterization of the precursor proteins of the capsule wall will be discussed. This characterization includes physical properties such as mass and amino acid composition, documentation and analysis of the complete primary sequence of four of these precursors, as well as structural studies of how they behave in solution. Next, the thermomechanical nature of egg capsule extensibility (entropic vs internal energies) will be examined, and experimental evidence for crystalline transitions in protein secondary structure will be presented. Following that, a more thorough characterization of this secondary structure transition, as well as shifts in hierarchical structure, derived from synchrotron source x-ray scattering, and how they relate to the stress-strain properties of the material will be introduced. Lastly, potential directions for future research and preliminary results will be outlined.

H. References

1. Am. Soc. for Testing of Materials Standards, Part 28, 1967
2. Harper, C. A. Handbook of Plastics and Elastomers. McMraw-Hill Book Company, New York, NY, 1975.
3. Pickett, A. G., & Lemcoe, M. M. *Handbook of Design Data on Elastomeric Materials Used in Aerospace Systems*. U.S. Air Force Communication, Wright-Patterson Air Force Base, Dayton, OH, 1961.
4. Treloar, L. R. G. *The Physics of Rubber Elasticity*. Oxford University Press, Oxford, U.K., 2005
5. Holden, G. *Understanding Thermoplastic Elastomers*. Hanser Gardner Publications, Inc. Cincinnati, OH, 2000
6. Gosline, J. M., Denny, M. W. & DeMont, M. E. Spider Silk as Rubber. *Nature* **309**, 551-552 (1984).
7. Weis-Fogh, T. A Rubber-Like Protein in Insect Cuticle. *Journal of Experimental Biology* **37**, 889-907 (1960).
8. Lillie, M. A. & Gosline, J. M. The Effects of Hydration on the Dynamical Mechanical Properties of Elastin. *Biopolymers* **29**, 1147-1160 (1990).
9. Urry, D. W. et al. Elastin: A Representative Ideal Protein Elastomer. *Philosophical Transactions of the Royal Society of London, Series B: Biological Sciences* **357**, 169-184 (2002).
10. Shadwick, R. E. & Gosline, J. M. Physical and Chemical Properties of Rubber-Like Elastic Fibres from the Octopus Aorta. *Journal of Experimental Biology* **114**, 239-257 (1985).
11. Tatham, A. S. & Shewry, P. R. Elastomeric Proteins: Biological Roles, Structures and Mechanisms. *Trends in Biochemical Sciences* **25**, 567-571 (2000).
12. Shewry, P. R., Tatham, A. S., & Bailey, A. J. *Elastomeric Proteins: Structures, Biomechanical Properties, and Biological Roles*. Cambridge University Press, Cambridge, U.K. 2002.
13. Fantner, G. E., Oroudjev, E., Schitter, G., Golde, L. S., Thurner, P., Finch, M. M., Turner, P., Gutsmann, T., Morse, D. E., Hansma, H., & Hansma, P. K. Sacrificial Bonds and Hidden Length: Unraveling Molecular Mesostructures in Tough Materials. *Biophysical Journal* **90**, 1411–1418 (2006).
14. Jackson, C. M., H. J. Wagner, & R. J. Wasilewski. 55-Nitinol- The Alloy With a Memory: Its Physical Metallurgy, Properties, and Applications: A Report. *Washington: NASA*, 1972.
15. Flory, P. J. Theory of Elastic Mechanisms in Fibrous Proteins. *Journal of the American Chemical Society*, 5222-5235 (1956).
16. Christodoulou, L., & Venables, J. D. Multifunctioal material systems: the first generation. *J. Min. Met. Mater. Sci.* **55**, 39-45 (2003).
17. Varadan, V. K., Varadan, V. V. Microsensors, microelectromechanical systems (MEMS) and electronics for smart structures and systems. *Smart Mat. Str.* **9**, 953-972 (2000).
18. Hui Shao, H., Bachus, K. N., & Stewart, R. J. A Water-Borne Adhesive Modeled after the Sandcastle Glue of *P. californica*. *Macromol. Biosci.* **9**, 464–471 (2009)
19. Kushner, A. M., Gabuchian, V., Johnson, E. G., & Guan, Z. Biomimetic design of reversibly unfolding cross-linker to enhance mechanical properties of 3D network polymers. *J. Am. Chem. Soc.* **129**, 14110-14111 (2007).
20. Lee, H., Lee, B. P., & Messersmith, P. B. A reversible wet/dry adhesive inspired by mussels and geckos. Nature **448**, 338-341 (2007).
21. Vincent, J. *Structural Biomaterials*, Revised ed; Princeton University Press, Princeton, NJ, 1990.
22. Holtman, K. M., Chang, H., Jameel, H., & Kadla, J., F. Elucidation of lignin structure through degradative methods: comparison of modified DFRC and thioacidolysis. *J Agric Food Chem* **51**, 3535-40 (2003).

23. Botkin, D. B., & Keller, E. A. *Environmental Science: Earth as a Living Planet*, 6th ed; John Wiley & Sons, Hoboken, NJ. 2005
24. Vogel, S. *Comparative Biomechanics Life's Physical World.* Princeton University Press, Princeton, NJ, 2003.
25. Currey, J. D. *Bones: Structure and Mechanics.* Princeton University Press, Princeton, NJ, 2002.
26. Khurana. S. *Advances in Molecular and Cell Biology #37: Aspects of the Cytoskeleton*, Elselvier LTD, London, U.K. 2006.
27. Alberts, B., Johnson, A., Lewis, J., Raff, M., Roberts, K., & Walter, P. *Molecular Biology of the Cell*, 5th ed; Garland Publishing Inc. New York, NY, 2008.
28. Broomell, C. C., Chase, S. F., Laue, T., & Waite, J. H. Cutting edge structural protein from the jaws of Nereis virens. *Biomacromolecules* **9** 669-677 (2008).
29. Miserez, A., Schneberk, T., Sun, C., Zok, F. W., & Waite, J. H. The transition from stiff to compliant materials in squid beaks. *Science* **319**,1816-1819 (2008).
30. Heiden, T. C., Haines, A. N., Manire, C., Lombardi, J., & Koob, T. J. Structure and permeability of the egg capsule of the bonnethead shark, Sphyrna tiburo. *J. Exp. Zool. A. Comp. Exp. Biol.* **303**, 577-589 (2005).
31. Lavelin, I., Meiri, N., & Pines, M. New insight in eggshell formation. *Poult Sci.* **79**, 1014-1017 (2000).
32. Hu, X., Kohler, K., Falick, A. M., Moore, A. M., Jones, P. R., Sparkman, O. D., & Vierra, C. Egg case protein-1. A new class of silk proteins with fibroin-like properties from the spider *Latrodectus hesperus. J Biol Chem.* **280,** 21220-21230 (2005).
33. Knupp, C., Chew, M., & Squire, J. Collagen Packing in the Dogfish Egg Case Wall. *J Struct. Biol.* **122**, 101–110 (1998)
34. Zhao, H., Sun, C., Stewart, R. J., & Waite, J. H. Cement proteins of the tube- building polychaete Phragmatopoma californica. *J Biol Chem.* **280**, 42938-42944 (2005).
35. Baden, H. P., & Maderson, P. F. Morphological and biophysical identification of fibrous proteins in the amniote epidermis. J Exp Zool **174**, 225–232 (1970).
36. Doolittle, R. F. Fibrinogen and Fibrin. *Annu Rev Biochem* **53**, 195-229 (1984).
37. Waite, J. H., Vaccaro, E., Sun, C. & Lucas, J. M. Elastomeric gradients: a hedge against stress concentration in marine holdfasts? *Phil. Trans. R. Soc. Lond. B* **357**, 143–153 (2002).
38. Creighton, T. E. *Proteins: Structures and Molecular Properties*, 2nd ed; W. H. Freeman and Company: New York, NY, 1993.
39. Hayashi, C. Y., & Lewis, R. V. Evidence from flagelliform silk cDNA for the structural basis of elasticity and modular nature of spider silks. *J. Mol. Biol* **275**, 773-84 (1998).
40. Lee, L. D., & Baden, H. P. Chemistry and composition of the keratins. *Int. J. Dermatol.* **14**,161-171 (1975).
41. Feughelman, M. *Mechanical Properties and Structure of Alpha-Keratin Fibres: Wool, Human Hair, and Related Fibres*, UNSW Press: Sydney, Australia, 1997.
42. Kastelic, J., & Baer, E. Deformation in Tendon Collagen. *Symp. Soc. Exp. Biol* **34**, 397-435 (1980).
43. Rogers, G. E. Biology of the wool follicle: an excursion into a unique tissue interaction system waiting to be re-discovered. *Exp. Dermatol* **15**, 931–949 (2006).
44. Koch, E. A., Spitzer, R. H., Pithawalla, R. B., & Downing, S. W. Keratin-like components of gland thread cells modulate the properties of mucus from hagfish (*Eptatretus stouti*). *Cell Tiss. Res* **264**, 79-86 (1991).
45. Coulombe, P. & Fuchs, E. Elucidating the early stages of keratin filament assembly. *J. Cell. Biol* 1990, 111, 153-169.
46. Kreplak, L., Aebi, U., & Herrmann, H. Molecular mechanisms underlying the assembly of intermediate filaments. *Exp. Cell. Res* 2004, 301, 77-83.
47. Pollard, T. D., Actin and actin-binding proteins. A critical evaluation of mechanisms and functions. *Ann. Rev. Biochem.* **55**, 987-1035 (1986).

48. Fessler, J. H., & Fessler, L. I. Biosynthesis of procollagen. *Ann. Rev. Biochem.* **47**,129-162 (1978).
49. Weigarten, M. D., Lockwood, A. H., Hwo, S. Y., & Kirschner, M. W. A protein factor essential for microtubule assembly. *Proc Natl Acad Sci U S A.* **172**, 1858-1862 (1975).
50. Broomell, C. C., Zok, F. W., & Waite, J. H. Role of transition metals in sclerotization of biological tissue. *Acta Biomater.* **4**, 2045-2051 (2008).
51. Pontin, M. G., Moses, D. N., Waite, J. H., & Zok, F. W. A nonmineralized approach to abrasion- resistant biomaterials. *Proc Natl Acad Sci USA.* **104,** 13559-13564 (2007).
52. Harrington, M. J., & Waite, J. H. pH-dependent locking of giant mesogens in fibers drawn from mussel byssal collagens. Biomacromolecules **9,** 1480-1486 (2008).
53. Gosline, J. M., Guerette, P. A., Ortlepp, C. S., & Savage, K. N. The mechanical design of spider silks: from fibroin sequence to mechanical function. *J. Exp. Biol* **202**, 3295–3303 (1999).
54. Fudge, D. S., & Gosline, J. M., Molecular design of the α-keratin composite: insights from a matrix-free model, hagfish slime threads. *Proc. R. Soc. Lond. B* **271**, 291–299 (2004).
55. Magalhaes, H. An Ecological Study of Snails of the Genus Busycon at Beaufort, North-Carolina. *Ecol. Monograph* **18**, 377-409 (1948)
56. Denny, M. W. *Biology and the Mechanics of the Wave-Swept Environment.* Princeton Univ. Press: Princeton, NJ, 1988.
57. Rawlings, T.A., Adaptations to physical stresses in the intertidal zone: The egg capsules of neogastropod molluscs. *American Zoologist* **39**, 230-243 (1999).
58. Rapoport, H. S., *Biomechanics, Biochemistry, and Molecular Biology of a Molluscan Scleroprotein Elastomer: Whelk Egg Capsule Biopolymer*, in *Marine Biology*. PhD thesis. University of California San Diego (2003).
59. Rapoport, H. S., & Shadwick R. E. Mechanical characterization of an unusual elastic biomaterial from the egg capsules of marine snails (*Busycon spp.*) *Biomacromolecules* **3**, 42-50 (2002).
60. Flower, N. E., Geddes, A. J., & Rudall, K. M. Ultrastructure of Fibrous Protein from Egg Capsules of Whelk *Buccinum Undatum. J Ultrastructure Research* **26**, 262-273 (1969).
61. Price, N. R. & Hunt, S. *Occurrence of Reducible Compounds in an Invertebrate Protein of Buccinum-Undatum (L). Cell. Mol. Life* **32**, 557- 558 (1976).
62. Goldsmith, L. A., & Lindberg, K. A. Nidamental Gland Precursor of Egg Capsule Protein of Gastropod Mollusk Busycon-Carica. Comp. Biochem. Physiol. B **59**, 133-138 (1978).
63. Rapoport, H. S., & Shadwick, R. E. Reversibly labile, sclerotization-induced elastic properties in a keratin analog from marine snails: whelk egg capsule biopolymer (WECB). *J. Exp. Biol* **210**, 12-26 (2007).
64. Cunningham, J. T. Formation of egg-capsules in Gastropoda. *Nature* **59**, 557 (1899)
65. Gathercole, L. J. *Studies on the protein of the egg capsule of whelks.* PhD thesis, University of Leeds: Leeds, UK (1969).
66. Hunt, S., Carbohydrate and amino-acid composition of egg capsule of whelk *Buccinum undatum* L. *Nature* **210**, 436-437 (1966).
67. Hunt, S., Comparison of 3 extracellular structural proteins in gastropod mollusc *Buccinum undatum* L, Periostracum, egg capsule and operculum. Comp. Biochem. and Physiol. **40**, 37-46 (1971).

Chapter 2. Characterization of precursor proteins from *Busycotypus canaliculatus*

Adapted from S.S. Wasko, and J.H. Waite, "Structural proteins from an egg capsule with nonentropic reversible extensibility," Biomacromolecules, under review.

A. Abstract:

The robust, proteinaceous egg capsules of marine prosobranch gastropods (genus *Busycotypus*) are extraordinary examples of shape memory polymers. Capsule material possesses long-range extensibility that is fully recoverable and is the result of a secondary structure phase transition from α-helix to β-sheet rather than from entropic elasticity. We report here the characterization of several precursor proteins that make up this material. Three different proteins have been purified and analyzed, and complete protein sequences deduced from mRNA transcripts. Circular dichroism spectra indicate that the proteins are strongly α-helical in solution and primary sequence analysis suggests these proteins have a propensity to form coiled-coil trimers. This is in agreement with previous wide-angle x-

ray analysis of intact egg capsules. TEM images of the purified proteins self-assembling into fibers of the same dimension as those observed in the bulk material further strengthen the hypothesis that these proteins are the main structural elements in the egg capsules. Finally, a structure-function model that is consistent with Flory's original theory on non-entropic elasticity at the scale of an individual protein is proposed.

Keywords: Egg capsule, elasticity, coiled-coil, α-helix β-sheet transition, shape memory

Abbreviations: Bc-cp, *Busycotypus canaliculatus* capsule protein; CP, capsule protein; IF, intermediate filament.

B. Introduction:

Rubbery proteins such as elastin, resilin, and abductin are well studied from a variety of organisms in which they endow specialized tissues such as aorta, insect wings, and scallop hinge ligaments with low modulus, high extensibility (>100%), high resilience (>90%), and an entropically driven elastic recovery[1-3]. Accordingly, the entropy of a rubbery protein chain at rest is much greater than of a chain pulled taut, hence its spontaneous recovery upon unloading.

In 1957, Flory[4] proposed another paradigm for protein stretchiness, in which a loaded protein or protein assembly extends by undergoing a transition from one crystalline structure such as alpha helix to another such as beta sheet. This paradigm parallels the rubbery proteins in providing large extensions but differs significantly in that the energy driving recovery is provided by internal energy rather than entropic changes. The original example cited, wool keratin, does indeed undergo an alpha to beta transition during extensions of up to 40%, but recovery is slow and incomplete. A better paradigm would be a material that exhibits a completely reversible structural transition during a large extension. Such a material actually exists and consists of proteins that prosobranch gastropod mollusks or whelks of the genus *Busycotypus* (formerly *Busycon*) use to encapsulate embryos during their extended development period[5]. Meter-long strings (mermaid necklaces) containing hundreds of interconnected egg capsules are deposited on the seabed, and rely chiefly on this protein casing to protect the developing embryos from the hydrodynamic forces associated with wave velocities in excess of 25m sec^{-1}, abrasion from sand and other particulate debris, predation, and damaging UV light[6-8].

Fully processed, or mature, whelk egg capsule wall is a highly extensible, self-assembled, proteinaceous material which possesses remarkable self-healing/shape-memory properties. The egg capsules approach the extensibility of the biological rubbers elastin and resilin but

have an initial stiffness two orders of magnitude higher. Strain energy density (toughness) of capsule wall is more than five times greater and resilience two thirds that of elastin[9] (Table 2.1). Furthermore, even after the material is extended beyond a mechanical yield point, upon relaxation it returns to its original size and shape and within seconds recovers its initial high stiffness[15] (Fig 2.1 and Table 2.1). This is a rare and highly desirable combination of properties in polymer fibers[16].

Previous studies have detailed the tensile properties of the capsule wall[15,17,18] as well as the structural conformation of the material[19,20], and have modeled the thermodynamics of the self-healing behavior[5]. It is suggested that a reversible protein secondary structure transition from α-helix to β-sheet, similar to that observed in hard α-keratin materials[10,21,22], rather than entropic elasticity of protein filaments, similar to elastin and resilin, accounts for this behavior. It is of critical importance to characterize the constituent proteins of this material, hereafter referred to as

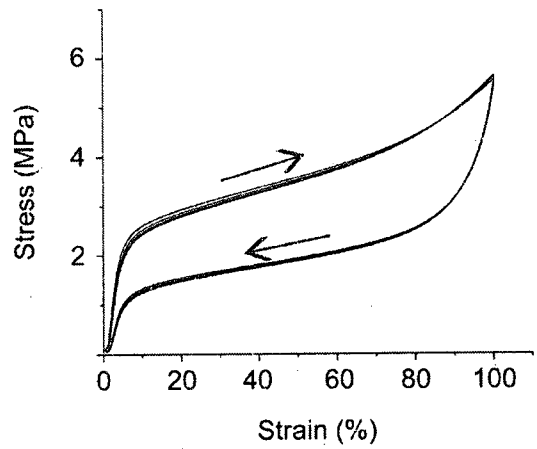

Figure 2.1. Typical engineering stress-strain curve for whelk egg capsule material in uniaxial tension. Sample was cyclicly strained multiple times at a rate of 5mm/min with no rest between cycles. Recovery of initial stiffness is complete and rapid.

the *Busycotypus canaliculatus* capsule proteins (Bc-cp), and wherever possible to reconcile the biochemistry with the observed tensile properties.

Protien Material	E_i (MPa)	Yield Stress (MPa)	Breaking Stress (MPa)	Yield Strain (%)	Breaking Strain (%)	Toughness (MJm)	Resilience (%)
Whelk Egg Capsule[a]	110	2.5	10.0	5	169	8.5	49
Wool Keratin[b]	3000	30	150	5	52	37.4	55
Resilin[c]	2	NA	4	NA	190	4	92
Elastin[d]	1	NA	2	NA	150	1.6	90
Tendon Collagen[e]	1200	20	39	1.5	12	4.1	90
Dragline Silk[f]	10000	160	1100	4	30	160	35

Table 2.1. A comparison of some mechanical properties of whelk egg capsules with other protein materials. The values presented here for egg capsules are taken from the authors' studies and differ slightly from previously published work. Values for other materials are taken from the following references- wool keratin: resilience[10] all others[11], elastin[9], resilin[2] tendon collagen: resilience (preyield)[12] all others (3 month rat tail)[13], dragline silk[14]. Strain rates for egg case, keratin, collagen, and silk are all comparable, but are unavailable for elastin and resilin.

Capsule proteins undergo at least two separate post-translational processing steps in the female whelk before the mature end product is formed: soluble precursor proteins first self-assemble into an immature scaffold for the egg capsule (which possesses neither high extensibility nor self-healing properties); then this scaffold is covalently crosslinked before the egg strings are released and abandoned on the ocean floor[17]. Consequently, it is extremely difficult to extract full-length, intact protein from the mature capsule. However, precursor capsule proteins are readily extractable from the female nidamental gland and easily purified. Previous

work has determined that the precursors extracted from gland tissue are the same as the proteins present in the immature capsules[18]. Using nidamental gland derived precursors, we determined the protein masses, amino acid composition, primary amino acid sequence, secondary structure in solution, and self-assembly behavior. From these data, as well as data from previous works, potential structure-function models for these proteins are proposed.

C. Materials and Methods:

All materials were purchased from Sigma-Aldrich or Fisher Scientific unless otherwise stated.

Live whelks (*Busycotypus canaliculatus*) were purchased from the Marine Biological Laboratories (Woods Hole, MA). Females were sacrificed by immersion in a cold ethanol bath and were immediately dissected to remove the nidamental gland which was placed at -80°C. Crude extract was prepared by treating gland material with 6M urea in 5% acetic acid and 50mM TCEP to reduce disulfide bonds. Reverse phase HPLC was performed on a C-8 Brown Lee Aquapore column, 7μm (Perkin Elmer, Norwalk, CT) with a Varian Pro-Star modular HPLC system (Varian Inc, Palo Alto, CA). Crude extract and purified protein HPLC fractions were assayed via SDS-PAGE using 15% acrylamide gels.

Henceforth in the Methods section, unless otherwise stated, when a solution is described as "CP-1" it is a mixture of CP-1a and CP-1b.

M/Z was determined by matrix-assisted laser desorption and ionization with time of flight (MALDI-TOF) mass spectrometry using a PerSeptive Biosystems Voyager DE model (AB Biosystems, Foster City, CA) as described elsewhere[23].

Lyophilized HPLC fractions were hydrolyzed *in vacuo* with 6N HCl at 110°C for 24 hours. Following hydrolysis, the samples were evaporated and washed with high purity water and methanol, twice each. Amino acid compositions were determined using a Beckman Coulter 6300 Amino Acid Analyzer using ninhydrin-based post column derivatization as described elsewhere[24].

Lyophilized HPLC fractions were subjected to Edman sequencing reactions using a Porton Instruments PI 2020 as described elsewhere[25]. For CP-2 and CP-3 N-terminal Edman sequencing was also performed by transferring protein from SDS PAGE gel to Immobilon-P PVDF membrane (Qiagen, Valencia, CA), excising bands, and submitting to the Protein Facility of Iowa State University (Ames, IA) for analysis.

RNA was purified from fresh (non-frozen) nidamental gland tissue immediately following dissection with Trizol reagent following the manufacturer's instructions. Total RNA was reverse transcribed to RACE ready cDNA using the GeneRacer Kit (Invitrogen, Carlsbad, CA), primers were purchased from Integrated DNA Technologies (Coralville, IA) and PCR reagents were purchased from Novagen (Darmstadt, Germany). PCR was

carried out on an Mastercycler Gradient thermocycler (Eppendorf, Hauppauge, NY). PCR products were purified on 1.1% agarose gels, visualized by ethidium bromide, and bands were excised and purified with a Qiagen Gel Extraction Kit. PCR products were directly sequenced by Genewiz Corp (La Jolla, CA).

Far UV (260-190nm) CD measurements were carried out on an OLIS RSM 1000 spectrophotometer (OLIS, Bogart, GA) in a 0.5 mm quartz cell at 1 nm resolution. Protein solutions between were prepared in 50 mM acetate buffer, pH 4.0. 10 spectra were taken at room temperature and the results were averaged. Spectra are presented in mean residue ellipticity with molecular weight determined by MALDI-TOF, and protein concentration determined by quantitative ninhydrin based amino acid analysis (see above) as described elsewhere[26]. Secondary structure analysis was performed by the Selcon3 algorithm using the SP2 37 soluble protein standard set provided by the OLIS Globalworks software package.

Based off of the output from the Selcon3 CD analysis and the number of residues per individual protein, the number of amino acids present in each secondary structure conformation was calculated for CP-1 and CP-2. These numbers were input into translational rise per amino acid relationships for those secondary structures. These relationships are as follows: 1.5Å per residue for α-helix, 3.2Å per residue for parallel β-sheet, and 3.4Å per residue for antiparallel β-sheet. For random coil length, statistical analysis of

steric restrictions were taken into account and a characteristic ratio, C_∞, of 9.0 was used as described by Creighton (1993)[27]. This results in a calculation dictated by the following equation

$$\langle r^2 \rangle_o^{1/2} = (130n)^{1/2} \quad (1)$$

Wherein the square root of the root mean square is taken as length.

These relationships are based on the assumption that the secondary structures are fixed at their ends in a scaffold versus tumbling freely in solution which is the case in the fully processed egg capsule material. Maximum end to end protein length takes the sum of the lengths of secondary structures and assumes no folding back within the protein.

Small aliquots of the protein samples used for CD measurements were diluted 1:5 v/v in 50 mM acetate buffer, pH 4.0. 5 mL of each solution were applied to Formar and Carbon Type-B coated Copper grids (Ted Pella Inc. Redding, CA) and allowed to dry. Samples were then washed with nanopure water, fixed with 2% gluteralydehyde and paraformaldehyde for 2 hours at room temperature, washed again, stained with uranyl acetate for 15 minutes, and then washed a final time. Imaging was performed using a FEI Tecnai G2 Sphera Microscope, 200 kV (FEI, Hillsboro, OR). Minimal currents were used to avoid significant beam damage.

***D. Results*:**

Consistent with previous findings SDS PAGE analysis of nidamental gland crude extract indicates a family of proteins around 50kD with three distinct bands: CP-1 the fastest migrating, CP-2 the intermediate, and CP-3 the slowest migrating. Using RP HPLC all three individual bands in this family can be purified from the extract (Fig 2.2) with CP-1 eluting at shorter retention times, CP-3 coming off in the middle, and CP-2 the last to elute.

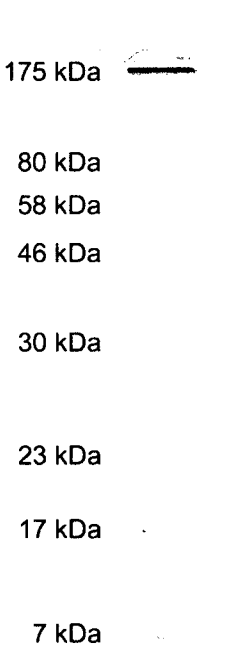

Figure 2.2. SDS-PAGE of Bc-cps purified from nidamental gland extract. Lanes 1, 2, 3, and 4 are, respectively, unpurified gland extract, purified CP-1, purified CP-2, and purified CP-3. Gel is 15% acrylamide and was run at constant current of 15mA.

MALDI-TOF mass spectrometry indicates the masses to be 47.4, 51.4, and 52.0kD (Fig 2.3). The proteins have amino acid compositions that are similar to one another as determined by ninhydrin based analysis and are also similar in composition to hard α-keratins (both being rich in Asx, Glx, and Leu), but with the notable differences that α-keratins have high disulfide content whereas the CPs have almost none, and CPs having much higher lysine content than keratins[28] (Table 2.2).

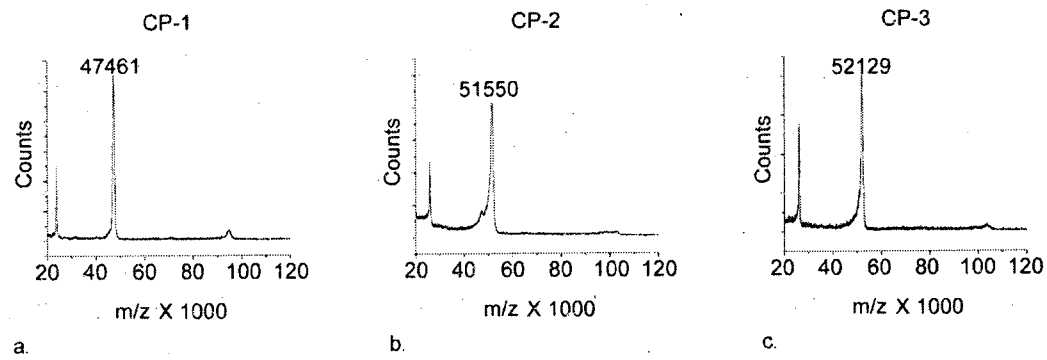

Figure 2.3. MALDI-TOF mass spectrum of purified Bc-cps. Figs a), b), and c) are CP-1, CP-2, and CP-3 respectively. Peaks from left to right are $[M + 2H]^{2+}$, $[M + H]^{+}$, and $[2M + H]^{+}$. Delayed extraction (200 ns) in positive ion mode with an accelerating voltage of 25 000 V, a grid voltage at 93%, and a guide wire voltage at 0.1%. The spectrum represents an average of 254 scans.

N-terminal amino acid sequence of the first 10 residues was obtained by automated Edman reaction from the HPLC purified fractions. CP-1 has a unique N-terminal sequence where as CP-2 and CP-3 share the first 10 amino acids. This sequence identity for CP-2 and CP-3 was verified by repeating the Edman reaction on SDS PAGE membrane transfers of crude extract.

Amino Acid	CP-1	CP-2	CP-3	Bulk Egg Capsule	α-Keratin[a]
Ala	9.0	6.4	6.3	7.5	7.7
Arg	4.7	4.2	4.1	3.9	7.9
Asx	10.1	10.8	10.7	13.5	9.6
Cys	0.0	0.0	0.0	0.0	6.0
Glx	18.6	16.1	16.7	15.6	16.9
Gly	5.1	5.9	6.3	8.0	5.2
His	2.2	3.4	3.7	1.5	0.6
Ile	5.9	5.4	6.1	4.9	3.8
Leu	9.5	9.1	8.6	9.5	10.2
Lys	12.0	12.2	12.6	9.4	4.1
Met	0.0	0.0	0.0	0.8	0.6
Phe	2.4	4.1	5.6	4.6	2.0
Pro	0.9	2.9	1.6	1.9	3.3
Ser	7.2	7.9	7.5	8.0	8.1
Thr	5.0	4.7	3.5	5.0	4.8
Tyr	0.3	0.5	0.0	0.4	2.7
Val	7.1	6.4	6.7	5.5	6.4
Total	100	100	100	100	100

Table 2.2. Amino acid composition of purified Bc-cps in mole percent (residues per 100 residues). Values for α-keratin are taken from J. Vincent (1990)[28].

```
                    10         20         30         40         50
Bc-cp 1a     MKVQLLLALI VLMQPLRGVF GDLDFDVPTE AAKKGRGFGD FKTSSPSDLK
Bc-cp 1b     MKVQLLLALI VLMQPLRGVF GALDFDVTKE AAKKGRGFGD FKTSSPSDLK
Bc-cp 2      MKLCVVLALV LLTREALGLF QGFNFGKKDG PFNLLHKHLD ILGSGVDSAL
Bc-cp 3      MKLCVVLALV LLTREALGLF QGFNFGKKDG PFNLLHKHLD ILGSGVDSAL

Bc-cp 1a     GLGQVEAKVK DIIVHTGKLV DIMTGNSRRQ DFFLDLCEKV AESQKVVKDS  100
Bc-cp 1b     GLGQVEAKVK DIIVHTGKLV DIMTGNSRRQ DFFLDLCEKV AESQKVVQNS
Bc-cp 2      HLAAFMTDQH REFSKSLDNV WKNQDKIVED VSTAESIASR VLQGTKDILN
Bc-cp 3      HLAAFMTDQH REFSKSLDNV WKNQDKIVED VSTAESIASR VLQGTKDILN

Bc-cp 1a     LKKVIETSTA ADSNTAQIKS NQDAMLKNQE GILNLVSGQH KITRKNIAQA  150
Bc-cp 1b     LRKVIETSTA AESNTAQIKS NQDAMLKNQE GILNLVLGQH KITRKNIAQA
Bc-cp 2      KQTQIFKGQS SIQQLINNEH RVTREQVADL QKNLQNNIDQ MGNNQKSILI
Bc-cp 3      KQTQIFKGQS SIQQLINNEH RVTREQVADL QKNLQNNIDQ MGNNQKSILI

Bc-cp 1a     ETTLVNGMGK LIESQGVIIS SLQKSEDFLA AGFNRIVEAE RRTQVLNSQV  200
Bc-cp 1b     ETTLVNGMQK LIQTQGDIDS SLQKSGDFLA AGFNRIVEAE RQTQVLNSQV
Bc-cp 2      KIAQGRSKAG NFFEQFLKVK AQTDNQVRVL LKTVLSSQAA NAKGQSRILE
Bc-cp 3      KIAQGRSKAG NFFEQFLKVK AQTDNQVRVL LKTVLSSQAA NAKGQSRILE

Bc-cp 1a     LKAVEESAAA NALGQANITA ELKDIRQETV EALNKALDQQ EIILNQISTA  250
Bc-cp 1b     LKAVEESAAA NALGQANITA ELKDIRQETV EALNKALDQQ ENTLNQISTA
Bc-cp 2      VVFSLRKDVA DRLSALSQSQ GTVLKRLASS QKNVENSIDK VIKQQAVIAN
Bc-cp 3      VVFSLRKDVA DRLSALSQSQ GTVLKRLASS QKNVENSIDK VIKQQAVIAN

Bc-cp 1a     EKSQLSKLDQ VQSNLLDILK LVGQSQKAVQ QSIHEANAIE RETQSLVKVS  300
Bc-cp 1b     EKSQLSKLDQ VQSNLLDILK LVGQSQKAVQ QSIHEANAIE RETQSLVKVS
Bc-cp 2      AVVVSQNAEL ADLEELKSEQ GKTQVRVKES TSAILGDISD IRNNEAGTQH
Bc-cp 3      AVVVSQNAEL ADLEELKSEQ GKTQVRVKES TSAILGDISD IRNNEAGTQH

Bc-cp 1a     QKVIQKELGE HKKDQKETQH LAKKCLENTK CDLDKVNDAL VQLVKLNTAS  350
Bc-cp 1b     QKVIQKELGE HKKDQKETQH LAKKCLENTK CDLDKVNDAL VQLVKLNTAS
Bc-cp 2      ILHKCKGSNC DPTKTINLIK HILKQVEEIE MEHKEHIHEI LAAESKTFSE
Bc-cp 3      ILHKCKGSNC DPTKTINLIK HILKQVEEIE MEHKEHIHEI LAAESKTFSE

Bc-cp 1a     RDSIREGLKE IRSKQSATQG RVKSTEKTVI KAIGAGFNTI NRNAAALVER  400
Bc-cp 1b     RDSIREGLKE IRSKQSATQG RVKSTEKTVI KAIGAGFNAI NRNAAALVER
Bc-cp 2      VGELEQNVLE VFSSNAAGTI HTLEDVENRL TDFLEQNEGI IGDFGREVHT
Bc-cp 3      VGELEQNVLE VFSSNAAGTI HTLEDVENRL TDFLEQNEGI IGDFGREVHT

Bc-cp 1a     LESSRSQSQN QFKVIEKNIR DTRNSQENAR GLIHQIHSII NKLLKH      450
Bc-cp 1b     LESSRSQSQN QFKVIEKNIR DTRHSQENAR GLIHEIHSII NKLLKH
Bc-cp 2      LEQIQESIEH ELKKLLHKLK DLHFPKGGKK KSDGFGKKFD FGKKDFDFDK
Bc-cp 3      LEQIQESIEH ELKKLLHKLK DLHFPKGGKK KSDGFGKKFD FGKKDFDFDK

Bc-cp 2      KDFVKKDFSF HKKDSDFGKK SFDFP                            500
Bc-cp 3      KDFVKKDFSF HKKDSDFGKK SFDFPRFKF
```

Figure 2.4. Complete amino acid sequence of Bc-cps 1a, 1b, 2, and 3 as deduced from cDNA. Red text at N-terminus represents signal peptide sequence. Green sequence represents heptad repeat regions that are predicted coiled-coils from the Lupas method using MTIDK matrix and scoring values >0.8.

From the partial N-terminal sequence, degenerate primers were designed for RT-PCR. First 5' RACE was performed to give sequence of the 5' untranslated region, then non-degenerate primers were designed for 3' RACE to amplify full-length transcripts. 3' RACE of the CP-1 cDNA transcript produced two PCR products, one at ~1500 bp and a second at ~2400 bp, whereas the reaction for the CP-2/CP-3 cDNA transcript produced only one PCR product at ~2400 bp (supplementary data). These three PCR products were gel excised and sequenced directly without cloning.

All three transcripts contain an open reading frame, which translates to a full length gene with start methionine and termination codon. Despite the difference in the size of the PCR products, the two CP-1 transcripts both translate to proteins of identical length (446 amino acids) and have 95% sequence identity. Hereafter these variants are referred to as CP-1a and CP-1b. The transcript for CP-2 and CP-3 translates to a single 479 amino acid protein (Fig 2.4). The fact that this transcript is responsible for the production of two different proteins can be explained by the potential of early termination in the translation process. Since sequencing was performed directly on gel purified PCR products without cloning, multiple variants may be present, resulting in different nucleotide sequences at the same position in the transcript. The primary codon at position 476 is AGA (arginine), however, in the raw sequencing chromatogram there is a lesser, but still significant, thymine peak in the first position. This would result in TGA, a

termination codon, which reduces the length of the protein by four amino acids with a combined weight of 578.6 daltons. This accounts for the mass difference observed between CP-2 and CP-3. The computed masses (not including signal peptides) of the cDNA–deduced protein sequences are consistent with the actual protein masses observed by MALDI-TOF mass spectrometry. Amino acid compositions of the purified proteins also agree with the compositions predicted from cDNA–deduced protein sequences (Table 2.3).

Amino	Bc-cp 1a		Bc-cp 1b		Bc-cp 2		Bc-cp 3	
Acid	Observed	Predicted	Observed	Predicted	Observed	Predicted	Observed	Predicted
Ala	9.0	8.5	9.0	8.9	6.4	5.7	6.3	5.6
Arg	4.7	4.5	4.7	4.5	4.2	3.1	4.1	3.3
Asx	10.1	11.5	10.1	11.6	10.8	12.9	10.7	11.8
Cys	0.0	0.7	0.0	0.7	0.0	0.4	0.0	0.4
Glx	18.6	16.2	18.6	16.9	16.1	14.8	16.7	14.8
Gly	5.1	4.9	5.1	4.9	5.9	5.9	6.3	5.9
His	2.2	1.9	2.2	2.1	3.4	3.7	3.7	3.7
Ile	5.9	7.5	5.9	6.8	5.4	6.6	6.1	6.5
Leu	9.5	9.6	9.5	9.9	9.1	9.4	8.6	9.3
Lys	12.0	10.6	12.0	10.4	12.2	11.4	12.6	11.5
Met	0.0	0.7	0.0	0.7	0.0	0.7	0.0	0.7
Phe	2.4	2.1	2.4	2.1	4.1	5.9	5.6	6.3
Pro	0.9	0.5	0.9	0.2	2.9	0.9	1.6	0.9
Ser	7.2	8.2	7.2	7.8	7.9	7.9	7.5	8.8
Thr	5.0	5.4	5.0	5.6	4.7	3.9	3.5	3.9
Trp	-	0.0	-	0.0	-	0.2	-	0.2
Tyr	0.3	0.0	0.3	0.0	0.5	0.0	0.0	0.0
Val	7.1	7.1	7.1	6.8	6.4	6.6	6.7	6.5
Total	100	100	100	100	100	100	100	100

Mass	Bc-cp 1a		Bc-cp 1b		Bc-cp 2		Bc-cp 3	
	Observed	Predicted	Observed	Predicted	Observed	Predicted	Observed	Predicted
m/z	47461	46880	47461	46962	51550	51437	52129	52016

Table 2.3. Comparison of amino acid composition and protein mass observed from experimental data (via ninhydrin based analysis and MALDI-TOF mass spec respectively), and predicted values derived from translated cDNA sequence.

In addition, all three transcripts code for a signal peptide sequence, indicating that these proteins are secreted via secretory vesicle pathways. Cleavage between G-21 and D/A-22 for the two CP-1 variants and between G-18 and L-19 in CP-2/CP-3 is predicted by "SIGNALP" (EXPASY) and matches the N-terminal sequence derived by Edman sequencing. BLAST searches (NCBI) resulted in no matches with E values of less than 10^{-9} for CP-1a and CP-1b and 10^{-5} for CP-2 and CP-3 in the database of sequences from eukaryotic species, indicating that the capsule proteins are not strongly homologous to any known eukaryotic proteins.

Far-ultraviolet (UV) CD spectroscopy was used to examine the secondary structure of CP-1 and CP-2 in solution. CP-3 was unable to be purified in large enough quantities to perform CD on. Lyophilized HPLC purified capsule proteins were resuspended in 50mM acetate buffer pH 4.0 (lyophilized proteins do not resolubilize at more neutral pH values), and spectra collected at room temperature. The CD spectra of both CP-1 and CP-2 (Fig 2.5) were characteristic for an single coil α-helical structure, exhibiting minima at 208 and 222nm and a $[\theta]_{222}:[\theta]_{208}$ ratio of <1 [29]. Analysis by the Selcon3 algorithm to derive secondary structure composition was performed and the results tabulated (Table 2.4). Selcon3 was chosen over

other algorithms because it most accurately predicted the secondary structure composition of human fibrinogen, a soluble protein trimer with coiled-coil structures (data not shown).

CD was also performed on a 1:1 molar concentration mixture of CP-1 and CP-2. This also produced similar α-helical spectra with a $[\theta]_{222}$:$[\theta]_{208}$ ratio of <1 which would indicate a single coil conformation (data not shown).

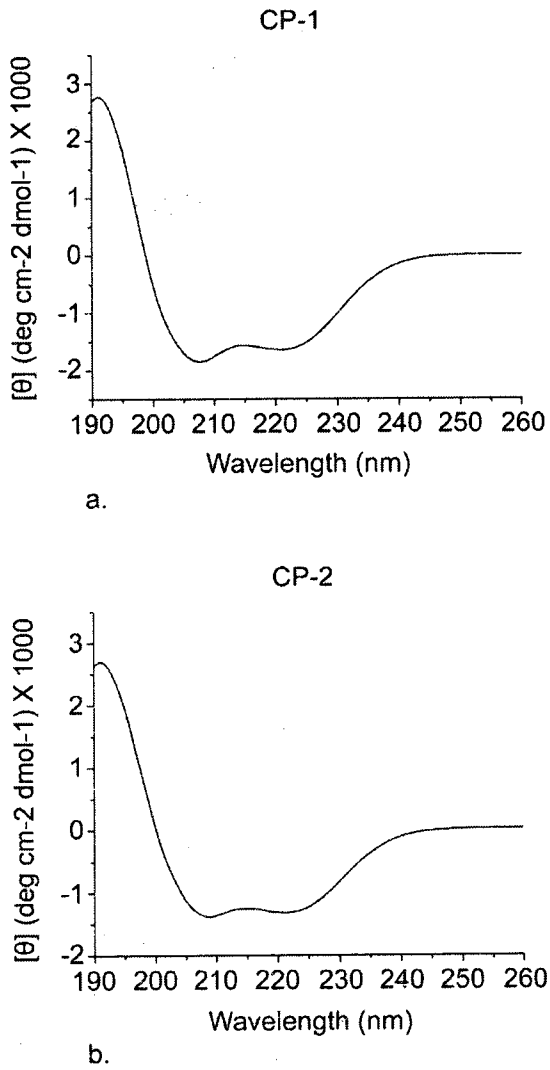

Figure 2.5. Circular dichroism spectra of purified Bc-cps. Figs a) and b) are CP-1 and CP-2 respectively. Bc-cp 3 was unable to be purified in sufficient quantities to measure with CD. Minima at 208nm and 222nm and a [θ]222:[θ]208 ratio of <1 are representative of single coil α-helix. The spectrum represents an average of 10 scans.

Purified protein solutions, upon the evaporation of solute, self-assemble into anisotropic nano-filaments < 20 nm in diameter, which bundle into fibers that are 200-500 nm across (Fig 2.6). This is similar in size to the fibers observed in mature egg capsules[5].

	α-helix	β-sheet	Random coil
Bc-cp1	36%	15%	49%
Bc-cp2	42%	15%	43%

Table 2.4. Protein secondary structure composition of Bc-cp1 and Bc-cp2 as predicted by the Selcon3 algorithm as provided by the Olis GlobalWorks CD analysis software. The SP2 set of 37 soluble proteins was used as the reference standard. Values are presented in percent amino acids in the secondary structure compared to total amino acids in the protein.

Both solutions of CP-1 and CP-2 exhibit this behavior and yield filaments that are the same size. A 1:1 molar concentration mixture of the two proteins also produces filaments that are identical to those from the homogeneous solutions.

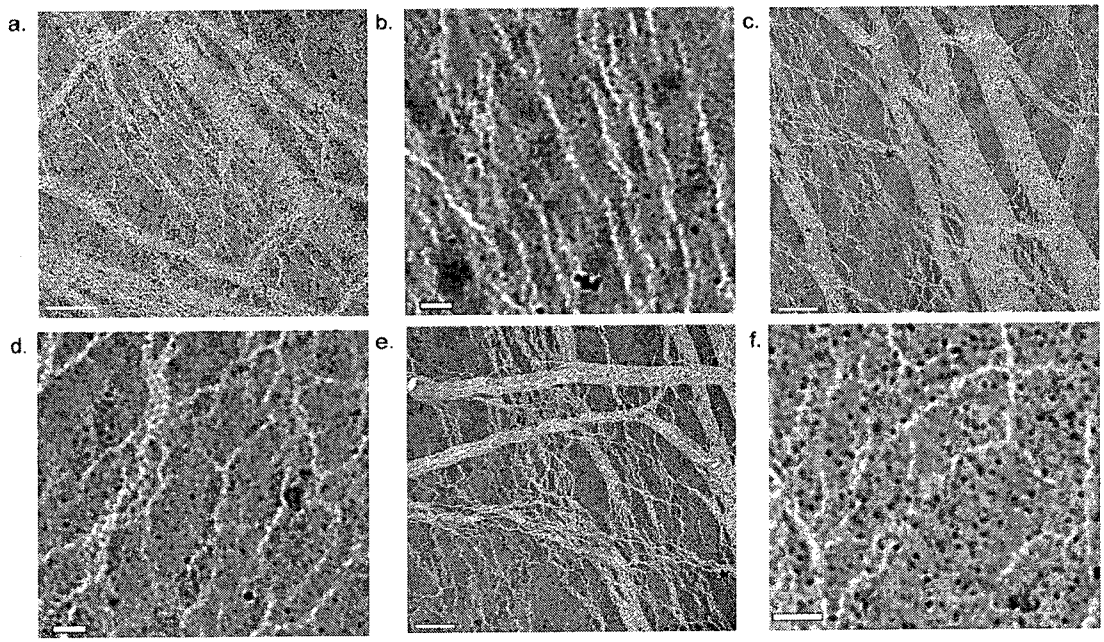

Figure 2.6. Transmission electron micrographs of purified capsule proteins. Figs a) and b) are of CP-1 only, Figs c) and d) are of CP-2 only, and Figs e) and f) are of a 1:1 molar ratio of the two. In all three preparations proteins form sub 20nm diameter filaments which bundle into 200 - 500nm diameter fibers. Scale bars are 500nm for a), c), and e) and 100nm for b), d), and f).

***E. Discussion*:**

α-Helical proteins are building blocks of diverse extra-organismal load-bearing scaffolds. The hard keratins found in horns, hair, and hooves[10] and hagfish slime[30,31] are familiar and esoteric examples, respectively. Unlike the proteinaceous egg capsules of other oviparous species, such as dogfish and spiders which produce collagen and silk based capsule proteins respectively [32,33], whelk egg capsule wall is included among the α-helical biomaterials. Although whelk egg capsule wall shares numerous similarities with the other members of this group, it also exhibits rather unique mechanical and biochemical properties.

Like intermediate filament (IF) based materials under uniaxial tension, capsule wall initially exhibits a high initial Young's modulus (Table 2.1). However, at 5% engineering strain, a mechanical yield occurs followed by plastic flow to nearly 65%[5,15]. In hard keratins and hagfish slimes, as well as in whelk egg capsule wall, it has been shown that the coordinated rupturing of the hydrogen bonds that hold together the α-helices allows for the elongation of protein fibers without fracturing the material as a whole. The α-helices unravel as the materials stretches through the post-yield region of the stress-strain curve, and once all of the α-helices are fully extended and lock into β-sheets with neighboring protein chains, the material re-stiffens as other structural interactions contribute to the tensile mechanics. This phenomenon is responsible for the high strain energy capacities[10,22,31] (Table

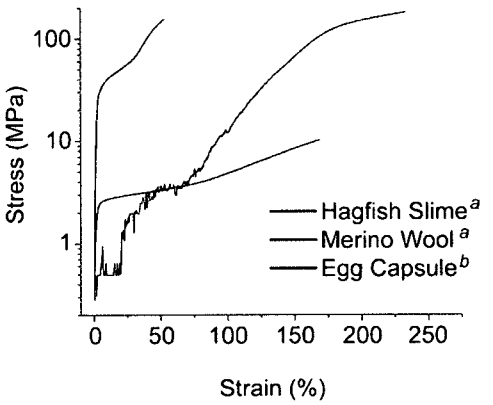

Figure 2.7. Engineering stress vs strain curves for whelk egg capsule material, hagfish slime, and wool. Values for hagfish slime and wool are taken from Fudge and Gosline (2004)[11].

2.1, Fig 2.7). However, it is the extensibility and recoverability of whelk capsule wall that sets it apart from these other materials. Although not quite as extensible as hagfish slime, capsule wall has the ability to recover its original conformation when the load is removed whereas hagfish slime remains extended even after unloading. Hydrated α-keratins also relax slowly, dissipating energy, but are not as extensible as the whelk capsule wall. Most remarkable is the capsule wall's ability to rapidly and completely recover initial stiffness following multiple cycles of tensile strain. Biochemical differences between these materials may help explain their differences in mechanical properties.

Proteins comprise over 90% of the dry weight in whelk egg capsule wall[5,15] and the CPs characterized in this work represent the most abundant of these[18]. The amino acid composition is consistent between both individual CPs as well as the bulk capsule wall material and is predominantly made up of helix forming and helix indifferent residues. The composition is also very similar to the filament component of hard keratins with the major difference coming in the cystine and lysine contents. Cystine is the primary crosslinking

molecule in keratins[10], and previous studies have suggested lysine as a potential crosslinker in capsule walls[34,35].

In agreement with the helix favoring amino acid composition, circular dichroism data presented here indicate that these precursors are strongly α-helical in solution. Very probably, these are the same proteins that contribute to the anisotropic α-helix x-ray scattering patterns and, hence, the α-helix ↔ β-sheet transition and associated mechanical properties reported earlier. Using the composition results from Selcon3 analysis geometric predictions of CP dimensions have been made using calculations detailed in the Methods section of this paper.

The maximum end-to-end distances for CP-1 and CP-2 in a relaxed state are 50.3 nm and 56.4 nm, respectively. This assumes that the intra protein β-sheet domains are antiparallel and are folded over on themselves to create this secondary structure. When egg capsule material is stretched α-helices are unraveled and β-sheets form between neighboring proteins. If these newly formed β-sheets are parallel in conformation, the end-to-end lengths increase to 76.3 nm and 89.1 nm, resulting in a 51.7% and 58.0% increase in end-to-end length. If the β-sheets are antiparallel, the lengths would increase to 79.3 nm and 93.0 nm respectively, causing a 57.7% and 64.9% gain respectively (Fig 2.8a). All of these values are close to the ~60% post-yield flow strain observed in bulk egg capsule material and further support the hypothesis that this is the result of an α-helix ↔ β-sheet

transition. Potential inter and intra-protein crosslinks in the random coil domains of the proteins would prevent unfolding during extension of the bulk material (Fig 2.8b). This is also hypothesized in the case of hard keratin materials, where disulfide linkages prevent the unraveling of the 1B and 2B helical domains[22].

Like IF materials, x-ray scattering studies have suggested that the α-helical filaments of whelk capsule walls are in a coiled-coil motif[5]. This tertiary structure is the result of a heptad repeat (amino acids A through G) in which apolar residues at positions A and D form a hydrophobic band that brings the two helices together, and the flanking charged residues E and G provide electrostatic stabilization[27]. Sequence analysis via the Lupas method[36] indicates several short patches of heptad repeat domains in each of the four capsule proteins (Fig 2.3). Additional analysis by Berger's method[37], suggests that these areas are more likely to form coiled-coil trimers in contrast to the dimers found in hagfish slime and keratin materials (Fig 2.8b).

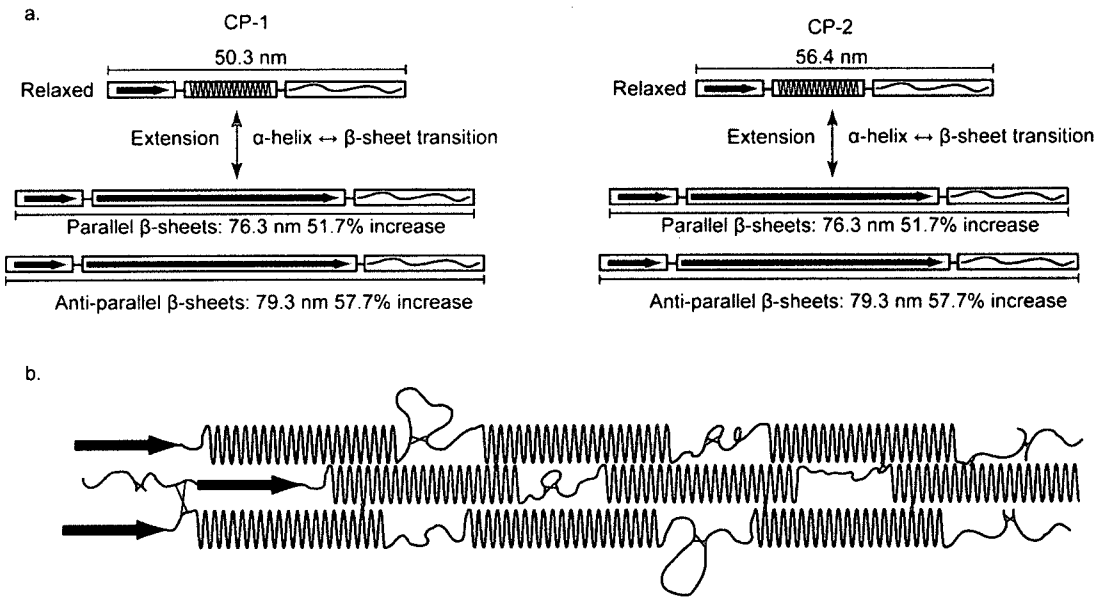

Figure 2.8. Schematics for the structure function model of both individual proteins, as well as predicted protein trimers. Fig a) shows single protein α-helical domains unraveling into β-sheets during extension. Secondary structures are presented in singular domains for clarity. The random coil and β-sheet domains in the relaxed protein remain unchanged under extension. Depending on whether the α-helices transition into parallel or antiparallel β-sheets, which is unknown as of this point, the increases in end to end length of the proteins are slightly different. Regardless of the β-sheet conformation, the percent increase in length of the individual proteins is close to the ~60% increase in flow strain that is hypothesized to be the result of an α-helix ↔ β-sheet transition in the bulk material. Fig b) shows a model for the capsule protein multi-domained coiled-coil trimer. Inter and intra-protein crosslinks prevent random coil regions from extending under tension. End to end crosslinks connect trimers to each other to maintain a continuous covalently linked protein

These heptad repeat domains are comparatively small, between 22 and 34 residues long for CPs 1a and 1b and between 15 and 30 residues long for CPs 2 and 3, and are separated by long stretches of non multi-coil sequence. This is far shorter than the >100 residue coiled-coil domains commonly found in IFs[38]. Additionally, the circular dichroism data suggest that in solution, purified capsule proteins preferentially adopt single coils rather than coiled-coils as indicated by the $[\theta]_{222}$:$[\theta]_{208}$ ratio of <1. Either the quantity of coiled-coil helices is too small compared to the single coiled

helices to shift the $[\theta]_{222}$:$[\theta]_{208}$ ratio from less than 1 to greater than 1, or the transition from single to multi-coils occurs during filament assembly.

During the egg laying process, egg capsule proteins first assemble into filaments in the immature egg capsule before they are crosslinked[18]. However, as with purified IF proteins, where it is postulated that changes in the pH and/or ionic strength of the solution cause electrostatic interactions in critical amino acid side-chains[39,40], egg capsule filament assembly can occur *in vitro* without the aid of additional accessory proteins/molecules. Based on the similar morphologies of the fibers created *in vitro* observed here by TEM, and those of the naturally produced fibers observed previously by SEM[5], purified capsule proteins form the filaments that the mature egg capsule material is composed of.

Intermediate filaments that form heterodimeric coiled-coil structures such as keratins *in vivo*, will not form filaments *in vitro* under any conditions unless both proteins are present in the solution[40]. It is therefore likely that the filaments formed in whelk capsule wall are not heterogeneous, as purified homogenous solutions of CP-1 and CP-2 are capable of forming filaments on their own. However, as both CPs form assemble into filaments of identical size, the exact roles of the two different proteins and whether both are necessary to form egg capsules *in vivo* remain to be determined. Proteins from IF based materials form coiled-coil tetramers, and sometimes octamers, in solution before assembling into filaments[39,40]. A more thorough

investigation into the self-assembly of capsule proteins will be necessary to determine whether they also form intermediate multimers in solution prior to filament assembly.

After assembly, crosslinking is the final processing step for the egg capsules before they are deposited on the ocean floor. It is only after crosslinking that the egg capsules exhibit the robust mechanical properties of the mature capsule that have been described. Previous work on both in the egg capsule material itself[34] as well as in the gland where this final processing step occurs[35] have suggested that these crosslinks are lysine derived. As mentioned above, all of the Bc-cps have high quantities of lysine in the amino acid composition. In CPs 1a and 1b, the distribution of lysine is fairly constant throughout the primary sequence, with some patches of higher density. In CPs 2 and 3, there is a very high proportion of lysine in the C-terminal region. CP-2 and CP-3 have 53 and 54 lysines in 475 and 479 amino acids respectively, but 20 and 21 of those lysines between residue 413 and the C-terminus (Fig 2.9). This region of the primary sequence seems a likely position for end-to-end crosslinking of these capsule proteins. However, until a chemical structure for the crosslink is determined, nothing definitive can be said about its location in the primary sequence of any of the capsule proteins.

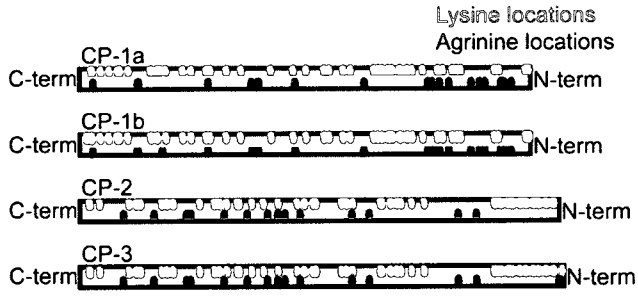

Figure 2.9. Distribution of lysine and arginine residues throughout the primary sequence of capsule proteins. Lysine is a suspected crosslinking amino acid in capsule wall material. It is shown here that there are distinct clusters of not only lysine but also arginine, which preliminary data suggests may also contribute to crosslinking, in each of the four capsule protein sequences.

Although there are striking similarities between whelk egg capsule wall and IF materials in terms of mechanics, amino acid composition of the precursor proteins, and the ability to self-assemble into filaments *in vitro* with no accessory molecules needed, primary sequence analysis, indicates that the capsule proteins are very different from intermediate filament proteins. An NCBI BLAST analysis of similar protein sequences results in no eukaryotic proteins in the database with E values of less than 10^{-9} for CP-1a and CP-1b, less than 10^{-5} for CP-2 and CP-3, and no homology to known IF proteins at all. Additionally each of the CPs contains a signal peptide sequence at the N-terminus. This short sequence, 21 residues long in CP-1a and CP-1b and 18 residues long in CP-2 and CP-3, indicates that the capsule proteins are exported from the cell via a controlled vesicle based secretory pathway. This is in direct contrast to hard keratins and hagfish slime both of which reach the extra cellular region by the programmed death of the specialized cells in which they are accumulated[41,42]. Based on the ClustalW2 alignment program[43] of the primary sequence and the strong suggestion of coiled coil trimers, the

capsule proteins may actually be more closely related to the fibrinogen family, an extracellular matrix protein involved in blood clotting and wound response, than it is to either α-keratin or hagfish slime filament proteins (data not shown).

There remain additional unanswered questions regarding whelk egg capsule wall processing and structure. The mature material is over 90% protein by dry weight, but the composition of the remaining mass is unknown. Furthermore, SDS PAGE of immature capsules and crude nidamental gland extract indicate that traces of additional proteins are present in this material, although in far lesser quantities than Bc-cp 1-3 [18], and the structure and function of these needs to be investigated. A potential role for these proteins involves composite matrix components. Hard keratin materials have globular, high-sulfur content matrix proteins which contribute significantly to mechanical properties[10,22], whereas hagfish slime does not[11]. Once these proteins are fully characterized, it will be possible to develop a model for how they interact with the CPs characterized here, and of the structure/function of the egg capsule material as a whole.

F. Conclusions:

In the present study the precursors of the primary structural proteins for whelk egg capsules were purified and characterized. The amino acid composition is very similar to intermediate filament proteins with the

exception of lysine and cystine, which are significantly higher in egg capsule walls and in IFs respectively. Circular dichroism and TEM studies indicate that, much like intermediate filament proteins, these precursors are strongly α-helical in solution and are capable of self-assembling into filaments on their own without the assistance of accessory molecules.

Using reverse genetics, the primary amino acid sequence for four variants was deduced from cDNA. The primary sequences are very unique as BLAST homology searches do not produce any significant matches to known proteins, including intermediate filaments. Analysis of these sequences indicates that the proteins are likely to form coiled-coil trimers, which is consistent with previous x-ray scattering studies. Furthermore, the end regions of the sequence are dense with lysine and arginine, both of which are suspected to play a role in the covalent crosslinking of egg capsule fibers.

From this data, as well as previous mechanical and structural studies, a structure-function model for the single protein unit of this material is proposed. In this model, the predicted increase in contour length of proteins due to an α-helix ↔ β-sheet structure transition ranges from 51.7% to 64.9%. This change corresponds well to the increase in overall length of the egg capsule material during the post-yield region of extension. This is the region in which the flow modulus decreases dramatically before restiffening later and is where the α-helix ↔ β-sheet transition is shown to take place.

This model further supports Flory's theory on non-entropic elasticity in proteins.

G. Accession Numbers:

The sequence data of Bc-cp1a, Bc-cp1b, Bc-cp2, and Bc-cp3 have been deposited in the NCBI database with the accession numbers GU205809, GU205810, GU205811, and GU205812 respectively.

H. Acknowledgments:

The authors would like to thank Krystyna Brzezinska and James R Neilson (Materials Research Lab, UC Santa Barbara) for assistance with the CD spectrometery and TEM imaging respectively; Douglas Fudge (University of Guelph, Ontario, Canada) for providing tensile data for Merino wool and Hagfish slime; Rebekah Ashley (Molecular Cellular and Developmental Biology, UC Santa Barbara) for assistance with cDNA sequencing; and Robert Shadwick (University of British Columbia, Vancouver, Canada) for insightful advice and communications through out the project.

This work was supported by a University of California Biotechnology Research and Education Program (UC BREP) Graduate Research and Education in Adaptive Biotechnology (GREAT) grant (#2007-02) and NIH grant #R01DE018468 (JHW). The work made use of MRL Central Facilities

supported by the MRSEC program of the NSF under Award # DMR05-20415.

I. References:

1. Urry, D. W., Hugel, T., Seitz, M., H. Gaub, E., Sheiba, L., Dea, J., Xu, J. & Parker, T. (2002). Elastin: a representative ideal protein elastomer. *Phil. Trans. R. Soc. Lond [Biol].* 357, 169-184.
2. Weis-Fogh, T. (1961). Molecular interpretation of the elasticity of resilin, a rubber- like protein. *J. Mol. Biol.* 3, 648-667.
3. Alexander, R. M. (1966). Rubber-like properties of the inner hinge-ligament of *Pectinidae*. *J. Exp. Biol.* 44,119-130.
4. Flory, P. (1956). Theory of Elastic Mechanisms in Fibrous Proteins. *J. Am. Chem. Soc.* 78, 5222-5235.
5. Miserez, A., Wasko, S. S., Carpenter C. F. & Waite, J. H. (2009). Non-entropic and reversible long-range deformation of an encapsulating bioelastomer. *Nat. Mater.* 8, 910-916.
6. Denny, M. W. (1988). *Biology and the Mechanics of the Wave-Swept Environment,* Princeton Univ. Press, Princeton.
7. Magalhaes, H. (1948). An Ecological Study of Snails of the Genus *Busycon* at Beaufort, North Carolina. *Ecol. Monograph.* 18, 377-409.
8. Rawlings, T. A. (1999). Adaptations to physical stresses in the intertidal zone: The egg capsules of neogastropod mollusks. *Am. Zool.* 39, 230-243.
9. Aaron, B. B. & Gosline, J. M. (1981). Elastin as a random-network elastomer: a mechanical and optical analysis of single elastin fibers. *Biopolymers.* 20, 1247-1260.
10. Feughelman, M. (1997). *Mechanical Properties and Structure of Alpha-Keratin Fibres: Wool, Human Hair, and Related Fibres.* UNSW Press, Sydney.
11. Fudge, D. & Gosline, J. (2004). Molecular design of the α-keratin composite: insights from a matrix-free model, hagfish slime threads. *Proc. R. S. Lond [Biol].* 271, 291-299.
12. Pollock, C. M. & Shadwick, R. E. (1994). Relationship between body mass and biomechanical properties of limb tendons of adult mammals. *Regul. Integrative Comp. Physiol.* 35, R1016-R1021.
13. Kastelic, J & Baer, E. (1980). Deformation in Tendon Collagen. *Symp. Soc. Exp. Biol.* 34, 397-435.
14. Denny, M. (1976). The physical properties of spider's silk and their role in the design of orb webs. *J. Exp. Biol.* 65, 483-506.
15. Rapoport, H. S. & Shadwick, R. E. (2002). Mechanical characterization of an unusual elastic biomaterial from the egg capsules of marine snails (*Busycon* spp.). *Biomacromolecules.* 3, 42-50.
16. Lendlein, A. & Kelch, S. (2002) Shape-memory polymers. *Angew. Chem. Int. Ed. Engl.* 41, 2035-57
17. Rapoport, H. & Shadwick, R. (2007). Reversibly labile, sclerotization-induced elastic properties in a keratin analog from marine snails: whelk egg capsule biopolymer (WECB). *J. Exp. Biol.* 210, 12-26.
18. Rapoport, H. S. (2003) Biomechanics, Biochemistry, and Molecular Biology of a Molluscan Scleroprotein Elastomer: Whelk Egg Capsules. PhD Thesis, University of California San Diego
19. Flower, N. E., Geddes, A. J. & Rudall, K. M. (1969). Ultrastructure of the fibrous protein from the egg capsules of the whelk *Buccinum undatum*. *J. Ultrastruct. Res.* 26, 262-273.
20. Goldsmith, L. A. & Lindberg K. A. (1978). Nidamental Gland Precursor of the Egg Capsule Protein of the Gastropod Mollusc *Busycon carica*. *Comp. Biochem. Physiol. B.* 59B, 133-138.
21. Bendit, E. G. (1957) The α-β Transformation in Keratin. *Nature.* 179, 535.

22. Hearle, J. W. S. (2000). A critical review of the structural mechanics of wool and hair fibres. *Int. J. Biol. Macromol.* 27, 123-138.
23. Vincent, J. (1990). *Structural Biomaterials* (revised ed). Princeton: Princeton University Press, Princeton.
24. Zhou, N. E., Zhu, B. Y., Kay, C. M. & Hodges, R. S. (1992). The two-stranded alpha- helical coiled-coil is an ideal model for studying protein stability and subunit interactions. *Biopolymers.* 32, 419-426.
25. Koch, E. A., Spitzer, R. H., Pithawalla, R. B. & Parry, D. A. D. (1994). An Unusual Intermediate Filament Subunit From the Cytoskeletal Biopolymer Released Extracellularly Into Sea Water by the Primitive Hagfish (*Eptatretus stouti*). *J. Cell Sci.* 107, 3133-3144.
26. Fudge, D., Gardner, K. H., Forsyth, V. T. & Riekel, C. (2003). The Mechanical Properties of Hydrated Intermediate Filaments: Insights from Hagfish Slime Threads. *Biophys. J.* 85, 2015-2027.
27. Gathercole, L. J., Atkins, E. D. & Goldbeck-Wood, E. (1993). Molecular Bending and Networks in a Basement Membrane-like Collagen: Packing in Dogfish Egg Capsule Collagen. *Int. J. Biol. Macromol.* 15, 81-88.
28. Hu, X., Kohler, K., Falick, A. M., Moore, A. M., Jones, P. R., Sparkman, O. D. & Vierra, C. (2005) Egg case protein-1. A new class of silk proteins with fibroin-like properties from the spider *Latrodectus hesperus*. *J. Biol. Chem.* 280, 21220–21230
29. Price, N. R. & Hunt, S. (1976). The occurrence of reducible compounds in an invertebrate structure protein of *Buccinum undatum* (L.). *Cell. Mol. Life. Sci.* 32, 557-558.
30. Price, N. R. & Hunt, S. (1976). An unusual type of secretory cell in the ventral pedal gland of the gastropod *Buccinum undatum* (L.). *Tissue and Cell.* 8, 217-228.
31. Creighton, T. E. (1993). *Proteins: Structures and Molecular Properties* (2nd ed). W. H. Freeman and Company, New York.
32. Lupas, A., Van Dyke, M. & Stock, J. (1991). Predicting coiled coils from protein sequences. *Science.* 252, 1162-1164.
33. Wolf, E., Kim, P. S. & Berger, B. (1997). MultiCoil: A Program for Predicting Two- and Three-Stranded Coiled Coils. *Prot. Sci.* 6, 1179-1189.
34. Parry, D. A. & Steinert, P. M. (1999). Intermediate filaments: molecular architecture, assembly, dynamics and polymorphism. *Q. Rev. Biophys.* 32, 99-187.
35. Coulombe, P. & Fuchs, E. (1990). Elucidating the early stages of keratin filament assembly. *J. Cell. Biol.* 111, 153-169.
36. Kreplak, L., Aebi, U. & Herrmann, H. (2004). Molecular mechanisms underlying the assembly of intermediate filaments. *Exp. Cell. Res.* 301, 77-83.
37. Koch, E. A., Spitzer, R. H., Pithawalla, R. B. & Downing, S. W. (1991). Keratin-like components of gland thread cells modulate the properties of mucus from hagfish (*Eptatretus stouti*). *Cell Tiss. Res.* 264, 79-86.
38. Rogers, G. E. (2006). Biology of the wool follicle: an excursion into a unique tissue interaction system waiting to be re-discovered. *Exp. Dermatol.* 15, 931–949
39. Larkin, M. A., Blackshields, G., Brown, N. P., Chenna, R., McGettigan, P. A., McWilliam ,H., Valentin, F., Wallace, I. M., Wilm, A., Lopez, R., Thompson, J. D., Gibson, T. J. & Higgins, D. G.(2007). Clustal W and Clustal X version 2.0. *Bioinformatics.* 23, 2947-2948
40. Zhao, H. & Waite, J. H. (2005). Coating Proteins: Structure and Cross-Linking in fp-1 from the Green Shell Mussel *Perna canaliculus*. *Biochemistry.* 44, 15915-15923.
41. Paz, M., Flückinger, R., Boak, A., Kagan, H. M. & Gallop, P. M. (1991). Specific detection of quinoproteins by redox-cycling staining. J. Biol. Chem. 266, 689-692.
42. Waite, J. H. (1991). Detection of peptidyl-DOPA by amino acid analysis and microsequencing techniques. *Anal. Biochem.* 192, 429-433.
43. Greenfield, N. (2006). Using circular dichroism spectra to estimate protein secondary structure. *Nat. Protoc.* 1, 2876-2890.

Chapter 3. Thermomechanical properties of *Busycotypus canaliculatus* egg capsules: entropic vs non-entropic

Adapted from A. Miserez, S.S. Wasko, C.F. Carpenter, J.H. Waite, "Non-entropic and reversible long-range deformation of an encapsulating bioelastomer," Nature Materials, 8 (11): 910-916 (2009).

Reproduced with permission from Nature Publishing Group.

A. Abstract

Encapsulation is a widespread biological process particularly in the formation of protective egg cases of oviparous animals. The egg capsule wall of the channelled whelk *Busycotypus canaliculus* is an effective shock absorber with high reversible extensibility and a stiffness that changes significantly during extension. Here we show that post-stretch recovery in egg capsules is not driven by entropic forces as it is in rubber. Indeed, at fixed strain, force decreases linearly with increasing temperature, whereas in rubber elasticity the force increases. Instead, capsule wall recovery is associated with the internal energy arising from the facile and reversible structural α-helix↔β-sheet transition of egg capsule proteins during extension. This behavior is extraordinary in the magnitude of energy

dissipated and speed of recovery and is reminiscent of strain-induced crystallization in some polymeric fibers and of superelastic deformations associated with diffusionless phase transitions in shape memory alloys.

B. Introduction

Engineering versatile encapsulants for pharmaceuticals and the transplantation of delicate cells and tissues is a very active area of medical research [1,2]. Surprisingly, engineers are largely unaware of how exquisitely well-tuned naturally occurring encapsulation strategies are. Oviparous animals, for example, all produce eggs that possess diverse protective capsules or shells specifically adapted to their anticipated wear and tear in the external environment. The familiar calcified eggshell of bird eggs is adequate protection in a nest of straw, but it would be a deathtrap for the eggs of the channeled whelk *Busycotypus canaliculus*, a large marine snail. *Busycotypus* eggs are released in meter-long helical strands known as mermaid necklaces that link up to 160 capsules (Figs. 3.1a and b). These are buffeted about for months by breakers at velocities up to 10 m/sec along the seashores of the east coast of North America [3]. Given the punishing environment, how the *Busycotypus* capsules shield the delicate embryos from damage is of fundamental interest. Recent investigations of the *Busycotypus* capsule wall have found it to consist of cross-plied sheets of protein fibers (Fig. 3.1c) with effective shock absorbing tensile properties [4,5].

The large and reversible extension of biopolymers in *Busycotypus* egg capsule wall is strongly suggestive of an elastomer. Elastomeric proteins play an essential role in a variety of extracellular structural tissues [6] and their long-range elastic properties are useful for instance as shock absorbers (*e.g.* in hydrated dragline spider silks [7]), for elastic energy storage capacity in jumping and flying insects [8], and to ensure adequate elasticity in the integument and arteries of various organisms [9-11]. Bioelastomers classically exhibit rubber-like entropic elasticity [10]. In this well-established framework [12], the force f acting on a strained specimen is expressed as the sum of the internal energy contribution and the entropic contribution, with the latter prevailing at sufficiently large extensions (larger than 10 %) [7,10] and typically contributing to 80-90 % of the total elastic force for rubbery materials. Our thermomechanical and *x*-ray scattering analysis shows that the *Busycotypus* egg capsule, albeit elastomeric in its high and reversible extensibility, is not dominated by entropic forces. Instead, our experimental data support the notion that high extensibility is due to a fully reversible α-helix ↔ β-sheet structural transition upon loading. This behaviour can be explained by simple thermodynamic equilibrium concepts and provides a clear experimental validation of the Flory [13] model predicting that forces arising from internal-energy can dominate long-range elasticity in polymorphic fibers. Whereas α ↔ β structural transitions have previously been described in α-keratin fibres, *Busycotypus* egg capsules show that it can be exploited to create

bioelastomers with higher extensibility and much less time-dependent recovery than previously recognized. This paradigm could prove useful in designing novel bioencapsulants for delicate tissue implants.

C. Materials and methods

Busyctypus canaliculus egg capsules were purchased from the Marine Biological Laboratory (Woods Hole, MA). Individual cases were split apart, the gelatinous contents including the embryos discarded, and the interiors were cleaned by repeated rinses with filtered water. Gentle physical disruption was necessary to dislodge the mucous lining. Rectangular strips about 10 mm long, and a 3-6 mm wide were cut from egg capsules with a razor blade, and the cross-sectional area was measured by light microscopy.

Stress-strain analysis was performed on an MTS (MTS, Eden Prairie, MN) Bionix 200 universal testing machine, at nominal strain rate of 10^{-2} s^{-1}, using a 50 N load cell and a built-in optical encoder to measure the load and displacement, respectively. All specimens were tested in seawater using a custom-made stainless steel container. The temperature of the seawater bath was regulated over the range –1 to 80 °C using an external thermocontroller unit. The seawater bath temperature was brought to prescribed levels by connecting the heating/coolant fluid from the thermocontroller to an inner copper tubing wrapped inside the water, hence allowing heat transfer by conduction. Styrofoam was used to insulate the seawater container from the ambient environment, and the temperature was

measured within 1 cm of the specimen with a thermocouple (accuracy +/- 0.5°C) during testing. Thermal expansion was corrected by re-setting the initial gauge length to zero before each test. In addition, swelling –which is known to significantly affect the actual volume of elastin samples at high temperatures [11]– was measured by heating an unstrained sample in water and observing size changes under an stereomicroscope. No detectable swelling was noticed. Control experiments were performed on a natural latex material under identical conditions.

Poisson's ratio was measured independently using a custom-made micrometer tensile frame. Fully hydrated samples were gripped and pulled to strains ranging from 20 to 100 % under a stereo-microscope. Width and thickness reductions were obtained in separate measurements, in which the micro-tensile grips were rotated by 90° to enable focus on the thickness or the width, respectively. All images were acquired with a Nikon D70 digital camera and analyzed with Adobe Photoshop software (Adobe Inc, San Jose, Ca, USA). Six measurements of width and thickness were obtained and averaged at each strain.

The elastic "Hookean" modulus was monitored at selected strains by partial unloading/reloading cycles as illustrated in Fig. 3.2a, at a strain rate during the unloading section that was half of that during monotonic loading (i.e. $5 \cdot 10^{-3}$ s^{-1}). The modulus at a given strain cycle was measured on true stress/strain curves as the slope of the tangent of an unloading cycle at the

unloading strain. This tangent modulus is a more accurate measure of the true elastic modulus at the instant of unloading; it also better captures micro-damage or stiffening due to structural changes during straining as observed in engineering composites and metal foams [30,31]. Each loading/unloading series was repeated three times per temperature and the relevant values for data analysis (force, modulus, stress, strain) were averaged.

X-ray diffraction patterns were obtained from dry specimens using a Huber Four-Circle goniometer Wide Angle X-ray Spectrometer (WAXS), equipped with a Cu rotating anode *x*-ray generator (Rigaku UltraX18, wavelength =1.54 Å), and a MAR345 image plate area detector. Spectra were acquired on pristine (unstrained), loaded, and cycled (loaded/ unloaded) specimens with a sample-to-detector distance of 282.5 mm. For loaded specimens, the hydrated specimen was deformed to a given strain, and then dried, thereby "locking" the specimen at that strain.

Diffraction patterns were acquired on fully hydrated samples using a high intensity synchrotron source at BESSY (Berlin Elektronenspeicherring Gesellschafft m.b.h, Berlin Germany) with *x*-ray wavelength of 1 Å. The beam line was equipped with a custom-made *in situ* tensile testing equipment [32] allowing to continuously monitor diffraction patterns during extension. A comprehensive description of the set-up can be found elsewhere [33]. In brief, experiments were conducted with a MarMosaic 225 2D CCD detector (MAR USA, Evanston, Il, USA), a having a 3072 x 3072

pixel resolution, a 30 μm beam size, and a sample-to-detector distance of 256.4 mm. Diffraction patterns were acquired at regular strain intervals for 30 sec, as well as at complete unloading.

Specimens for SEM imaging were freeze-fractured following immersion in liquid nitrogen. Fixation was done in a mixture of 1% glutaraldehyde and 1% paraformaldehyde, followed by serial de-hydration in ethanol/water mixtures up to 100% ethanol. Final dehydration was done in a hexamethyldisilazane overnight. Fixed samples were gold-coated for 1 min. Low magnification imaging was performed using a Vega Tescan TS5130-MM thermionic emission SEM (Brno, Czech Republic), whereas high-resolution imaging was done on a field emission gun FEI XL-40 microscope (FEI, Hillsboro, Oregon). Working-distance was set at 5 mm for high resolution imaging.

For amino acid copositional analysis, egg capsules were thoroughly washed in milli-Q water and subsequently hydrolyzed *in vacuo* in a 6M HCl/ 5% phenol solution at 110°C for 24 hours. The supernatant was separated from the solid residue by centrifugation, flash-evaporated and subsequently washed with water and methanol to remove traces of acid and the amino acid composition was obtained with and analyzed in a ninhydrin-based Beckman Autoanalyzer (Beckman-Coulter, Fullerton, CA)

D. Results and Discusson

The microstructure of a mature *Busycon* capsule wall resembles plywood in consisting of stacked sheets, each about 10-20 μm thick [14]. Each sheet is an array of aligned fibers in which the preferred fiber orientation is rotated by 90° from one sheet to the next (Fig. 3.1c) and results in orthotropic mechanical properties when measured in the plane of the capsule. At higher magnification, individual fibers with diameters of 200-500 nm and characteristic surface ridges are evident (Fig. 3.1d). Capsule microstructure and formation is described at length elsewhere [4].

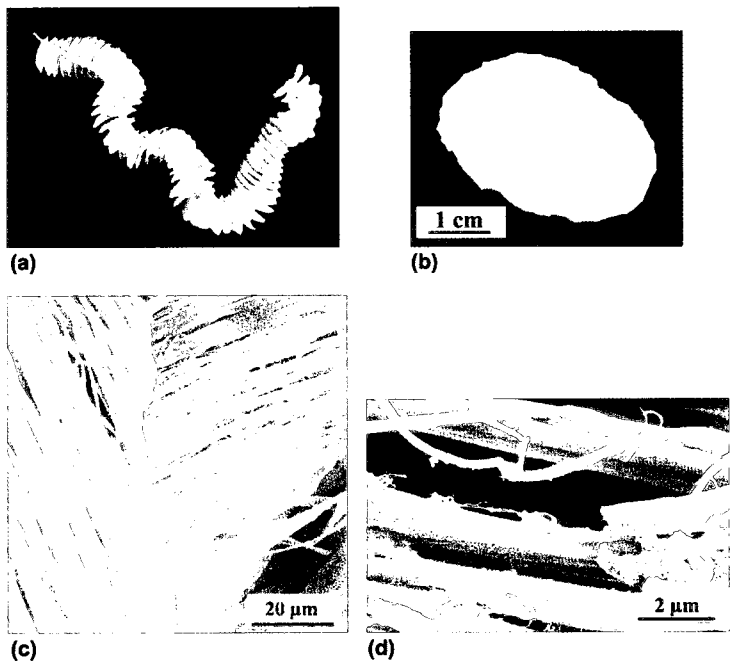

Figure 3.1. Busycon canaliculum photographs and SEM micrographs. a, Helical strand ('mermaid's necklace') containing dozens of interconnected capsules, with a total length of about 1 m. b, Close-up view of a dissected capsule from which tensile specimens were extracted. c, Low-magnification SEM image after freeze-fracture illustrating the cross-plywood structure, with the preferred fibre orientation at about 90◦ between adjacent sheets. d, High-magnification SEM micrograph of a few individual fibres within one sheet; fibres are typically 200–500 nm in diameter and contain characteristic surface ridges.

A typical stress-strain curve (strain rate 10^{-2} s^{-1}) with both engineering and true properties reproducibly illustrates the four regimes reported earlier [5] (Fig. 3.2a): (1) an initial stiff region to about 5 % strain with an elastic modulus of about 100 MPa; (2) a pseudo-yield region with a much lower increase of flow stress with strain; (3) at strains beyond 70 %, increased stiffening; and (4) a large hysteresis loop upon unloading during which up to 40 % of the total energy is dissipated.

The material exhibits a quasi-instantaneous recovery of strain and modulus with the residual strain at zero load attributed to viscoelastic effects (the residual strain was recovered in fully unloaded specimens after a few minutes). The representative stress-strain curves in the temperature range – 1 to 80°C clearly show diminished initial stiffness as well as decreased flow stress and hysteresis with increasing temperature (Fig. 3.2c). Additional tests (data not shown) performed at various strain rates confirmed earlier data [5] regarding a slight reduction of hysteresis (10 %) at higher strain rates (10^{-1} s^{-1}).

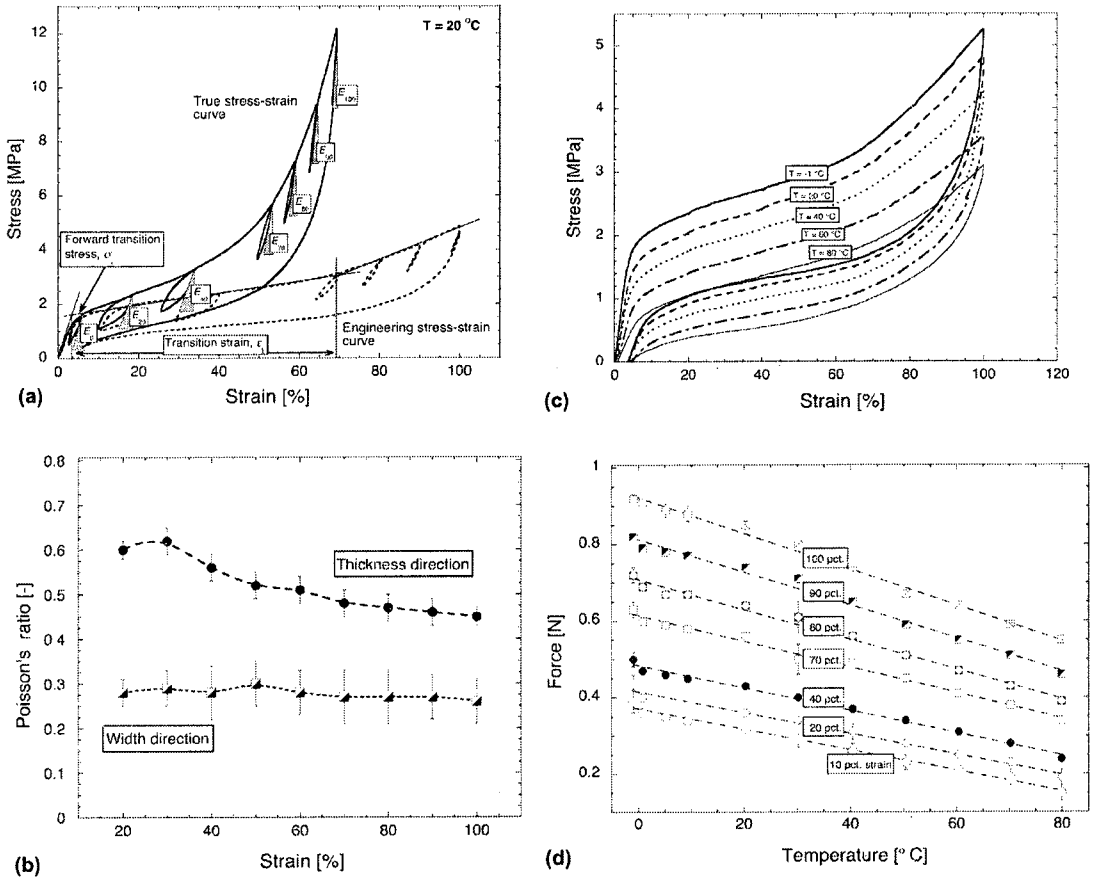

Figure 3.2. Thermomechanical properties of whelk egg capsule material. a, Typical whelk egg capsule stress–strain curves (engineering curve and true tensile curve corrected for the measured Poisson's ratios). At fixed engineering strains during loading, unloading/reloading cycles were carried out, and the true modulus was obtained from the tangent of the unloading portion of a cycle on the true stress–strain curve, as illustrated. Forward transition stress and transition strain (defined in text) are calculated with reference to the engineering properties. The slight residual deformation on unloading is due to viscoelastic effects, and full recovery was observed by letting the sample rest for a few minutes before the next cycle. b, Poisson's ratio versus strain (engineering values); each data point is the average of two samples measured at six different locations (n = 12) and error bars are the standard deviation; note the distinct anisotropy of Poisson's ratios in the thickness and the width directions. c, Stress–strain curves with full unloading at various temperatures (±0.5◦). Unloading/reloading loops at given strain intervals as illustrated in a were also carried out for each temperature but are omitted for clarity. d, Force versus temperature plots at various values of strains, measured from plots in b. For both c and d, each data point is the average of three measures and error bars are the standard deviation.

Wide angle X-ray scattering (WAXS) analysis *Busycon* capsule wall

during deformation resulted in distinctly recognizable diffraction patterns (Fig. 3.3a). At 0 % strain, two classical features of α-helices are detectable [15,16], *i.e.* (1) a broad equatorial peak centered at 1.03 nm corresponding to the mean distance between α-helical axes (the presence of that reflection on the meridian axis is attributed to the orthotropic arrangement of the egg capsules), and (2) the 0.52 nm peak along the meridian due to projection of the α-helix along the coiled-coil axis [15]. At 70 % strain, a β-sheet formation is indicated by (1) the 0.465 nm equatorial reflections, due to lateral periodicity between chains in the β-sheet [17], and (2) the 1.03 nm peak which is now due to the mean inter-sheet distance. Upon further stretching to 120 %, the 0.465 nm reflection on the equatorial arc was intensified, as were the 1.03 nm spots. The faint peak at 0.33 nm on the meridian approximates the translational rise between successive residues along the protein chain in a β-sheet [17]. At full unloading the diffraction pattern returns to that of a pristine unstretched specimen; notably, the 0.465 nm β-sheet feature is absent. Time-resolved diffraction patterns acquired by synchrotron radiation of fully hydrated samples during *in-situ* extension confirm earlier trends in the 0.52 nm meridian and equatorial 0.465 nm reflections (Fig. 3.3b), and the diffraction pattern returns to that of the unstrained material upon unloading. The slightly higher *D*-spacing corresponding to inter-helix and inter-sheet distances, respectively, in hydrated samples (1.26 nm vs. 1.03 nm for dry samples) is attributed to swelling. Taken together, the patterns are consistent

with a structural and *reversible* transition between α-helices and β-sheets during a stretch/relaxation cycle.

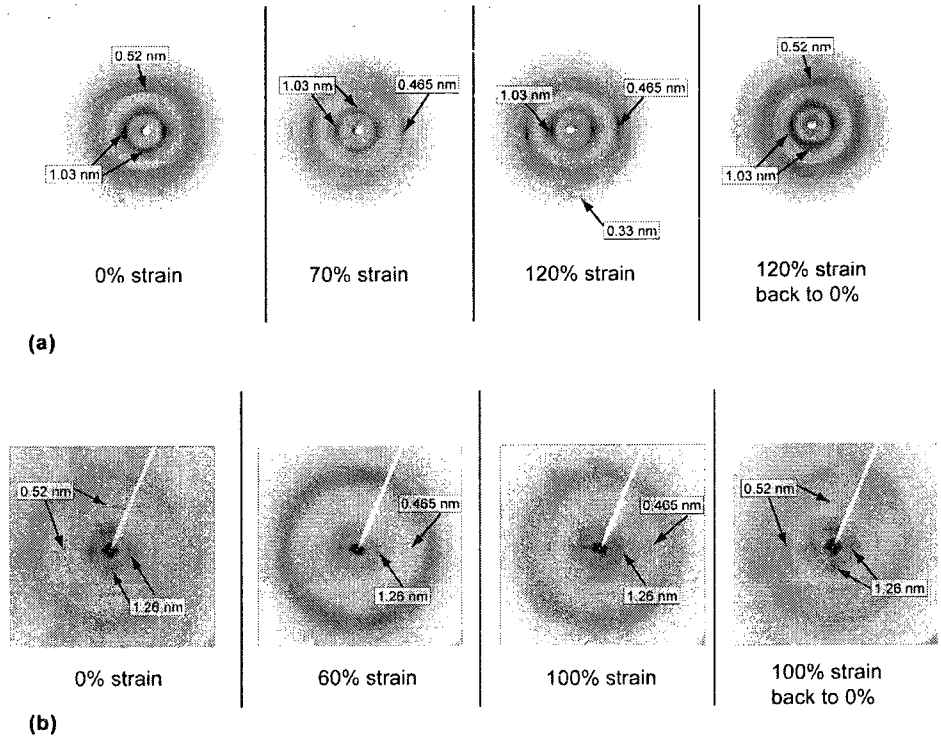

Figure 3.3. WAXS diffraction patterns at various strains and after full unloading. a, 'Dried frozen' sample, diffraction pattern acquired with a standard X-ray tube (0, 70, 120%, back to 0%). b, Time-resolved diffraction pattern of a hydrated sample acquired with a high-intensity synchrotron beam. Diffraction patterns were integrated with the Fit2D software and peaks were assigned according to refs 14, 15. The larger inter-helical and inter-sheet distances observed in the hydrated specimen (1.26 nm versus 1.03 nm in the dry state) are attributed to swelling.

Entropic elasticity manifests distinct thermoelastic properties. In force *vs.* temperature plots (f *vs.* T), the force at a fixed strain increases with temperature, with the values of force being nearly proportional to absolute temperature. This behavior is described by established thermodynamic concepts relating the total elastic force f with its internal (f_U) and entropic

energy (f_S) components as:

$$f = f_U + f_S = \left(\frac{\partial U}{\partial l}\right)_{V,T} - T\left(\frac{\partial S}{\partial l}\right)_{V,T} = \left(\frac{\partial U}{\partial l}\right)_{V,T} + T\left(\frac{\partial f}{\partial T}\right)_{V,l}$$

(3.1)

where U and S are the internal energy and the entropy of the system, respectively; the right-hand side is from the Maxwell relationship - $(\partial S/\partial l)_{V,T} = (\partial f/\partial T)_{V,l}$. On f vs. T plots at constant strain, the slope at any given point on the curve thus corresponds to the entropy change per unit extension, whereas the intercept at $T = 0$ is equal to the change of U per unit extension. Capsule wall stress-strain curves at various temperatures (Fig. 3.2b) re-plotted as corresponding f *vs.* T plots for engineering strains in the range 10 to 100 % (Fig. 3.2d) unequivocally show that force decreases with temperature at all strains tested, contrary to rubbery elastomer behavior: latex rubber at various temperatures conformed to the classical increase of force with temperature (Supplementary Materials). Poisson's ratios showed significant dimensional anisotropy (Fig. 3.2b), with values around 0.48 and 0.27 for capsular thickness and width dimensions, respectively, at extensions of 50 % and above (calculated in engineering strain, with corresponding true strain values of 0.83 and 0.43, respectively). Interestingly, this results in a 15 % volume decrease during uniaxial

extension, a phenomena quite unusual for synthetic elastomers, but not unexpected in biological materials [18]. A correction to Eq. (1) for the observed volume change shows that the internal energy contribution is slightly overestimated at constant pressure [12] but does not alter the inverse stress/ temperature trend apparent from our experiments. The implication is that vis-à-vis most known elastomers, the extensibility of *Busycon* egg capsules is not dominated by entropic forces.

X-ray analysis supports a transition from α-helices present at low strain to β-sheets structures at high strain (Fig. 3.3), as previously speculated in [5]. In keratin fibers, α-helical coiled-coils start to unravel at roughly 5 % strain [16], resulting in an intermediate random coil structure as well as some α and β structures between 20 and 40 % engineering strain. We measured the change in tangent modulus with strain to gain additional insight into structural reorganization occurring during deformation (see Materials and Methods) (Fig. 3.4). At low temperature (< 30°C), the modulus decreased from its initial value to a minimum at about 20 % strain. The modulus then increased slightly to 65 % strain. Upon further stretching, noticeable and rapid stiffening occurred. Based on the *x*-ray and modulus data and similarity with results reported for keratin [16], four distinct structural domains were identified during extension, and schematically illustrated in Fig. 3.5 for fibers oriented along the loading axis. In domain 1, from unstrained to 5 % strain, α-helices dominate in the capsule wall. At the

initiation of pseudo-yielding (5 %), unfolding of α-helices into random coils occurs, leading to a semi-amorphous structure that is accompanied by a decrease in stiffness. Domain 2 is present from 5 to 20 % strain. The observed modulus is lower and consistent with semi-crystalline polymers and elastomers in which amorphous domains leads to a reduction of stiffness [12,19]. The third domain prevails at 20 to roughly 60 % strain; here random coils and β-sheets coexist with the latter progressively replacing the former (transition regime 3). Domain 4 is a β-sheet dominated structure, in which random coils have mostly disappeared and re-crystallized into β-sheets. At such high strains, the increased modulus results from the inherently stiffer nature of β-sheets as well as sheet alignment along the loading axis during stretching - a stiffening mechanism recognized for semi-amorphous polymer fibers [19]. The much-reduced hysteresis during partial loading cycles is further suggestive of a single-phase material in this domain (see Fig. 3.2). At higher temperatures,

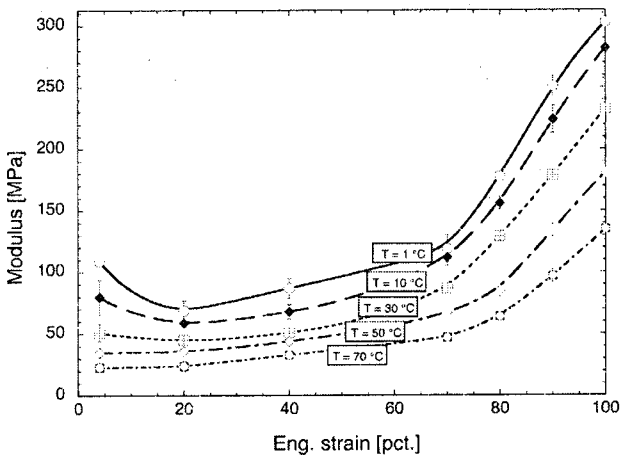

Figure 3.4. Tangent modulus versus strain at various temperatures. In the temperature range 0−30 ◦ C, the modulus initially decreases up to 20%. strain and then increases on further straining. At T > 30 ◦ C, the modulus is initially constant, and tangent modulus versus strain then follows the trends at lower temperatures. Each data point is the average of three measurements and error bars are the standard deviation.

the α-helices are thermodynamically less stable, consequently, the initial decrease in modulus was not observed at T > 30C°. Instead the modulus remained constant up to 60 % strain, where stiffening then occurred as at lower temperatures.

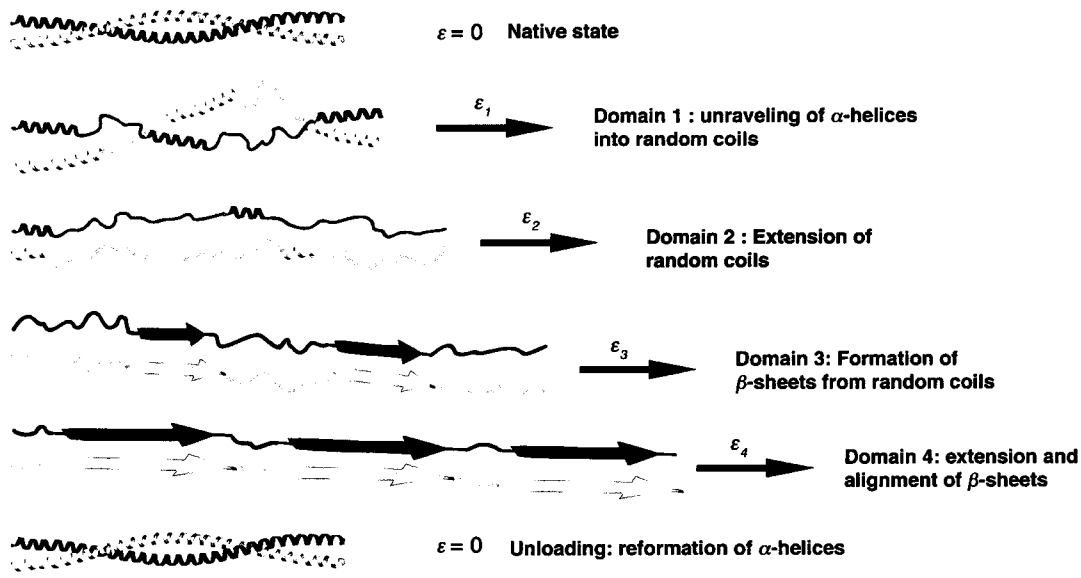

Figure 3.5. Schematic diagram of α-helix ↔ β-sheet transition during straining. For fibrils oriented along the loading axis, transition is accommodated by the presence of intermediate random coils. Fibrils oriented at 90◦ relative to the loading axis (not shown) do not undergo the structural transition. The coiled coil dimer was arbitrarily chosen to illustrate the

A stress dependent interconvertibility of secondary structures is thermodynamically analogous to that of axially oriented polymer fibers with both crystalline and amorphous phases [19]. For this type of polymorphic system, it is convenient to use the Gibbs free energy *G* as the thermodynamic potential, from which it can be shown that the melting temperature *T* is a function of applied force *f*, [13] and given by:

$$\left(\frac{\partial f}{\partial T}\right)_P = \frac{f}{T} - \frac{\Delta H}{T \cdot \Delta L} \qquad (3.2)$$

with ΔL equal to the total length increment during crystallization and ΔH, the enthalpy of crystallization. In the present case ΔL can be seen as the length increment necessary to fully transform α-helices into β-sheets, whereas ΔH is the enthalpy of the α→β phase transformation under a tensile force *f*. Equation (2) is simply a restatement of the Clausius-Clapeyron relation, with force and length replacing pressure and volume. Interestingly, this reversible behavior is reminiscent of shape memory effects in metallic alloys in which high reversible deformation is obtained through a reversible, diffusionless solid-phase transformation - the martensitic transformation [20,21] - and is also modeled by the Clausius-Clapeyron relation. Recalling that α-helices start to unravel at the yield point in *Busycon* egg capsules (Figs. 3.3 and 3.4), it is tempting to interpret our results within this framework, using *f* as the force at initiation of yield for the conformational phase transition. Rewriting equation (2) as:

$$\left(\frac{\partial (f/T)}{\partial (1/T)}\right)_P = \frac{\Delta H}{\Delta L} \qquad (3.3)$$

,or equivalently in terms of stress and strain:

$$\left(\frac{\partial (\sigma_t/T)}{\partial (1/T)}\right)_P = \frac{\Delta H}{\varepsilon_t \cdot V_0} \qquad (3.4)$$

where σ_t is defined as the "forward transition stress". According to equation (4), a plot of (σ_t / T) *vs.* $(1/T)$ should be linear with the enthalpy of transformation or ΔH per unit volume V_0 deduced from the slope. This analysis is shown in Fig. 3.6, which indicates that the slopes for 3 different specimens are closely comparable, although there are some differences in stress intensity (due to uncertainties in specimen thickness and slight variations in orientation). Equation (3) implicitly requires the transformation *strain* ε_t to be temperature-independent. Plots of experimental ε_t vs 1/T confirm this independence (Fig. 3.6). The whelk capsule wall is thus an unequivocal validation of the theoretical proposition by Flory [13] that high extensibility in some elastic proteins could be achieved via an internal-energy dominated mechanism. It must be noted that the entropic forces are not fully absent, especially in the regime of random-coils extension. However their contribution is much lower than that

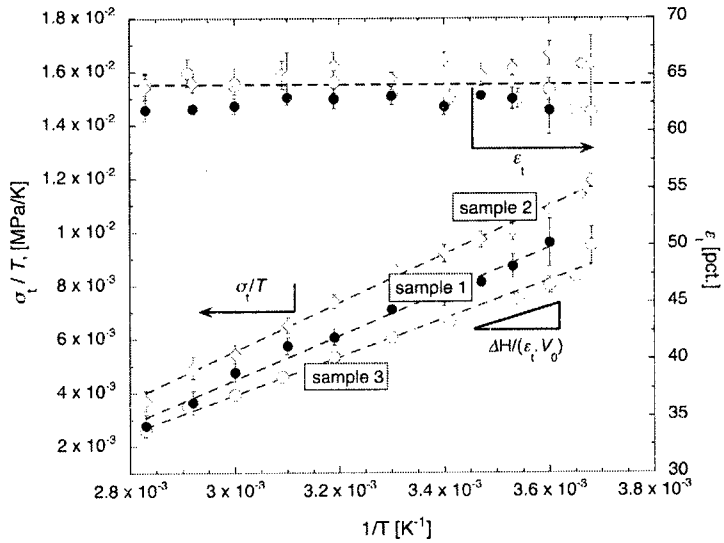

Figure 3.6. Transition stress and strain at various temperatures.(σ_t/T) versus (1/T) plot (left y axis) with σt being the forward transition stress, and ε_t versus (1/T) plot (right y axis) with ε_t being the transition strain, for three different samples. Each data point is the average of three cycles and error bars are the standard deviation. The linear relationship (σ_t/T) versus (1/T) agrees with equation (4), whereas ε_t is essentially independent of T.

of the internal energy of the phase transition happening simultaneously, and are hence not distinguished in the experiments. Solving Eq.3 for the capsule data yields an enthalpy of transformation ΔH = 1.26 cal/cm^3. Approximating the density of the egg capsules as 1.45 g/cm^3 [22] and the average molecular weight of *Busycon* egg capsule proteins as 50 kDa [23], and finally assuming that only half of initial coiled-coils undergo the structural transition because of the orthotropic microstructure, we calculate a value ΔH of 86.8 kcal/mol or 207 cal/mol residue (average residue mass 119 g/mole). This is in the range of the 170 cal/mol residue reported for the $\alpha \rightarrow \beta$ transition of poly-*L*-lysine measured by differential scanning calorimetry at pH ≈ lysyl pK_a [24] at which the prevailing secondary structure is α-helical below a critical temperature. It should be noted that our approximation of the $\alpha \rightarrow \beta$ transition enthalpy is contingent on its being a first-order transition, an assumption that has been considered at some depth elsewhere in connection with the $\alpha \rightarrow \beta$ transition of hair keratins [25] and is accepted [26].

In the $\alpha \rightarrow \beta$ transition regime, the stress increases with strain (Figs. 3.2a and b). This behavior is not consistent with simple thermodynamic equilibrium concepts discussed above and merits further scrutiny. In a one-component ideal system (*i.e.* fibers composed of a single protein with uniform sequence and cross-link density) and with all fibers aligned along the loading axis, a constant transformation stress would be expected. The actual material deviates from ideality in three ways, and the combined

deviations reshape the stress/strain curve. First, nanofibrils are not uniquely oriented to the loading axis. Fibers in different layers of the orthotropic cross-lamellar structure experience at least two levels of local stresses *along their longitudinal axis,* σ_y. Consider a sample with one family of fibers oriented at an angle θ from the loading axis. At a given external load σ_a, these fibers will start transforming into β-sheets when σ_y equals the critical stress, σ_T. This condition hence is satisfied by $\sigma_a = \sigma_T/\cos\theta$. A second group of fibers oriented at 90° relative to the first group will require an external load $\sigma_a = \sigma_T/\cos(90-\theta)$, which differs from the first group. The presence of fibers at various angles in the structure would necessarily lead to the coexistence of α and β forms in the intermediate region, spreading the transition over a range of tensile forces rather than at a unique force.. Keeping also in mind that the capsules do not exhibit a perfect orthotropic organization across their thickness, one will expect a distribution of angles θ and, in turn, a distribution of critical transformation stresses in the intermediate two-phase region. Second, the diameter distribution of the capsule nanofibrils is not monodisperse. At a given external force, the local stress sustained by individual fibrils of various diameters varies, and such variations will lead to different critical transformation stresses. A third deviation from ideality pertains to the assumption of a one-component system. Protein extraction from the capsules and nidamental glands suggests three electrophoretically

distinct proteins [23], all of which may undergo α ↔β transitions. The Gibbs free energy for a multi-component system under uniaxial force and constant pressure accounts for an additional chemical potential term:

$$dG = -SdT + fdL + \sum_i \mu_i dn_i \qquad (3.5)$$

where S is the entropy, n_i the concentration of component i in the mixture and μ_i its chemical potential. At equilibrium, ΔG is at a minimum and impacted by the relative concentrations and chemical potential of each phase in the system. Under such conditions, it can be shown that equation (3) is re-written as [19]:

$$\left(\frac{\partial(f/T)}{\partial(1/T)}\right)_{P,\lambda} = \frac{\Delta\overline{H}}{\Delta\overline{L}} \qquad (3.6)$$

where λ denotes the fraction of fibers in the α state, $\Delta\overline{H}$ now consists of the enthalpy of transformation *plus* the enthalpy of dilution of the α-phase, and $\Delta\overline{L}$ is similarly defined. Because the $\Delta\overline{H}$ and $\Delta\overline{L}$ terms are dependent on the composition, the critical force f (or critical stress σ_t) is not constant at a given temperature. Instead, the force varies with the length as the transformation progresses.

The large macroscopic deformation associated with egg capsule α ↔ β *t*ransitions is consistent with the behavior of a number of coiled-coil proteins examined by atomic force microscopy. In myosin [27,28] for example,

reversible extensibility as high as 200 % has been reported in individual fibers, and is explained in terms of unraveled coiled-coils. Indeed, the myosin force-extension curves reveal a plateau of constant force that resembles the present macroscopic experiments with *Busycon* capsule. Reversible extension to 65 % during unfolding of helical to amorphous structure prior to formation of β-sheets is therefore not uncommon. The large capsule hysteresis, however, in combination with instantaneous recovery of initial modulus is rare. Myosin exhibits almost no hysteresis (< 5 %), and keratin, which does have significant hysteresis, shows only slow recovery [25]. The slow recovery of keratin, as well as its more limited extensibility, can be attributed to the high density of disulfide cross-links, which are absent in whelk egg capsules [5]. Disulfide bonds are also permanently broken at high strains and temperature, resulting in incomplete strain recovery under those conditions. Hagfish slime also exhibits an $\alpha \rightarrow \beta$ transition [29] but this transformation is irreversible.

The implications of these subtleties for engineering protective encapsulants for delicate tissues such as a developing embryo are significant. Imagine an embryo in a fluid filled rubbery sac. Given the high resilience of rubbers, extensive deformation of the capsule walls by buffeting would result in release of most of the stored energy, thus the fluid and embryo would be vigorously jostled. This is not possible in *Busycon* capsules because only a fraction of the energy invested in deforming the

capsule walls is released and the rest dissipated. Like an ideal rubber, however, egg capsule elastomer will be as good as new for the next challenge.

E. Conclusions

The *Busycon* egg capsule wall is endowed with high extensibility, durability, and shock-absorbing capability. Thermomechanical and structural analyses indicate that the long-range elasticity of the capsules is not entropically dominated. Instead internal energy changes associated with a fully reversible $\alpha \leftrightarrow \beta$ phase transition seem to be the main determinant. Capsule thermomechanical behavior conforms to the Clausius-Clapeyron relation as applied to phase equilibrium previously developed to model crystallization of polymer fibers under stress, and deviations from an ideal system are invoked to explain the increase of stress during the structural transition. Although $\alpha \leftrightarrow \beta$ transitions during extension are not unique to *Busycon* egg capsules, the capsules are extraordinarily distinctive in the magnitude of reversible strain and their almost instantaneous strain recovery. Complete characterization and recombinant expression of *Busycon* egg capsule proteins should ultimately enable the engineering of capsule-like materials that combine high modulus, reversible extensibility (> 100 %), and impact-absorbing properties for the insulation of damage prone tissues.

F. Acknowledgements

Thanks are due to B. Shadwick (University of British Columbia, Vancouver, Canada) and F. Zok (Materials Department, UCSB) for helpful criticism. Y. Li (Materials Research Laboratory (MRL), UCSB) and H. Gupta (Max-Planck Institute for Colloids and Interfaces, Golm, Germany) provided critical guidance for WAXS and time-resolved synchrotron experiments, respectively. K. Field (Mechanical Engineering Department, UCSB) helped in developing the microtensiometer. S.W. was financially supported by a California Sea Grant # R/MP-97B and UC BREP GREAT traineeship #2007-02. This work made use of MRL Central Facilities supported by the MRSEC Program of the National Science Foundation under award No. DMR05-20415.

H. References

1. Ma, P. X. & Elisseeff, J. H. *Scaffolding in Tissue Engineering* (CRC Press, 2006).
2. Capito, R. M., Azevedo, H. S., Velichko, H. S., Mata, A. & Stupp, S. I. Self- Assembly of Large and Small Molecules into Hierarchically Ordered Sacs and Membranes. *Science* **319**, 1812-1816 (2008).
3. Denny, M. W. *Biology and the Mechanics of the Wave-Swept Environment* (Princeton University Press, Princeton, N.J., 1988).
4. Rapoport, H. S. & Shadwick, R. E. Reversibly Labile, Sclerotization-induced Elastic Properties in a Keratin Analog from Marine Snails: Whelk Egg Capsule Biopolymer (WECB). *Journal of Experimental Biology* **210**, 12-26 (2007).
5. Rapoport, H. S. & Shadwick, R. E. Mechanical Characterization of an Unusual Elastic Biomaterial from the Egg Capsules of Marine Snails (*Busycon spp). Biomacromolecules* **3**, 42-50 (2002).
6. Tatham, A. S. & Shewry, P. R. Elastomeric Proteins: Biological Roles, Structures and Mechanisms. *Trends in Biochemical Sciences* **25**, 567-571 (2000).
7. Gosline, J. M., Denny, M. W. & DeMont, M. E. Spider Silk as Rubber. *Nature* **309**, 551-552 (1984).
8. Weis-Fogh, T. A Rubber-Like Protein in Insect Cuticle. *Journal of Experimental Biology* **37**, 889-907 (1960).
9. Lillie, M. A. & Gosline, J. M. The Effects of Hydration on the Dynamical Mechanical Properties of Elastin. *Biopolymers* **29**, 1147-1160 (1990).
10. Urry, D. W. et al. Elastin: A Representative Ideal Protein Elastomer. *Philosophical Transactions of the Royal Society of London, Series B: Biological Sciences* **357**, 169-184 (2002).
11. Shadwick, R. E. & Gosline, J. M. Physical and Chemical Properties of Rubber-Like Elastic Fibres from the Octopus Aorta. *Journal of Experimental Biology* **114**, 239-257 (1985).
12. Treloar, L. R. G. *The Physics of Rubber Elasticity* (ed. Sciences, O. C. T. i. t. P.) (Oxford University Press, Oxford, U.K., 2005).
13. Flory, P. J. Theory of Elastic Mechanisms in Fibrous Proteins. *Journal of the American Chemical Society*, 5222-5235 (1956).
14. Shadwick, R. E. (2009), personal communication.
15. Busson, B., Briki, F. & Doucet, J. Side-Chains Configurations in Coiled Coils Revealed by the 5.15-A Meridional Reflection on Hard α-Keratin X-Ray Diffraction Patterns. *Journal of Structural Biology* **125**, 1-10 (1999).
16. Kreplak, L., Doucet, J., Dumas, P. & Briki, F. New Aspects of the α-Helix to β-Sheet Transition in Stretched Hard α-Keratin Fibers. *Biophysical Journal* **87**, 640-647 (2004).
17. Fraser, R. D. B., MacRae, T. P., Parry, D. A. D. & Suzuki, E. The Structure of β-Keratin. *Polymer* **10**, 810-826 (1969).
18. Vogel, S. *Comparative Biomechanics: Life's Physical World* (Princeton University Press, 2003).
19. Mandelkern, L. *Crystallization of Polymers* (Cambridge University Press, Cambridge, U.K., 2002).
20. Wollants, P., Roos, J. R. & Delanay, L. Thermally- and Stress-Induced Thermoelastic Martensitic Transformation in the Reference Frame of Equilibirium Thermodynamics. *Progress in Materials Science* **37**, 227-288 (1993).
21. Liu, Y. & Yang, H. Strain Dependence of the Clausius-Clapeyron Relation for Thermoelastic Martensitic Transformations in NiTi. *Smart Materials and Structures*, S22-S27 (2007).
22. Quillin, M. L. & Matthews, B. W. Accurate Calculation of the Density of Proteins. *Acta Crystallographica, Section D: Biological Crystallography* **D56**, 791-794 (2000).
23. Rapoport, H. S. PhD Thesis, in *Scripps Institution of Oceanography* (University of California, San Diego, La Jolla, CA, 2003).

24. Chiou, J.-S. et al. The α-Helix to β-Sheet Transition in Poly(L-lysine): Effects of Anesthetics and High Pressure. *Biochimica et Biophysica Acta* **1119**, 211-217 (1992).
25. Feughelman, M. *Mechanical Properties and Structure of Alpha-keratin Fibres: Wool, Human Hair, and Related Fibres* (University of South Wales Press, 1997).
26. Hearle, J. W. S. A Critical Review of the Structural Mechanics of Wool and Hair Fibres. *International Journal of Biological Macromolecules* **27**, 123-138 (2000).
27. Schwaiger, I., Sattler, C., Hostetter, D. R. & Rief, M. The Myosin Coild-Coil is a Truly Elastic Protein Stucture. *Nature Materials* **1**, 232-235 (2002).
28. Root, D. D., Yadavalli, V. K., Forbes, J. G. & Wang, K. Coiled-Coil Nanomechanics and Uncoiling and Unfloding of the Superhelix and *a*-helices of Myosin. *Biophysical Journal* **90**, 2852-2866 (2006).
29. Fudge, D. S., Gardner, K. H., Forsyth, V. T., Riekel, C. & Gosline, J. M. The Mechanical Properties of Hydrated Intermediate Filaments: Insights from Hagfish Slime Threads. *Biophysical Journal* **85**, 2015-2027 (2003).
30. Kouzeli, M., Weber, L., SanMarchi, C. & Mortensen, A. Quantification of Microdamage Phenomena During Tensile Straining of High Volume Fraction Particle Reinforced Aluminium. *Acta Materialia* **49**, 497-505 (2001).
31. Despois, J.-F., Mueller, R. & Mortensen, A. Uniaxial Deformation of Microcellular Metals. *Acta Materialia* **54**, 4129-4142 (2006).
32. Gupta, H. S. et al. Cooperative Deformation of Mineral and Collagen in Bone at the Nanoscale. *Proceedings of the National Academy of Sciences of the United States of America* **103**, 17741-17746 (2006).
33. Paris, O. et al. A New Experimental Station for Simutaneous X-Ray Microbeam Scanning for Small- and Wide-Angle Scattering and Fluorescence at BESSY. *Journal of Applied Crystallography* **40**, S466-S470 (2007).

Chapter 4. Using wide angle x-ray scattering to characterize the phase transition from α-helix to β-sheet as a result of uniaxial tension

***A. Abstract*:**

Synchrotron source x-ray radiation has been a valuable tool in the structural analysis of biological materials. This tool can be coupled with *in situ* tensile testing to provide additional information on how structural changes directly effect the mechanical properties of such materials. The following study uses this approach to analyze the α-helix ↔ β-sheet transition in a proteinaceous material that marine gastropods use in egg capsules. This material displays remarkable shape memory behavior and it has been theorized that an α-helix ↔ β-sheet transition is responsible for the mechanical properties associated with that behavior. Evidence is presented that the cooperative rupturing and reforming of the hydrogen bonds that stabilize these two protein secondary structure is directly related to changes in modulus, as well as hysteresis throughout an entire shape memory cycle.

B. Introduction:

Shape memory materials are being developed for a wide range of applications including heavy construction (in bridges, for example)[1-3], switches and actuators[4-6], and implanted biomedical devices (vascular stents[7-9] and encapsulants[10]). Reversible crystalline transitions have been implicated in a variety of shape memory materials including metal alloys[11], synthetic polymers[12-14], and biological materials[15]. In these systems, when an external force is placed on the material, a shift in the atomic lattice occurs to accommodate it, resulting in a change in crystal structure to a metastable state. Once the force is removed, the material returns to the original, more thermodynamically favorable crystalline conformation.

The strain induced α-helix ↔ β-sheet transition has been observed in keratin fibers via x-ray scattering since 1931[16]. As coiled-coil α-helices are subjected to a load along the fiber axis, the hydrogen bonds responsible for the stabilization of the helices rupture and the peptide unravels and elongates. During this elongation, new hydrogen bonds are created between adjacent fibers, forming a β-sheet crystalline structure. When load is removed the process reverses, hydrogen bonds stabilizing the β-sheets rupture, and fibers return to the preferred α-helical conformation. This reversible transition contributes to a degree of shape memory properties in keratins[15,17].

This phenomenon has been observed in a variety of other intermediate filament-like fibers such as vimentin[18] and hagfish slime

threads[19], and has been conjectured to occur in other materials such as desmin[20] and fibrin in blood clots[21]. Once thought to be a one step transition wherein β-sheet content increased in direct correspondence with α-helix destruction and vice-versa[22], new evidence indicates that the transition is actually a two-step mechanism wherein α-helices unravel into non-crystalline random coils before a critical strain is reached, at which point the peptides will form hydrogen bonds and adopt a β-sheet conformation[23]. Numerous examples of human diseases are believed to result from the irreversible structural transition of α-helices to β-sheets[24] and of mutations to intermediate filament proteins[25,26]. As such, it is of fundamental importance that this phase transition be thoroughly examined.

The effect that a crystalline phase transition has on the tensile mechanical properties of a material has been reported for non-biological systems such as shape memory alloys[11] and synthetic shape memory polymers[12]. However, although there is considerable speculation on the subject[17,23], how the α-helix ↔ β-sheet transition affects the tensile properties of protein fibers has not been directly investigated. One model system that is particularly well suited for doing this is the egg capsule wall of marine prosobranch gastropods, commonly know as whelks. This material demonstrates long-range reversible extensibility and recent studies have shown that this property is the result of the α-helix ↔ β-sheet transition rather than entropic elasticity[10]. It is suggested that this transition contributes

heavily to the remarkable shape memory properties of this material which have been studied extensively[10,27,28]. The following report utilizes wide angle x-ray scattering (WAXS) with *in situ* tensile testing to directly correlate changes in protein secondary structure to mechanical properties in real time and on the same sample.

C. Materials and Methods:

Busycotypus canaliculatus egg capsules were purchased from the Marine Biological Laboratories (Woods Hole, MA). Capsules were cut with a razor into approximately 5 X 10 mm strips and washed repeatedly in DI water using gentle physical disruption to remove the mucous lining. The exact thickness and width of each strip was measured by micrometer.

A custom-made, portable uniaxial tensile testing apparatus called the Micro-mechanical Tensile Apparatus (MiTA) was used[29]. A nebulizer directed water vapor to ensure complete hydration of the sample throughout the complete tensile cycle. A strain rate of 8 μm/sec was used for both extension and relaxation and grip separation distance of the device calipers was used for sample length. There was no pause between extension and relaxation. Results are given in Engineering stress vs strain.

Data collection was performed on the MuSpot beamline at the BESSY synchrotron source (Berlin Elektronenspeicherring Gesellschaft m.b.H., Berlin, Germany)[30] with an X-ray wavelength of 1.0 Å and a beam

size of 30 μm. Beamline calibration was carried out with a corundum (Al_2O_3) standard, giving a sample to detector distance of 256.39 mm. A 2D CCD detector (MarMosaic 225, Mar USA, Evans- ton, USA) with pixel size of 73.24 μm and resolution of 3072 X 3072 pixels was used to acquire the WAXS frames.The MiTA was situated so that the sample was directly in the beamline to perform realtime *in situ* tensile testing. Samples were exposed to x-rays for 30 second durations while the MiTA was actively recording tensile data. As the strain rate was so low, the engineering strain of the sample sample changed by no more than 2% during exposure times.

Analysis was performed using the Fit2D program[31]. Intensity around the meridian and equator was integrated radially using the CAKE command, and the shift and change in peaks were tracked as a function of externally applied stress and strain. Background (empty beam) intensities were at least an order of magnitude smaller than the intensity from the sample at the wavevectors corresponding to both the α-helix 0.53 nm and β-sheet 0.47 nm reflections, and were not subtracted separately but were included in the linear background term. To account for the decrease in sample thickness during stretching, a scaling factor that allowed the intensity profiles to superimpose at wide diffraction angles was applied, as described previously[23].

***D. Results*:**

When a protein material is exposed to x-rays, the two dimensional scattering pattern can indicate the secondary structure crystallinity, as well as the orientation of these structures in the material. The the WAXS data presented below focus on the α-helix and β-sheet specific peaks corresponding to 0.53 nm along the meridian and 0.47 nm along the equator respectively (Fig 4.1). These values have been previously established and detailed[23]. The weak β-sheet specific 0.33 nm peak along the meridian was unfortunately obscured by an amorphous halo in the scattering data.

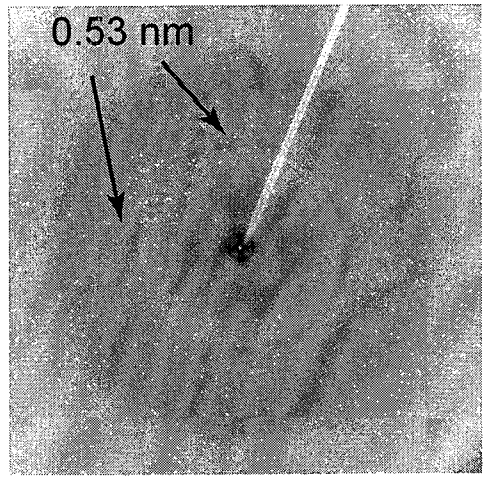

0% Strain

WAXS of an unstrained sample produces a double peak around 0.53 nm along both the meridian and the equator indicative of coiled-coil α-helices. (Fig 4.2). These data suggest that this material has coiled-coil α-helical fibers running orthogonally at

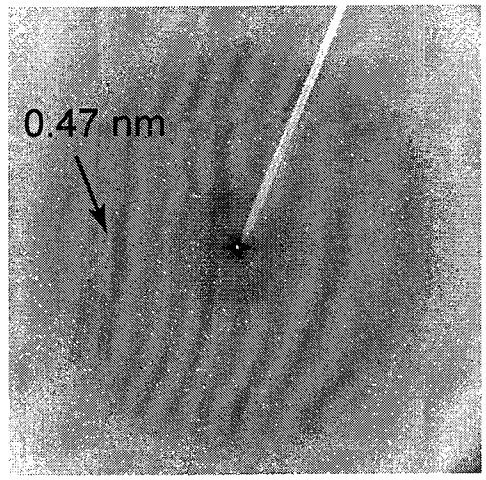

100% Strain

90° to each other, producing these spacings along both equatorial and meridianal axes which is in agreement with previously published findings[10].

Figure 4.1. Two dimensional WAXS frames of whelk egg capsules at 0% and 100% strain. At 0%, the material displays banding patterns characteristic of α-helical fibers orthogonal to each other (0.53 nm along both axes). At 100%, the pattern changes to displaying β-sheet structure along the axis of extension (0.47 nm along the equator).

WECB is comparatively stiff at strains up to ~4% with a modulus of 69.67 MPa. After this point, there is a yield event as flow modulus drops dramatically to 1.69 MPa. This results in a post-yield plateau between 4% and 45% where this stiffness is maintained. Just past 45% strain, flow modulus increases to 12.31 MPa and is maintained until 100% strain which is in agreement with previous work[32].

The recovery curve differs drastically from the deformation curve, resulting in an energy dissipating hysteresis. First there is a very steep drop in stress as strain decreases from 100% to 65%. Then there is a recovery plateau wherein stress does not decrease much as strain lowers further to 10%. Below this point, stress decreases rapidly until it reaches 0 at 2.5% strain, indicating some non-recoverable plastic deformation in the material. (Fig 4.3).

Previous studies have detailed the repeatability of multiple load cycles on the same sample (Fig 4.3 inset)[32]. As the tensile data here are consistent with these previous works through one complete cycle, multiple cycles on these samples were not conducted.

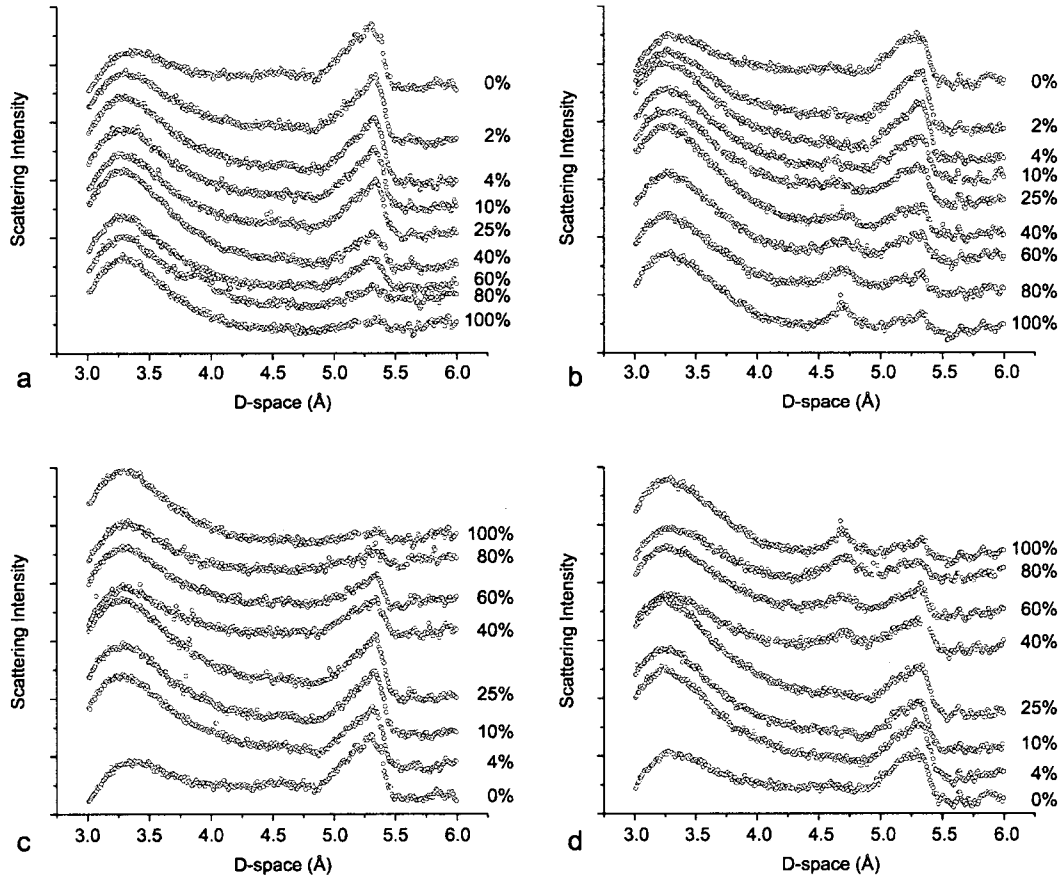

Figure 4.2. One dimensional WAXS plots of whelk egg capsules as they are being extended to 100% strain, and as they are being relaxed back to 0% after this extension. a) and b) represent the meridian and equator respectively under tension. The 0.53 nm meridian peak corresponding to α-helix structure decreases while the 0.47 nm equator peak corresponding to β-sheet structure increases. c) and d) are the meridian and equator during relaxation after extension. Here the transition reverses with α-helix intensity increasing while β-sheet intensity decreases.

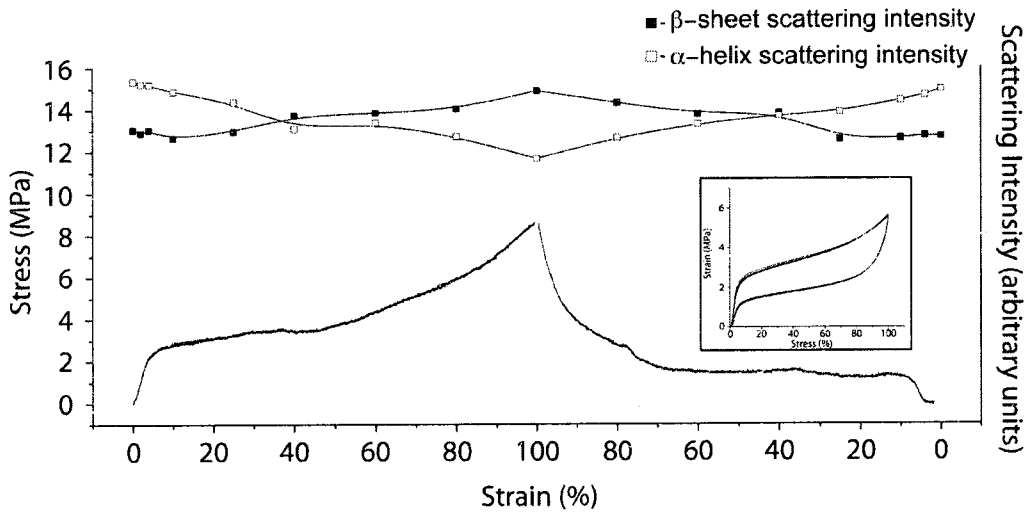

Figure 4.3. Tensile and structural data for a complete shape memory cycle, extension to 100% strain and relaxation back down to 0% strain. α-helix unraveling during extension and formation during relaxation occurs at a fairly constant rate while β-sheet formation and destruction happens in a stepwise manner, supporting the two step α-helix ↔ β-sheet transition model. Inset is a stress strain curve of whelk egg capsules undergoing sequential shape memory cycles to demonstrate the repeatability of the tensile behavior.

As the material is uniaxially strained from 0% - 4%, the intensity and location of the double peak at 0.53 nm does not change (Figs 4.2a,b and 4.3). However, once the material is strained beyond the yield point, the intensity of the meridian 0.53 nm peak begins to decrease indicating that the α-helices aligned along this axis of stress are unraveling. However, there is no indication of β-sheet formation as there is no increase in the 0.47 nm equatorial peak. This peak does not appear until the material reaches 40% strain, just before the material starts to restiffen at 45% strain. As it is extended past 45% strain, this β-sheet specific peak increases in intensity

until 100% strain is reached. By this point the 0.53 nm meridian peak has almost completely vanished.

It should also be noted that during this loading cycle that the 0.53 nm peak on the equator, corresponding to the α-helices that are perpendicular to the axis of tension decreases in intensity. This is not due to unraveling of α-helices, but is likely due to the decrease in α-helical fiber density along this axis. A model for this has been previously published[27].

Upon relaxation after 100% strain, the order of events is similar to a step by step reversal of the α ⟶ β transition that occurred under tension (Figs 4.2c,d and 4.3). First the 0.47 nm equator peak decreases in intensity as the material relaxes towards 40% strain while, simultaneously, the 0.53 nm meridian peak intensity increases. Once the material relaxes further, the 0.47 nm peak disappears entirely, but the 0.53 nm does not return to maximum intensity until strain drops below 10%. This corresponds in the downward "jump" in the stress strain relationship at ~9%.

***E. Discussion*:**

Recently synchrotron source x-ray radiation has been combined with *in situ* tensile mechanical testing to directly investigate the change in morphological crystallinity in materials while they are being put under uniaxial load. Studies have focused on both wide angle and small angle scattering on synthetic polymers[33-35] as well as biological materials such as

collagen[36], silk[37], and the mussel byssus[38]. Although synchrotron x-ray studies have been applied to study the α-helix ↔ β-sheet transition in keratins while extended[23], this is the first study to couple WAXS with *in situ* mechanical testing on the same sample to examine the secondary structure changes throughout a complete shape memory cycle (extension and relaxation).

Data presented here are in agreement with previous studies suggesting that the α-helix → β-sheet transition is a two step mechanism wherein the α-helices first unravel into an non-crystalline intermediate before locking into β-sheets after extended further[23]. α-helix structure is completely maintained throughout the pre-yield region up to ~5% strain and it is only after the mechanical yield point that the α-helix content begins to decrease. This provides clear evidence that helix-stabilizing hydrogen bonds remain intact during the initial high modulus region, and that the rupturing of these bonds directly corresponds with the decrease in stiffness of the material, and supports the model that some supramolecular mechanism, such as fibril sliding, is responsible for the initial high modulus, but that when the hydrogen bonds rupture under load, the unzippering of the α-helices causes the dramatic decrease in stiffness observed at the yield point (Fig 4.4).

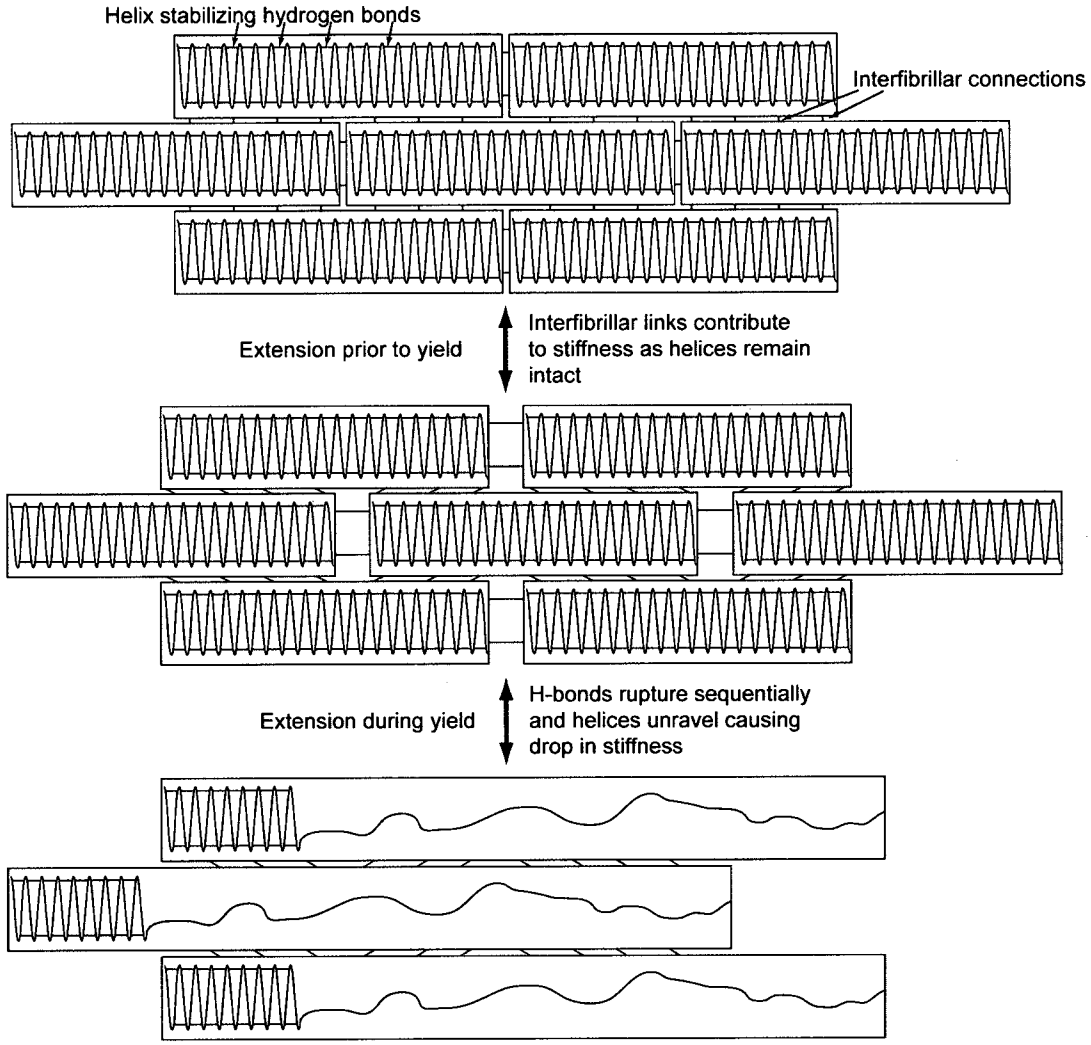

Figure 4.4. Schematic for the contributions of interfibrillar interactions and hydrogen bonding to modulus before and during yielding. The exact nature of the interfibrillar interactions (direct crosslinks, matrix interactions, etc) is unknown as of this point.

Stiffness does not increase again until β-sheet formation begins. A previous model contends that this restiffening in keratin is the result of α-helix unraveling reaching high density cystine crosslink regions in the fiber.

Although this cannot be discounted in the keratin system, whelk egg capsule proteins do not have cystine crosslinks. Additional work into the precise nature of covalent crosslinks in these proteins will be needed to apply this model to the whelk egg capsule system. However, data here provide direct evidence to support a hypothesis that the increase in hydrogen bond density resulting from β-sheet formation causes this increase in modulus.

As the material relaxes from 100% to 0% strain, the secondary structure transition reverses. It is proposed here that this is also a two step mechanism wherein β-sheets first break down into random coils before forming α-helices. This is supported by the fact that although β-sheet destruction is complete somewhere between 40% and 25% strain, α-helix formation continues until past 10% strain, indicating that helices are being formed from random coils at this point. However, although this β-sheet $\longrightarrow$ α-helix crystalline phase transition is seemingly a mirror image of the α-helix $\longrightarrow$ β-sheet transition observed during extension, the stress strain profile is vastly different upon relaxation, resulting in a large hysteresis loop.

Hysteresis is typically attributed to either internal friction of material components, the existence of metastable equilibria associated with the system dynamics, or a combination thereof[11,39,40]. Although there is a great body of literature on the mechanics of the α-helix $\longrightarrow$ β-sheet transition in keratins, there a relative dearth regarding the β-sheet $\longrightarrow$ α-helix transition and the hysteresis that accompanies it. One model suggests that the

reforming of stabilizing electrostatic interactions is slowed during relaxation and that this combined with interfibrillar friction causes the observed hysteresis, and is based off of tensile testing in media at varied pH[41]. As the pH is lowered further, the proteins shift to positive net charges, disrupting native electrostatic interactions and reducing hysteresis. However, the same effect is observed when whelk egg capsules are exposed to heated water[10] and non-charged denaturants such as urea[42], both of which should have no effect on electrostatics. Likely, the acidity of the media changes the charge structure of helix forming residues' side chains, such as glutamate, and render them less prone to forming α-helices.

Additionally, this model does not take into account that once β-sheets are formed and stabilized by hydrogen bonds, it will take an energy input to rupture these bonds. The amount of force required to rupture a hydrogen bond is ~4 pN, and force spectroscopy studies on β-amyloid fibers has shown that upwards of several hundred pN is required to rupture all of the β-sheet structure of a single molecule[43]. Figure 4.5 shows that during relaxation, β-sheets are stable at much lower stresses than they are during extension indicating that additional energy is required to rupture these bonds.

Although the energy required to rupture the β-sheet stabilizing hydrogen bonds does contribute to the hysteresis of the material, there must be an additional component. This is evidenced by the fact that during

relaxation the stress values at a given strain are always less than those values at the same strain during extension. If the energy to break β-sheets was the only contributing factor, the relaxation stress values would equal the corresponding extension values once all of the β-sheets were destroyed. However, this is not the case, and it is possible that interfibrillar friction is responsible for this.

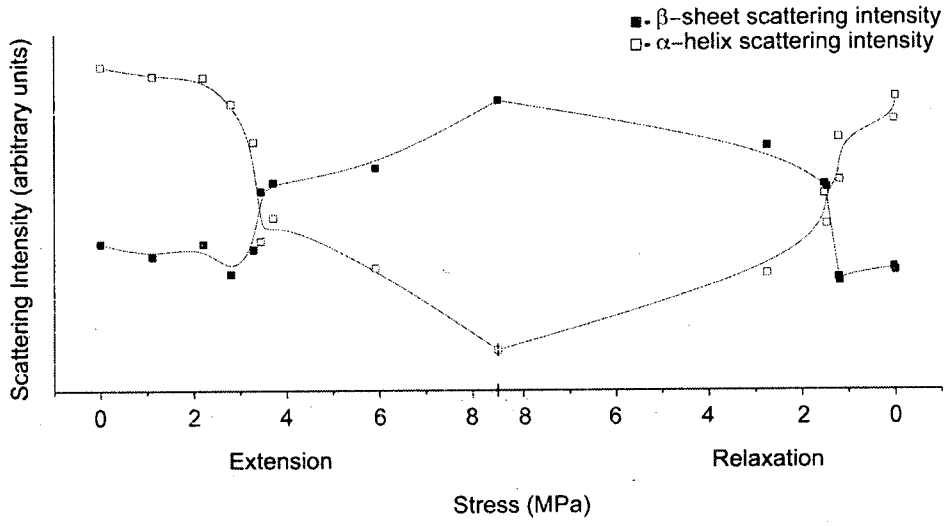

Figure 4.5. Plot of α-helix and β-sheet scattering intensities versus stress. During the relaxation part of the cycle, β-sheets exist at lower stresses suggesting that they are more stable and require additional energy be destroyed.

Figure 4.6 summarizes the current model for how the α-helix ↔ β-sheet transition directly affects tensile mechanics.

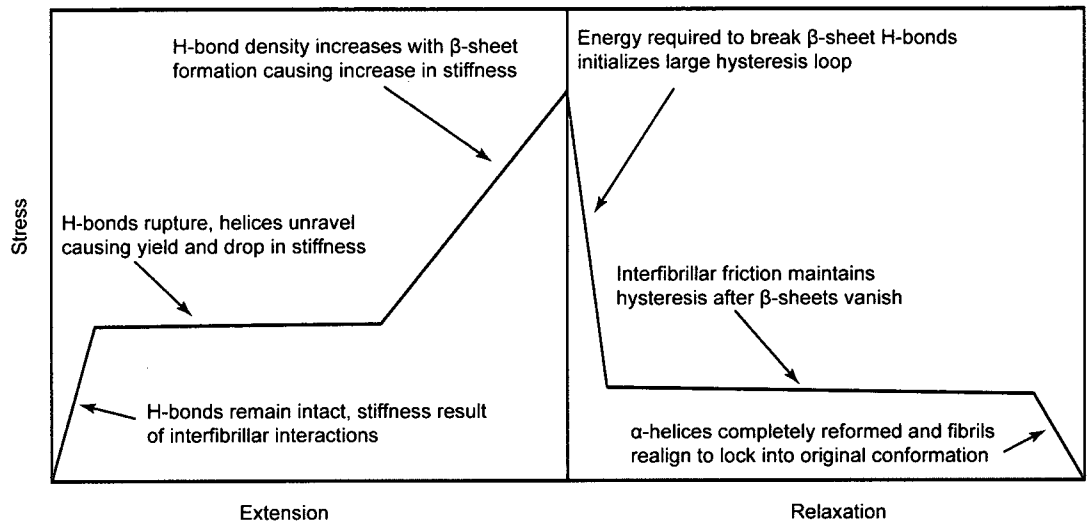

Figure 4.6. Schematic for how the hydrogen bond formation and breaking during the α-helix ↔ β-sheet transition contributes to tensile properties during a complete shape memory cycle. Figure not drawn to scale.

F. Conclusions:

Data presented here indicate that the destruction and formation of secondary structure stabilizing hydrogen bonds directly correspond with the changes in mechanical properties of whelk egg capsules. The α-helix ↔ β-sheet transition is a two step mechanism wherein the cooperative forming and rupturing of these hydrogen bonds throughout a shape memory cycle contribute to tensile properties such as modulus and hysteresis. During extension, initial high stiffness is attributed to α-helices remaining intact and interfibrillar slippage. When hydrogen bonds rupture at the yield point, helices unravel causing a decrease in modulus until β-sheets form. At this

point, hydrogen bond density increases again, increasing stiffness. During relaxation, the energy required to break these β-sheet stabilizing hydrogen bonds initiates the hysteresis loop. Once all β-sheets have broken down, interfibrillar friction likely contributes to the continued hysteresis until the material relaxes back to 0% strain.

G. Acknowledgements

Thanks are due to H. Gupta (Max-Planck Institute for Colloids and Interfaces, Golm, Germany) for assistance with the time-resolved WAXS synchrotron experiments. S.W. was financially supported by a California Sea Grant # R/MP-97B and UC BREP GREAT traineeship #2007-02.

I. References:

1. DesRoches, R., & and Delemont, M. Seismic retrofit of simply supported bridges using shape memory alloys, *Eng. Struct.* **42**, 325-332 (2002).
2. Song, G., Ma, N., & Li, H. N. Applications of shape memory alloys in civil structures. *Eng Struct.* **28**, 1266-1274 (2006).
3. Desroches, R., & Smith, B. Shape memory alloys in seismic restraint design and retrofit: A critical review of their potential and limitations. *J. Earthquake Eng.* **7**, 1–15 (2003).
4. Seelecke, S., & Müller, I. Shape memory alloy actuators in smart structures: Modeling and simulation. *Appl. Mech. Rev.* **57**, 23-46 (2004).
5. Liang, C., & Rogers, C. A. Design of Shape Memory Alloy Actuators. *J. Intell. Mater. Syst. Struct.* **8**, 303-313 (1997).
6. Tabib-Azar, M., Sutapun, B., & Huff, M. Applications of TiNi thin film shape memory alloys in micro-opto-electro-mechanical systems. *Sens. Actuators A* **77**, 34-38 (1999).
7. Wache, H. M., Tartakowska, D. J., Hentrich, A., & Wagner, M. H. Development of a polymer stent with shape memory effect as a drug delivery system. *J. Mater. Sci. - Mater. Med.* **14**, 109-112 (2003).
8. Morgan, N. B. Medical shape memory alloy applications—the market and its products. *Mater. Sci. Eng. A.* **378**, 16-23 (2004).
9. Lendlein, A., & Langer, R. Biodegradable, Elastic Shape-Memory Polymers for Potential Biomedical Applications. *Science* **296**, 1673 - 1676 (2002).
10. Miserez, A., Wasko, S. S., Carpenter, C. F., & Waite, J. H. Non-entropic and reversible long-range deformation of an encapsulating bioelastomer. *Nat Mater* **8**, 910-916 (2009).
11. D. C. Lagoudas (Editor). *Shape Memory Alloys*. Springer Science Media LLC. New York, NY. (2008)
12. Pereira, I. M., & Orèfice, R. The morphology and phase mixing studies on poly(ester–urethane) during shape memory cycle. *J. Mater. Sci.* **45**, 511-522 (2010).
13. Ichikawa, Y., Washiyama, J., Moteki, Y., Noguchi, K., & Okuyama, K. Crystal Transition Mechanisms in Poly(tetramethylene succinate). *Polym. J.* **27**, 1230 -1238 (1995).
14. Apostolov, A. A., Fakirov, S., Stamm, M., Patil, R. D., & Mark, J. E. Alpha-Beta Transition in Poly(butylene terephthalate) As Revealed by Small-Angle X-ray Scattering. *Macromolecules* **33**, 6856-6860 (2000).
15. Feughelman, M. *Mechanical Properties and Structure of Alpha-Keratin Fibres: Wool, Human Hair, and Related Fibres*, UNSW Press: Sydney, Australia, 1997.
16. Ashbury, W. T., & Street, A. X-ray studies of hair, wool, and related fibres - I: General. *Philos. Trans. R. Soc. London, Ser. A* **230**, 75-101 (1931).
17. Hearle. J. A critical review of the structural mechanics of wool and hair fibres. *Int. J. Biol. Macromol.* **27**, 123–138 (2000).
18. Qin, Z., Kreplak, L., & Buehler, M. J. Nanomechanical properties of vimentin intermediate filament dimers. *Nanotechnology* 20, 425101-9 (2009).
19. Fudge, D., Gardner, K., Forsyth, V., & Riekel, C. The Mechanical Properties of Hydrated Intermediate Filaments: Insights from Hagfish Slime Threads. *Biophys. J.* **85**, 2015–2027 (2003).
20. Kiss, B., Karsai, A., & Kellermayer, M. S. Z. Nanomechanical properties of desmin intermediate filaments. *J. Struct. Biol.* **155**, 327–339 (2006).
21. Lim, B. B.C., Lee, E. H., Sotomayor, M., & Schulten, K. Molecular basis of fibrin clot elasticity. *Structure* **16**, 449-59 (2008).
22. Bendit, E. G. A quantitative x-ray diffraction study of the alpha-beta transformation in wool keratin. *Text. Res. J.* **30**, 547–555 (1960).

23. Kreplak, L., Doucet, J., Dumas, P., & Briki, F. New Aspects of the α-Helix to β-Sheet Transition in Stretched Hard α-Keratin Fibers. *Biophys. J.* **87**, 640–647 (2004).
24. Stefani, M., & Dobson, C. M. Protein aggregation and aggregate toxicity: new insights into protein folding, misfolding diseases and biological evolution. *J. Mol. Med.* **81**, 678-699 (2003).
25. Lazarides, E. Intermediate filaments as mechanical integrators of cellular space. *Nature* **283**, 249–256 (1980).
26. Bonne, G., Di Barletta, M. R., Varnous, S., Becane, H. M., Hammouda, E. H., Merlini, L. et al. Mutations in the gene encoding lamin A/C cause autosomal dominant Emery-Dreifuss muscular dystrophy. *Nat Genet* **21**, 285–288 (1999).
27. Rapoport, H. S., & Shadwick, R. E. Reversibly labile, sclerotization-induced elastic properties in a keratin analog from marine snails: whelk egg capsule biopolymer (WECB). *J. Exp. Biol* 210, 12-26 (2007).
28. Rapoport, H. S., *Biomechanics, Biochemistry, and Molecular Biology of a Molluscan Scleroprotein Elastomer: Whelk Egg Capsule Biopolymer*, in *Marine Biology*. PhD thesis. University of California San Diego (2003).
29. Gupta, H.S., Seto, J., Wagermaier, W., Zaslansky, P., Boesecke, P., Fratzl, P., Cooperative deformation of mineral and collagen in bone at the nanoscale. *Proc. Natl. Acad. Sci. USA* **103**, 17741–17746 (2006).
30. Paris, O., Li, C.H., Siegel, S., Weseloh, G., Emmerling, F., Riesemeier, H., Erko, A., Fratzl, P. A new experimental station for simultaneous X-ray microbeam scanning for small- and wide-angle scattering and fluorescence at BESSY II. *J. Appl. Crystallogr.* **40**, S466–S470 (2007).
31. Hammersley, A. FIT2D: an introduction and overview. ESRF Internal Report ESRF97HA02T. (1997)
32. Wasko, S. S., & Waite, J. H. Structural proteins from an egg capsule with nonentropic reversible extensibility. Submitted to: *Biomacromolecules*, under review (2010).
33. Feldman A. Y., , Wachtel, E., Zafeiropoulos, N. E., Schneider, K., Stamm, M., R. J., Davies· Weinberg, A., & Marom, G. In situ synchrotron microbeam analysis of the stiffness of transcrystallinity in aramid fiber reinforced nylon 66 composites. *Compos. Sci. Technol.* 66, 2009-20015 (2006).
34. Davies, R. J., Zafeiropoulos, N. E., Schneider, K., Roth, S. V., Burghammer, M., Riekel, C., Kotek, J. C., & Stamm, M. The use of synchrotron X-ray scattering coupled with in situ mechanical testing for studying deformation and structural change in isotactic polypropylene. *Colloid. Polym. Sci.* 282, 854-866 (2004).
35. Wu, J., Schultz, J. M., Yeh, F., Hsiao, B. S., & Chu, B. In-Situ Simultaneous Synchrotron Small- and Wide-Angle X-ray Scattering Measurement of Poly (vinylidene fluoride) Fibers under Deformation. *Macromolecules*, 33, 1765 – 1777 (2000).
36. Gupta, H.S., Seto. J., Krauss, S., Boesecke, P., & Screen H. R. C. In situ multi-level analysis of viscoelastic deformation mechanisms in tendon collagen. *J. Struct Biol.* **169**, 183–191 (2010)
37. Seydel, T., Kölln, K., Krasnov, I., Diddens, I., Hauptmann, N., Helms, G., Ogurreck, M., Kang, S., Koza, M. M., & Müller, M. Silkworm Silk under Tensile Strain Investigated by Synchrotron X-ray Diffraction and Neutron Spectroscopy. *Macromolecules* **40**, 1035-1042 (2007).
38. Harrington, M. J., Gupta, H. S., Fratzl, P., Waite, J. H. Collagen insulated from tensile damage by domains that unfold reversibly: In situ X-ray investigation of mechanical yield and damage repair in the mussel byssus. *J. Struct. Biol.* **167**, 47-54 (2009).
39. Sethna, J. P., Dahmen, K., Kartha, S., Krumhansl, J. A., Roberts, B. W., & Shore, J. D. Hysteresis and Hierarchies: Dynamics of Disorder-Driven First-Order Phase Transformations. *Phys. Rev. Lett.* **70**, 3347 (1993)

40. Dahmen, K., Kartha, S., Krumhansl, J. A., Roberts, B. W., Sethna, J. P., & Shore, J. D. Disorder-driven first-order phase transformations: A model for hysteresis, Karin Dahmen, Sivan Kartha, *J. Appl. Phys.* **75**, 5946 (1994)
41. Feughelman. M. Mechanical hysteresis in wool keratin fibers. *J. Macromol. Sci. Part B Phys.* **7**, 569 - 582 (1973).
42. Non-published observations.
43. Kellermayer, M. S. Z., Grama, L., Karsai, A., Nagy, A., Kahn, A., Datki, Z. L., & Penke, B. Reversible Mechanical Unzipping of Amyloid β-Fibrils. *J. Biol Chem.* **280**, 8464–8470 (2005)

Chapter 5. The supramolecular hierarchical ordering of *Busocotypus canaliculatus* egg capsules and its role in tensile mechanics

A. Abstract

Whelk egg capsules are peculiar biomaterials with extraordinary shape memory properties resulting, not from entropic elasticity, but from a crystalline phase transition in the protein components. Although the behavior of these components has been extensively studied at the single protein and multimer level, little is known about the hierarchical ordering of this material and how that may contribute to the unique mechanical properties exhibited. Scanning electron microscopy (SEM) and atomic force microscopy (AFM) along with small angle x-ray scattering (SAXS) were employed to investigate this ordering. Then, using a combination of time-resolved synchrotron SAXS together with tensile testing of egg capsule walls under physiologically wet conditions, the deformation at the nanoscale was measured from changes in the meridianal diffraction pattern. Results show that this material is very hierarchical in its structure, and that effects from single protein phase transitions as well as nanometer scale fibrillar components combine in different proportions at different regions of the stress strain relationship to dictate the overall mechanical properties of whelk egg capsules in tension.

B. Introduction

The proteinaceous egg capsules produced by marine prosobranch gastropods (whelks) are remarkable examples of shape memory/self healing materials. The tensile properties have been studied extensively[1-3] and models for the long range, reversible extensibility have been presented[4]. Briefly, the material undergoes a crystalline phase transition from α-helix to β-sheet when placed under tension. When the load is removed, the material relaxes back to the original α-helical conformation.

Although the unraveling of α-helices makes a major contribution to the extensibility and shape memory of this material, the involvement of larger (nanometer rather than Å) scale ordering has not yet been investigated. The supramolecular ordering of protein fibers into hierarchical assemblies is a common theme in biological materials[5-7] and is known to play a critical role in the mechanics of these systems. Indeed in some keratin models, while an α-helix ⇔ β-sheet phase transition is certainly responsible for long range deformation, changes in the surpamolecular ordering also play significant role in tensile properties[7,8]. Therefore, it is of great importance to look into the hierarchical arrangement of the egg capsule fibers in order to gain a more complete understanding of the structure-property relationships of this material under tension, from the single protein level, up through the fiber level, and eventually to the bulk material.

Utilizing the same methods that have greatly advanced the understanding of tendon collagen structure under loading[9-12], this study combines scanning electron microscopy and tapping mode atomic force microscopy with high-resolution synchrotron based small angle x-ray scattering (SAXS) with real time tensile testing to investigate the structural reorganization occurring at the nano-length scales of the egg capsule fiber hierarchy during uniaxial loading, and builds a more detailed understanding of the local material mechanics. This, combined with what is already known about this material on a single protein level will provide a much more thorough knowledge of the structure/function relationship of egg capsules under mechanical tension.

C. Materials and Methods

Busycotupus canaliculatus egg capsules were obtained and prepared for experimentation exactly as described in the Materials and Methods section of Chapter 4 of this dissertation.

SEM sample preparation and image acquisition was performed as described in Chapter 3 of this dissertation. Analysis of the distances between bands in the micrographs was performed using the Vega TC software program (Tescan USA, Cranberry Twp., PA).

Egg capsule samples were cut into narrow strips with a razor and washed repeatedly with deionized water using gentle physical agitation to

remove the mucous lining. Measurements were taken using an MFP-3D AFM system (Asylum Research, Santa Barbara, CA) in tapping mode according to the manufacturers instructions. Dry measurements were taken by applying a wetted strip of egg capsule on a glass slide so that the cross section was exposed to the AFM probe. When the water evaporated, the sample adhered to the glass surface. Silicon probes were used for these measurements (Olympus America, Lakewood, CO). Wet measurements were taken by applying a strip of egg capsule to double-sided tape on top of a glass slide so that the cross section was exposed to the AFM probe. Silicon nitride probes were used for the measurements (Olympus America, Lakewood, CO). Data were analyzed by the Argyle software program provided by Asylum Research.

Tensile testing during x-ray analysis was conducted using the Micro-mechanical Tensile Apparatus (MiTA) described in the Chapter 4, using identical parameters. All other tensile testing was preformed using an MTS Bionix 200 (MTS, Eden Prairie, MN) tensile apparatus as described in Chapter 3. X-ray data collection was performed on the MuSpot beamline at the BESSY synchrotron source (Berlin Elektronenspeicherring Gesellschaft m.b.H., Berlin, Germany) also described in the Materials and Methods section of Chapter 4 using the same parameters for data acquisition, with the exception that the sample to detector distance was determined to be 906.39 mm using a corundum (Al_2O_3) standard.

Analysis of 2D SAXS frames was performed using the CAKE command of the Fit2D program, as described in Chapter 4. This resulted in a one-dimensional intensity profile of peak reflections from the 4th to the 9th order that are visible on both sides of the primary beam. The peaks corresponding to the different orders were fitted to a series of Gaussian functions to determine changes in D-spacing and measure fibril strain, ε_F, as described previously[11,12]. The current analysis only examines the meridian reflections.

D. Results

SEM images clearly show the fibrous nature of this material, with fiber strands typically ranging from 200 - 500 nm in diameter with some >1 μm (Fig 5.1a). These fibers occasionally, but not always, appear to be braided to form larger rope-like structures. Higher magnification of these fibers reveals a lateral banding pattern with elevated ridges of different widths occurring at repeated intervals (Fig 5.1b). The width of these bands was determined by analysis with the Vega TC software program and these numbers along with the pattern of the banding repeats is detailed in (Fig 5.2). Cross sections of the fibers were also imaged. These show a smaller scale ordering within the fibers that appear to be between 10 and 20 nm in diameter as well as some pores/voids (Fig 5.1c, d).

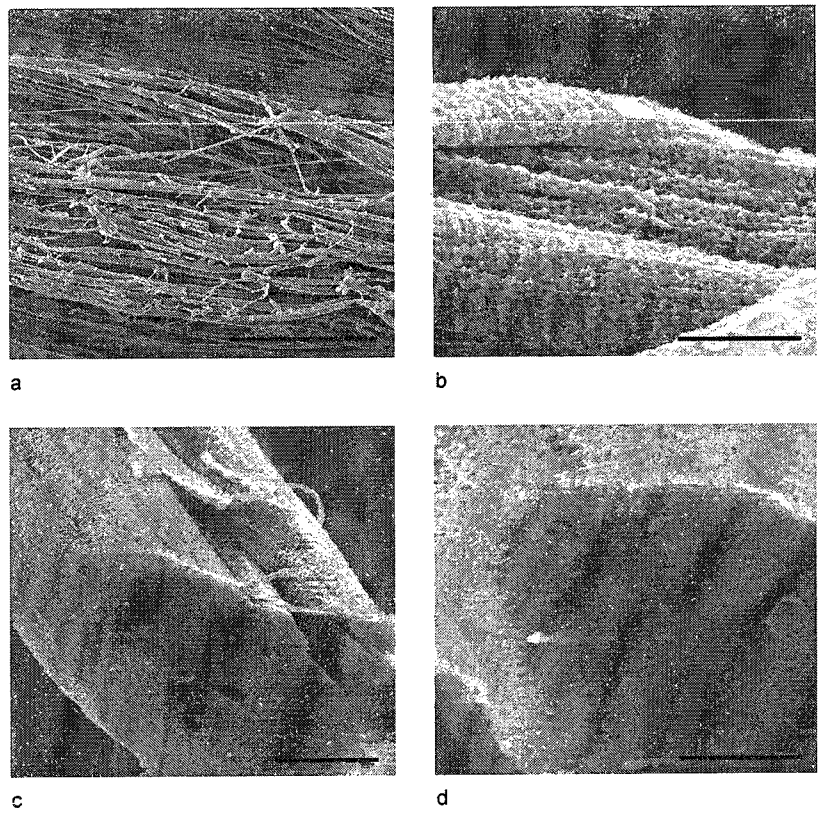

Figure 5.1. SEM images of whelk egg capsule fibers. a) shows fibrous nature and orientation of single fiber sheet. b) is a close up of a single braid of fibers which clearly show the lateral banding pattern. c) and d) are of cross sections of fibers and show some porosity as well as 10 - 20 nm structures that may be the cross sections of the smaller fibrils. Scale bars are as follows a) 20 μm, b) 500 nm, c) 1 μm, d) 500 nm.

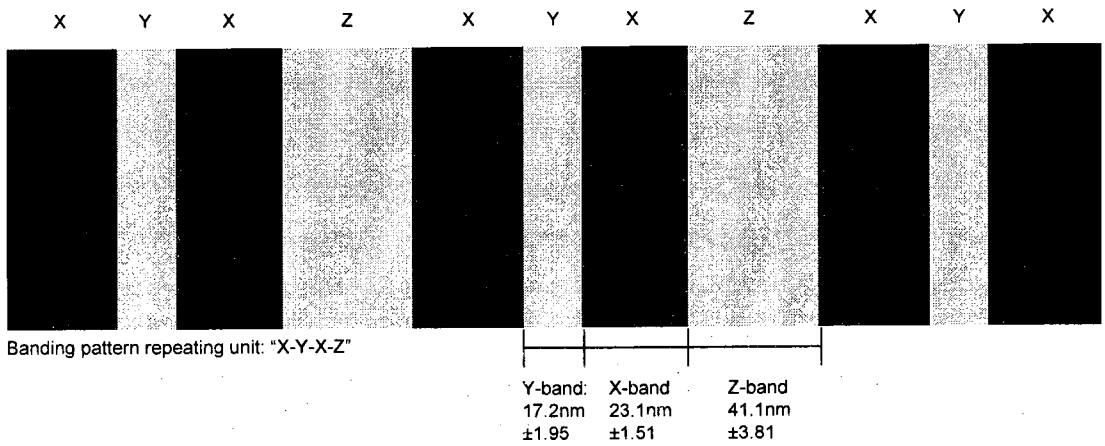

Figure 5.2. Schematic of the banding pattern observed in SEM images. Not drawn to scale.

Tapping mode AFM in air produced similar images to those taken by SEM, revealing fibers that are several hundred nanometers in diameter and with lateral ridges going across the fiber (Fig 5.3a). However, the banding patterns of these ridges is noticeably different than those observed by SEM. Here, there is no complex periodicity, rather there is just a constant sigmoidal ridge that is 93.8 ±8.5 nm (STDEV) across from peak to peak (Fig 5.3b). Furthermore, when AFM is performed under fully hydrated conditions, the pattern persists, but the peak to peak width changes to 98.0 ± 1.2 nm (STDEV) (Fig 5.4). One possible explanation for the inconsistencies between imaging methods is that sample preparation is vastly different: SEM requires a series of dehydration treatments as well as gold coating of the sample; dry AFM does not require coating of the sample and while the dehydration steps are not as thorough or harsh as those for SEM, the sample is still in a non-native (dehydrated) state; wet AFM keeps the sample in the most biologically native condition. As the SAXS studies also kept the samples fully hydrated during testing, all comparisons and analysis combining microscopy images with x-ray data will use the wet AFM images.

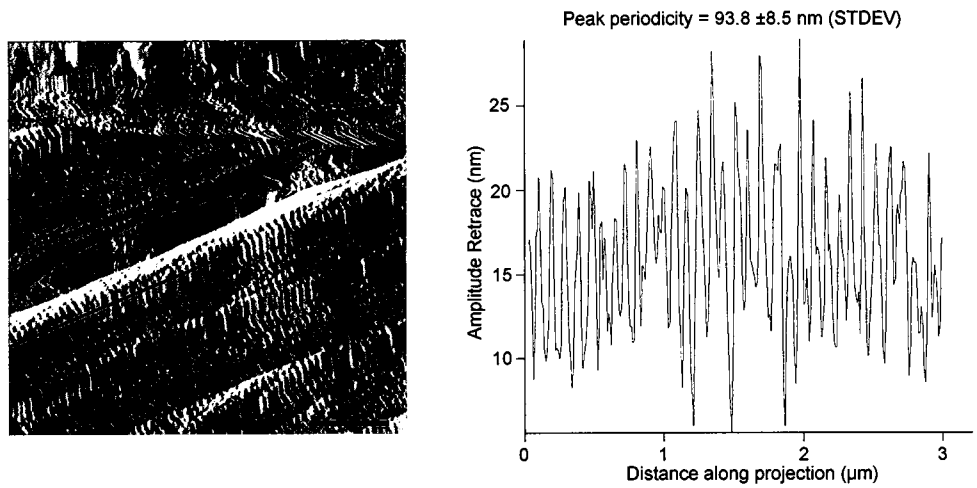

Figure 5.3. Tapping mode AFM done in air. The banding pattern observed is slightly different than what was observed in SEM. b) represents the amplitude of the topography taken along the blue projection line in a). Scale bar in a) is 1 µm.

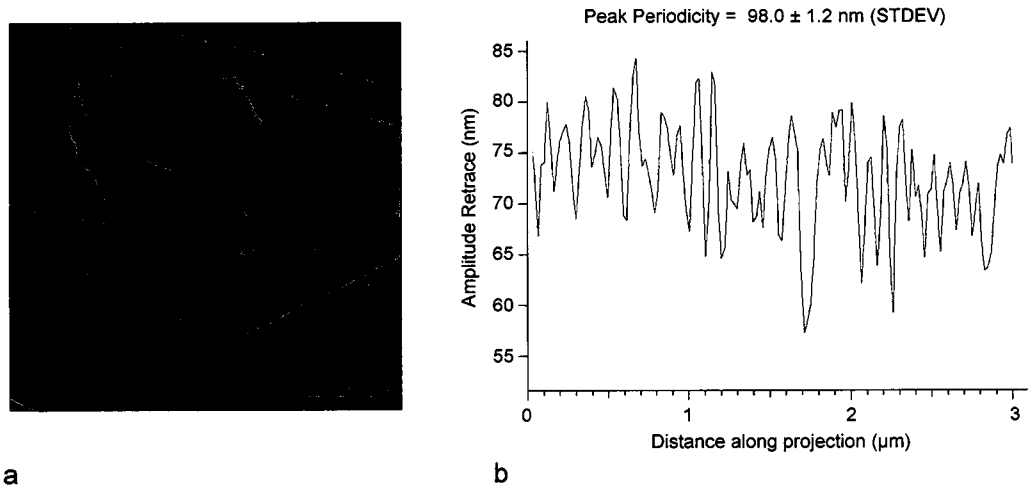

Figure 5.4. Tapping mode AFM done in water. The banding pattern observed is similar to that of the AFM done in air. However, the exact distances between peaks and valleys of the topography are slightly different. b) represents the amplitude of the topography taken along the blue projection line in a). Scale bar in a) is 2 µm.

X-ray scattering produced visible reflections from orders 4 - 9 along both the meridian and equator (Fig 5.5). To calculate the lateral diameter, R, of the scattering unit the relationship $R \propto 1/\delta q_{\perp}$ was applied. Using values from the n = 5 reflection for the equation

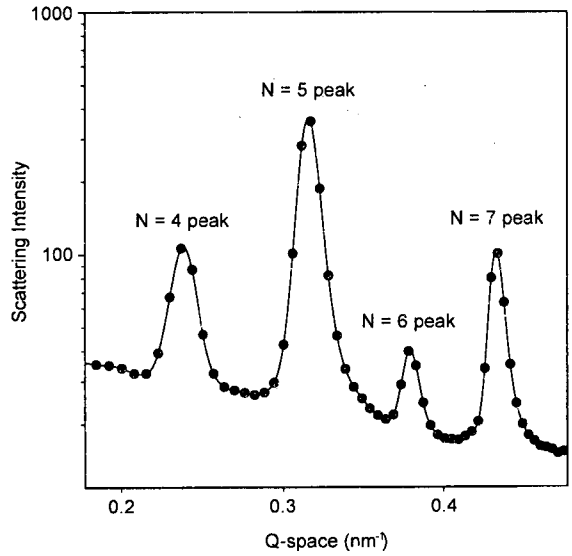

Figure 5.5. One dimensional plot of x-ray scattering intensity along the meridian axis showing the N = 4 - 7 peak reflections.

$$\delta q_{\perp} = 2q_m \times \sin(\delta\chi_{\perp}/2) \qquad (5.1)$$

Wherein χ is the angular coordinate of the reflection. $\delta q_{\perp} = 2 \times 0.315 \times \sin(20°/2) = 0.11\ nm^{-1}$. Previous studies[13] indicate that this value corresponds to a coherent length of ~9.1 nm for the radius of a single fibril (Fig 5.6). These may correspond to the 10 - 20 nm structures observed in the SEM cross sectional images of the fibers. This suggests that the several hundred nanometer diameter structures that were observed by microscopy are bundles of these fibrils.

To examine the axial ordering of these fibrils the relationship $q_n = 2\pi n/D$ was applied to each of the visible reflections. All resulted in a D space value of 99.8 nm which corresponds to the distances between lateral bands across fibrils (Fig 5.6). This is consistent with the 98.0 nm value measured by wet AFM.

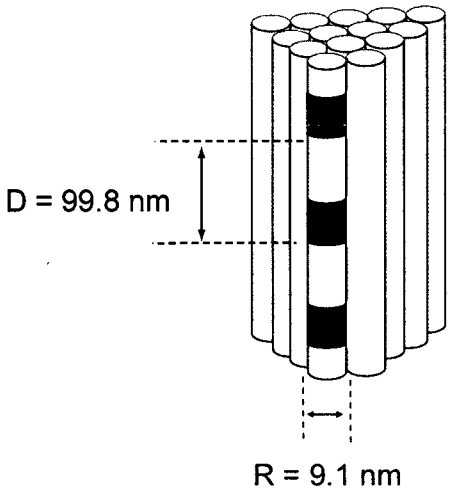

Figure 5.6. Schematic of fibril diameter and band distances as derived from SAXS data. Image is not

Tensile mechanical data for samples undergoing SAXS analysis were nearly identical in every way to the samples that underwent WAXS analysis in Chapter 4. No significant differences between the two data sets were noted.

As the material is extended in the pre-yield region (from 0% - ~5% engineering strain) there is little change in the intensity and location of the SAXS reflections. Once extended into the yield region (~5% - ~45% engineering strain) there is a significant decrease in peak intensity, but a negligible shift in peak position suggests a decrease in the crystalline ordering within these fibrils. As the material restiffens, the peak intensity increases again, and there is a significant shift in peak position suggesting a

new crystalline order has been established and is contributing to the mechanics (Fig 5.7).

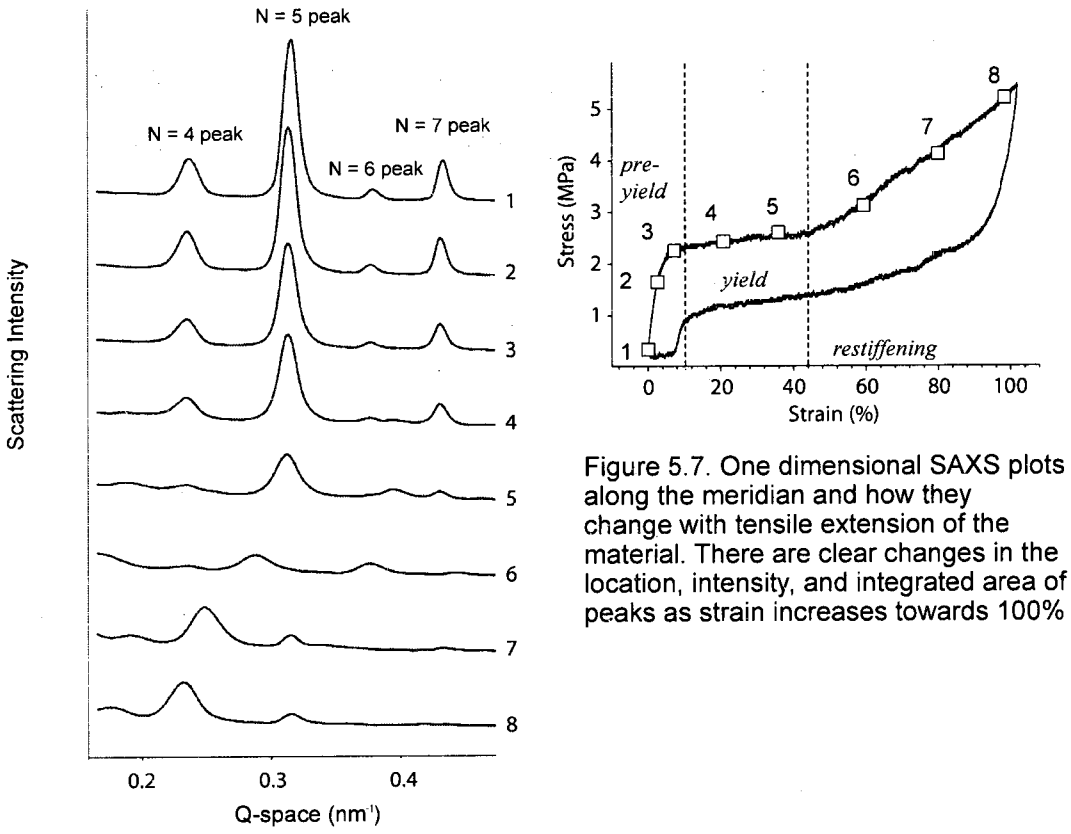

Figure 5.7. One dimensional SAXS plots along the meridian and how they change with tensile extension of the material. There are clear changes in the location, intensity, and integrated area of peaks as strain increases towards 100%

Fibril strain, ε_F, was calculated by the relationship:

$$\varepsilon_F = (D(\varepsilon)-D_o)/D_o \qquad (5.2)$$

wherein D_o is the 99.8 nm D-spacing of the fibril at rest and $D(\varepsilon)$ is the D-spacing of a fibril at any given engineering strain. ε_F increases slightly during

extension in the pre-yield region, but remains fairly constant throughout the yield region before increasing dramatically in the restiffening region (Fig 5.8). This fibril strain corresponds to the ~10 nm diameter structures. The resolution of the SAXS setup used does not permit examination of the effects of macroscopic extension on the larger fibril bundles as observation of much smaller angles of diffraction, beyond the detector's limitations, would be necessary.

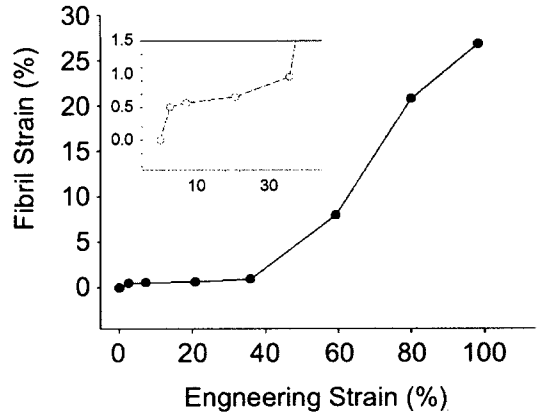

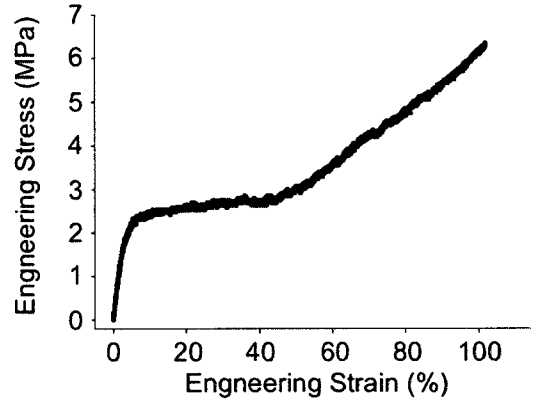

Figure 5.8. Plots of Fibril Strain vs Strain, and Stress vs Strain. Fibril strain increases in the pre-yield region, remains fairly constant in the yield region, and then increases again in the restiffening region. Inset zooms in on the pre-yield and yield region to more clearly demonstrate that the pre-yield fibril strain is significant.

E. Discussion

The findings presented here reveal useful details about the nanostructural hierarchical ordering in proteinaceous whelk egg capsules. There is additional information about some of the mechanisms affiliated with these structures

and how they are involved in the capsule's remarkable mechanical properties in uniaxial tension[14]. Building upon previous work indicating that individual α-helical protein components, 1.2 nm in diameter[15], form coiled-coil trimers[16] which are 4 - 5 nm in diameter[17]. The data suggest that these are then organized into ~10 nm fibrils which then bundle into the 200 - 500 nm fibers, with the occasional fiber being >1 μm, that further braid in co-alignment to make up the laminar sheet structure (Fig 5.9).

The lateral D-spacings of ~100 nm that are observed at the fibril level by x-ray scattering may be caused by the alignment of secondary structures in the individual proteins making up the fibrils, as in intermediate filaments like nuclear lamins[18], or could potentially be caused by gaps in between the end to end linkages of proteins within the fibrils, as is the case with tendon collagen[19]. It is the stretching and lengthening of the distances between these structures and/or gaps that causes increases in D-space reflections and, hence, fibril strain. The banding that is visible on the fiber level in via microscopy (wet mode AFM) has the same dimensions as the fibril D-spacings, ~100 nm, suggesting that the two are possibly related. However, the amplitude of the bands on the fiber surface can be in excess of 20 nm (Fig 5.4b), whereas the diameter of the individual fibrils is only ~10 nm, indicating that this banding pattern cannot be the result of single fibrils on the surface, but rather must be caused by a ordered stacking of multiple

fibrils. Further studies will be needed to determine the relationship, if any, between the fibril D-spacings and the fiber banding pattern.

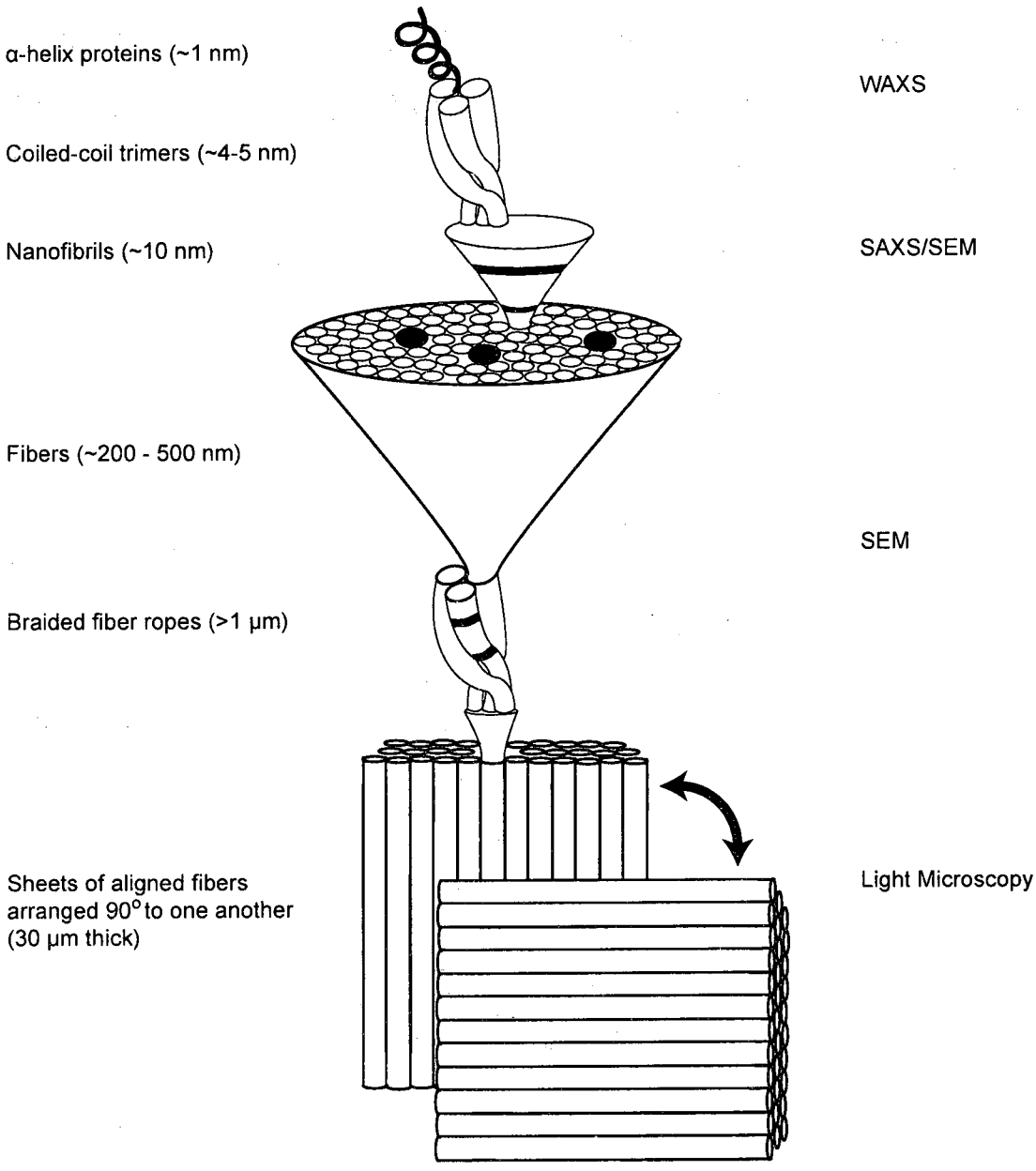

Figure 5.9 Schematic of the hierarchical ordering of whelk egg capsules

When an external load is applied, an initial slight increase in fibril strain is observed in the pre-yield region. At the protein level, coiled-coil α-helix trimers are being strained and the hydrogen bonds stabilizing these structures remain intact[7]. Many biological fibers demonstrate supercoiling in their relaxed state, which can cause crimping of the fibers[20-22]. The observed pre-yield increase in fibril strain may be the result of unraveled supercoiling and the fiber crimps being straightened out.

As the egg capsule is pulled beyond the mechanical yield point at ~5% engineering strain, fibril strain does not increase much as the material extends further. Typically this is the result of either a sliding between fibrils caused by delamination of the structures connecting them, or by an inhomogeneous destruction of the crystalline elements of the fibril after the yield point, corresponding to strain localization. SAXS data presented here are suggestive of the second mechanism, and indicate that both the intensity as well as the integrated area of the peaks corresponding to fibril crystallinity decrease while the location of these peaks remains constant. Furthermore, previous studies detail how the α-helix ↔β-sheet phase transition occurs in this region and how this transition is a two step mechanism which begins with the destruction of the α-helix crystal structure. However, some degree of interfibrillar slipping cannot be completely ruled out. Any actual slippage must be reversible to account for the recoverability and shape memory of this material.

Once the egg capsule is strained beyond 45%, it begins to restiffen. At this point there is a shift in the peak location in the SAXS profile as well as an increase in peak intensity and integrated area. This indicates an increase in crystalline content as well as a change in D-spacings of the crystal structures of the fibril, corresponding perfectly to the formation of β-sheets at the single protein level detailed before[4,14]. As these structures propagate throughout the material the fibril strain increases as well. In collagen fibrils, two different models for this increase have been presented. 1) a homogeneous stretching in the crystalline poly-proline helix during elongation leads to changes in the D-spacings, and 2) a side by side gliding of neighboring molecules within the fibrils causing an increase in gap size and distance[9].

In egg capsules the first model would translate to a homogeneous increase in β-sheet content in the restiffening region. The second model would relate to a sliding of the protein trimers which form the fibrils along each other resulting in an increase in D-spacings due to either a realignment of secondary structures, or an increase in gap sizes (Fig 5.10). This second model would also imply that covalent crosslinks between trimers would either be ruptured, or that there is an additional matrix component in between trimers that accommodates this slipping without rupturing covalent bonds.

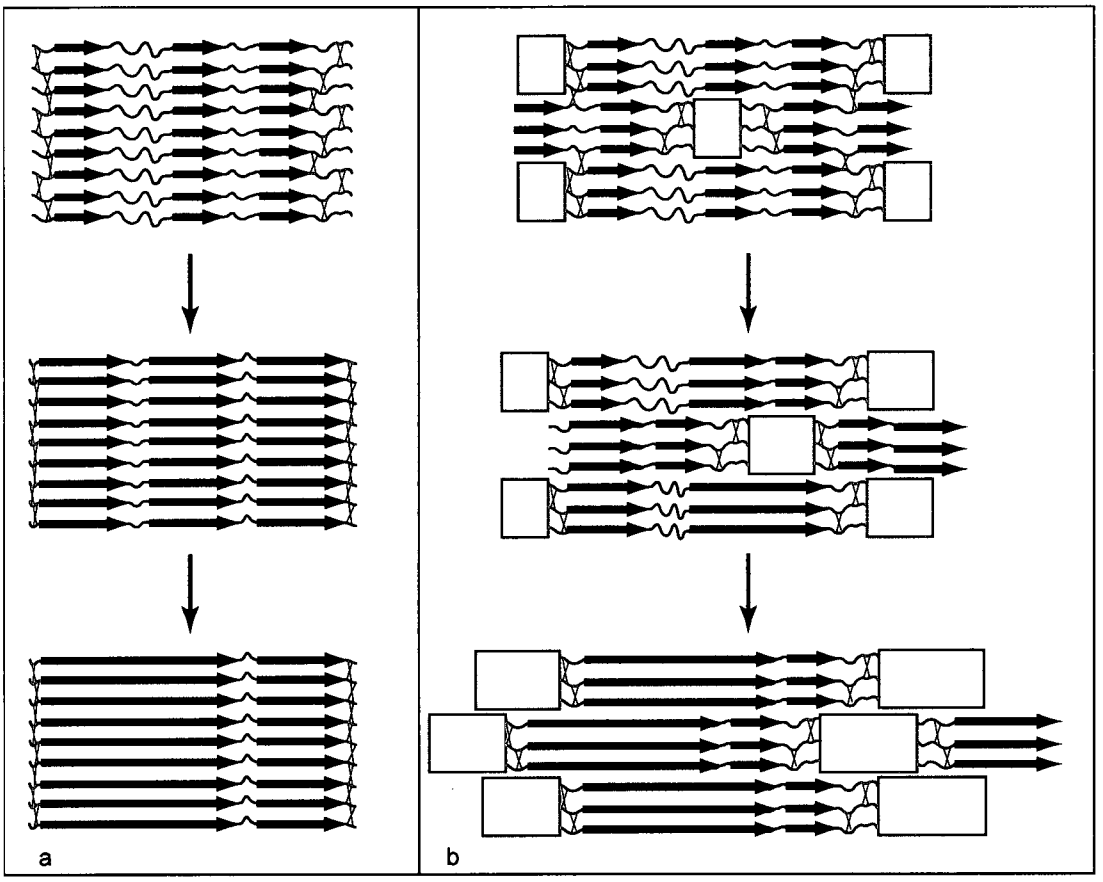

Figure 5.10. Schematic of two models for increase in fibril strain in restiffening region. a) represents a homogenous formation and elongation of β-sheet structures in unison responsible for an increase in D-spacings due to alignment of secondary structures and random coils. b) shows a heterogeneous increase in β-sheets with a sliding of neighboring trimers causing changes in gap size and location resulting in increased D-spacings. It is not yet determined whether there are gaps in this material, and the sliding model shown in b) could also be applied to a realignment of secondary structures and random coils causing D-space changes.

In tendon collagen, the second model has been experimentally confirmed as molecular shearing causes changes in the gap/overlap patterns[9] with a proteoglycan matrix allowing for this slippage without rupturing crosslinks until critical strains are met[23]. While it is not yet known if

the egg capsule material has matrix components, the rupturing of covalent cross-links would imply some non-recoverable deformation resulting from extension of samples into the restiffening zone. Indeed it is observed that the further into the restiffening zone a sample is extended, the more non-recoverable plastic deform-

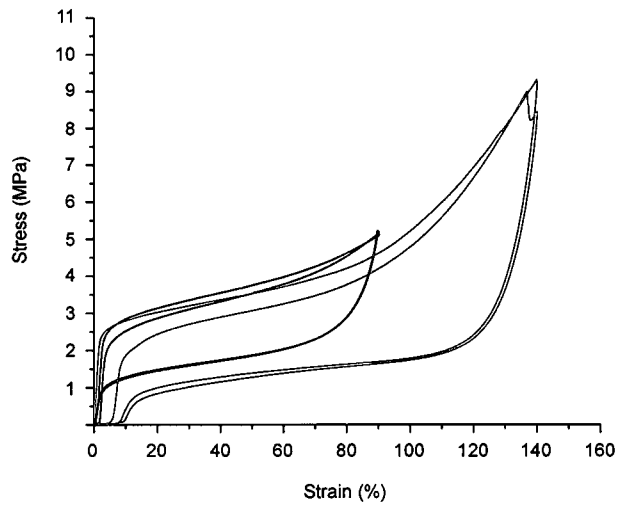

Figure 5.11. Stress strain curves of egg capsules cyclically extended to 90% (black) and 140% (red). As the material is extended further into the restiffening region, the amount of plastic deformation between cycles increases, which could be the result of the rupturing of covalent crosslinks between trimers.

ation is incurred (Fig 5.11). However, until ad-ditional work is performed, and crosslink characterization is complete, no model can be completely discounted or confirmed in whelk egg capsules.

Figure 5.12 summarizes what is currently known about the various established mechanisms and how they interact to dictate the mechanical properties of the egg cases. Additional analysis will be needed to determine how these mechanisms contribute to the relaxation mechanics of the egg capsule material.

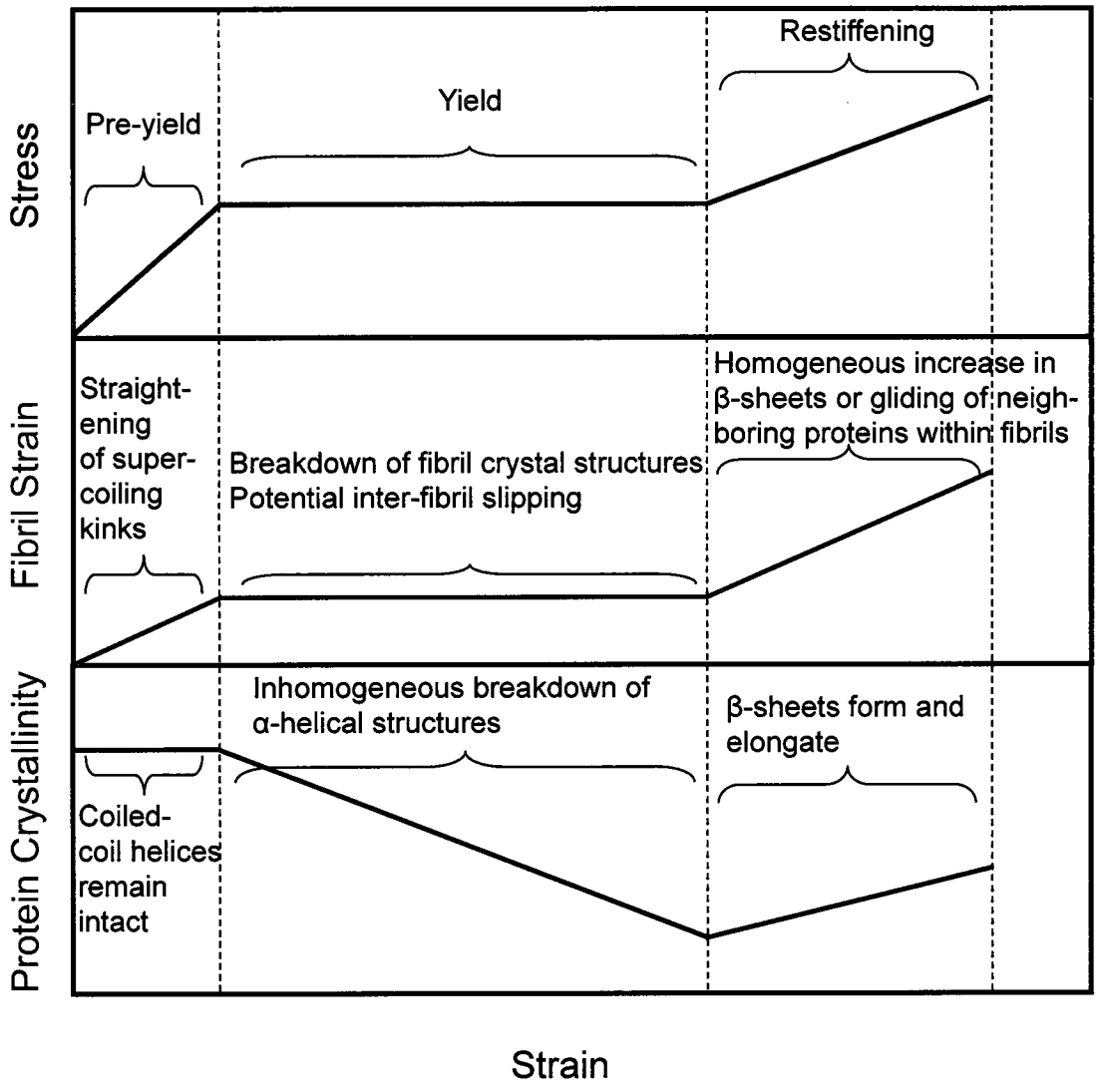

Figure 5.12. Model of how fibril strain and the α-helix ⟷ β-sheet crystalline protein phase transition combine to affect the mechanical properties under tension. Not drawn to scale.

F. Conclusions

Using scanning electron microscopy, atomic force microscopy, and small angle x-ray scattering techniques, the supramolecular ordering of

whelk egg capsules has been observed down to the nanometer scale. This combined with the wide angle x-ray scattering data from Chapter 4 has elucidated the structural hierarchy of this material from the single protein level up through the macroscopic level. When the egg capsules are put under uniaxial tension there is a slight increase in the strain of the 10 nm fibril component as measured by the change in D-spacing of the banding patterns. Once the material is pulled past the yielding point, fibril strain remains constant while the coiled-coil α-helices inhomogeneously break down. Some interfibrillar slipping may also be occurring in this region. Once the material begins to restiffen after ~45% strain, fibril strain increases again as does β-sheet content. Several possible models are proposed, and more work is required to confirm which of these is occurring in this system.

G. Acknowledgements

Thanks are due to H. Gupta (Max-Planck Institute for Colloids and Interfaces, Golm, Germany) and A. Miserez (Materials Department, UCSB) for providing guidance and assistance with the time-resolved SAXS synchrotron experiments and SEM imaging respectively. S.W. was financially supported by a California Sea Grant # R/MP-97B and UC BREP GREAT traineeship #2007-02. This work made use of MRL Central Facilities supported by the MRSEC Program of the National Science Foundation under award No. DMR05-20415.

I. References

1. Rapoport, H. S., & Shadwick R. E. Mechanical characterization of an unusual elastic biomaterial from the egg capsules of marine snails (*Busycon spp.*) *Biomacromolecules* **3**, 42-50 (2002).
2. Rapoport, H. S., & Shadwick, R. E. Reversibly labile, sclerotization-induced elastic properties in a keratin analog from marine snails: whelk egg capsule biopolymer (WECB). *J. Exp. Biol* **210**, 12-26 (2007).
3. Rapoport, H. S., *Biomechanics, Biochemistry, and Molecular Biology of a Molluscan Scleroprotein Elastomer: Whelk Egg Capsule Biopolymer*, in *Marine Biology*. PhD thesis. University of California San Diego (2003).
4. Miserez, A., Wasko, S. S., Carpenter, C. F., & Waite, J. H. Non-entropic and reversible long-range deformation of an encapsulating bioelastomer. *Nat Mater* **8**, 910-916 (2009).
5. Fratzl, P., & Weinkamer, R. Nature's hierarchical materials. *Prog. Mater. Sci.* **51**, 1263-1334 (2007)
6. Kastelic, J. & Baer, E. Deformation in Tendon Collagen *Symp. Soc. Exp. Biol* **34**, 397-435 (1980).
7. Feughelman, M. *Mechanical Properties and Structure of Alpha-Keratin Fibres: Wool, Human Hair, and Related Fibres*, UNSW Press: Sydney, Australia, 1997.
8. J Hearle. A critical review of the structural mechanics of wool and hair fibres. *Int. J. Biol. Macromol.* **27**, 123–138 (2000).
9. Fratzl, P., Misof, K., & Zizak, I. Fibrillar Structure and Mechanical Properties of Collagen. *J Struct. Biol.* **122**, 119-122 (1997).
10. Krauss, S., Fratzl, P., Seto, J., Currey, J. D., Estevez, J. A., Funari, S. S., & Gupta, H. S. Inhomogeneous fibril stretching in antler starts after macroscopic yielding: Indication for a nanoscale toughening mechanism. *Bone* **44**, 1105–1110 (2009).
11. Gupta, H. S., Seto, J., Krauss, S., Boesecke, P., & Screen, H. R. C. In situ multi-level analysis of viscoelastic deformation mechanisms in tendon collagen. *J. Struct. Biol.* **169**, 183–191 (2010).
12. Gupta, H .S., Seto, J., Wagermaier, W., Zaslansky, P., Boesecke, P., Fratzl, P., Cooperative deformation of mineral and collagen in bone at the nanoscale. *PNAS* **103**, 17741–17746 (2006).
13. Kreplak, L., Franbourg, A., Briki, F., Leroy, F., & Dalle, D. A New Deformation Model of Hard α-Keratin Fibers at the Nanometer Scale: Implications for Hard α-Keratin Intermediate Filament Mechanical Properties. *Biophys. J.* **82**, 2265–2274 (2002).
14. Chapter 4 of this dissertation.
15. Creighton, T. E. *Proteins: Structures and Molecular Properties*, 2nd ed; W. H. Freeman and Company: New York, NY, 1993.
16. Wasko, S. S., & Waite, J. H. Structural proteins from an egg capsule with nonentropic reversible extensibility. Submitted to: *Biomacromolecules*, under review (2010).
17. Håkansson, K., Lim, N. K., Hoppe, H., & Reid, K. B. M. Crystal structure of the trimeric α-helical coiled-coil and the three lectin domains of human lung surfactant protein D. *Structure* **7**, 255-264 (1999).
18. Ben-Harush, K., Wiesel, N., & Frenkiel-Krispin, D. The supramolecular organization of the *C. elegans* nuclear lamin filament. *J. Mol. Biol.* **386**, 1392–1402 (2009).
19. Fratzl. P. *Collagen: Structure and Mechanics*, P Fratzl Editor, Chapter 1. Springer Science Media LLC, New York, NY, (2008).
20. Beck, K., & Brodsky, B. Supercoiled Protein Motifs: The Collagen Triple-Helix and the α-Helical Coiled Coil. *J. Struct. Biol.* **122**, 17-29 (1998).

21. Vazina, A. A., Bras, W., Dolbnya, I. P., Korneev, V. N., Lanina, N. F., Matyushin, A. M., Sergienko, P. M., & Zabelin A. V. Peculiarities of human hair structural dynamics. *Proc. XV. Inter. Synch. Rad. Con.* **543,** 153-157 (2005).
22. T. I. Nikolaeva, T. I., Tiktopulo E. I., Il'yasova, E. N., & Kuznetsova, S. M. Collagen type I fibril packing in vivo and in vitro. *Biofizika* **52**, 899–911 (2007).
23. Gupta, H. S. *Collagen: Structure and Mechanics*, P Fratzl Editor, Chapter 5, Springer Science Media LLC, New York, NY, (2008).

Chapter 6. Conclusions and future directions

A. Abstract

The biochemical composition, thermomechanical properties, and structure-function relationship at multiple length scale orders of *Busycotypus canaliculatus* egg capsules have been presented in this dissertation. Four variants of the precursor protein family were purified from a crude extract and thoroughly characterized. The cDNA deduced sequences were derived, and studies into protein behavior relating to structure and assembly in solution were carried out. The thermomechanical properties - specifically, the behavior of the hydrated material in uniaxial tension at various temperatures - were investigated and modeled. The results were applied to formulae derived from standard thermodynamic relations in order to determine entropic and internal energy contributions to the tensile properties. Finally structural studies were performed to examine the changes in molecular architecture that occur as the egg capsule material goes through a complete strain cycle. A combination of wide and small angle x-ray scattering, Raman spectroscopy, and microscopic techniques provided structural data that ranged from the Å (single protein) level, through the micron (bundled protein fiber) level.

B. Conclusions from this Work

The family of precursor proteins that migrates near 50kD has been purified and characterized, and the sequence deduced from cDNA. These proteins are highly related to each other, but are not homologous to any other protein sequence in the collective databases. Named *Busycotypus canaliculatus* capsule proteins, or Bc-cp, variants 1 through 3, the masses of the proteins as obtained via MALDI-TOF matches very closely with the calculated masses of the cDNA deduced sequences, suggesting that the sequences do correspond with the proteins of interest. Further supporting this is the fact that the amino acid composition determined experimentally via automated ion exchange chromatography with ninhydrin detection also matches the composition from the cDNA sequences. This composition is rich in α-helix favoring and α-helix indifferent residues, similar to the composition of intermediate filaments which are known α-helix structures.

Circular dichroism studies indicate that the precursor proteins are strongly α-helical in solution, and also suggest that the helices tend to form single coil helices rather than coiled-coils. However, analysis of the cDNA derived primary sequence suggest that there are short regions that favor the formation of coiled-coil trimers. This is in agreement with wide angle x-ray scattering studies (described in detail below) which indicates coiled-coil structures in the mature egg capsule material.

TEM micrographs clearly show the purified proteins self-assembling into fibers out of solution *in vitro*. The dimensions of the fibers are consistent with SEM and AFM images taken of the fibers from intact egg capsules, and suggest that the Bc-cps are responsible for forming these structural fibers in the mature material.

Thermomechanical as well as structural tests of the mature material were performed to determine the exact nature of the high reversible extensibility of the egg capsules. The two theories that were tested are classic entropic elasticity (wherein entropic energy constantly drives the system to a greater disordered state, which in the case of extensible materials typically means a contracted, isotropic polymer) and Flory's theory on protein extensibility (in which internal bond energies dictate a loaded protein or protein assembly extending by undergoing a transition from one crystalline structure such as α-helix to another such as β-sheet).

Via uniaxial tensile testing at temperatures ranging from -1°C to 80°C, and analysis of the data via formulaic derivations of the Hemholtz free energy relationship, it was determined that any entropic contribution to the reversible extensibility of the egg capsule material is far less than the contribution due to internal bond energy. This behavior conforms to the Clausius–Clapeyron relation of phase transition as applied to a phase equilibrium previously developed to model crystallization of polymer fibers under stress. Additionally, wide-angle x-ray scattering demonstrates such a

phase transition in the egg capsule material coming in the form of a reversible crystalline shift from α-helix to β-sheet. As such, Flory's paradigm wherein protein extensibility is the result of a reversible phase transition is the accepted explanation for extensibility in the whelk egg capsule material.

Both synchrotron x-ray and con-focal Raman microprobe analysis with *in situ* tensile testing demonstrates that at the single protein level, coiled coil α-helices dominate the pristine material and remain intact as the egg capsules are extended throughout the stiff pre-yield region of the stress strain curve. The α-helical component does not begin to break down until after the yield point, when modulus decreases dramatically. The sequential rupturing of the hydrogen bonds responsible for stabilizing the α-helices is hypothesized to be the primary contributing factor to this decrease in stiffness. However, β-sheet formation does not begin until the restiffening region is entered. When β-sheet specific hydrogen bonds form, flexibility is lost at the single protein level, which contributes to the restiffening of the material as a whole.

Upon relaxation, a large hysteresis loop is observed. Data suggest that this is due to the energy required to rupture the β-sheet stabilizing hydrogen bonds in order to reverse the phase transition back from β-sheet to α-helix. However, the contribution of internal friction resulting from the sliding of hierarchical fibrils and other components of the material cannot be discounted.

Whelk egg capsules, like many other biological materials, are very hierarchical structures with multiple levels of supramolecular ordering ranging from the Å up through the micron and millimeter levels as observed from WAXS, SEM, AFM, SAXS, and light microscopy. These different levels of ordering contribute to the tensile mechanical properties of the bulk material in different ways. The contribution of the α-helix ⟷ β-sheet transition has already been mentioned, but there is a significant contribution from 10 nm diameter fibril structures as well.

Although more data analysis is required, there is clear evidence indicating that fibrillar strain contributes to tensile behavior in the pre-yield and restiffening regions, and multiple models for how this phenomenon is linked with mechanical properties have been presented in this dissertation. Furthermore, in the pre-yield and restiffening regions, only a small fraction of the bulk strain is being converted into fibrillar strain, suggesting that there are even more mechanisms contributing to the tensile properties of the bulk material that have not yet been examined.

Overall, whelk egg capsule is a very unique material in terms of its biochemistry, biophysics, structural ordering, and mechanical properties. This dissertation although providing a sizable contribution to illuminating some of the structure-function relationships involved, has really only scratched the surface of what is possible. A great deal of additional work will

be needed to more thoroughly understand this system to the point where the synthesis of an effective mimic of the material can be explored.

C. Future Directions

Although this system does indeed show promise towards biomimetic applications, there is clearly much more to be learned before this comes to fruition. This biomaterial is ~90% protein by dry weight. The composition of that additional 10% has not yet been determined let alone it's structure or function, although it is suggested to be carbohydrate[1]. And although four variants of the precursor protein family have been described, the crude extract contains additional proteins that are, as of yet, uncharacterized[2]. The proteins that have been described likely contribute to the structural fibers of the egg capsule material and participate in the α β transition that has been described. The uncharacterized proteins that appear on the SDS PAGE of the crude extract, although present in lower amounts, are not similar in size, what-so-ever, to the characterized CPs 1-3 which are all in the 50kD range. Rather the unknowns come in at 24kD, 37kD, and 120kD according to their migration patterns. A full characterization of these precursor proteins will be necessary to determine the roles that they play in the structure/function of the egg capsule material as a whole. One possibility for the function of these unknowns is as matrix proteins. Hard keratins are a composite of both

structural fibers and amorphous matrix, both of which contribute significantly to mechanical properties[3].

Of the precursor proteins that have been characterized, the nature of the self-assembly as well as the post translational modification steps that guide the synthesis of the fully mature and functional material are also unknown. Although it has been shown that CPs 1 and 2 will self-assemble *in vitro* into fibers that are the same size as those seen in the mature material, the specifics of this assembly including the trigger, the intermediate steps and structures formed, the kinetics, etc, are all unknown. Further elucidating these mechanisms could lead the way to developing synthetic self-assembling materials.

After assembly, covalent crosslinks are formed to stabilize the material. The nature of these crosslinks, the exact chemical structure (a suspected lysine or other borohydride reducible derivative[4]) as well as the location within the protein sequence, is unknown. This information will be invaluable to both confirming the individual coiled-coil protein trimer model presented in Chapter 2, as well as determining how that model can be applied to a complete fiber of protein trimers that are linked together. Work into this has been started and the preliminary results will be presented later in this chapter.

Other ideas for future work include single molecule force spectroscopy to examine the unfolding of single proteins or of protein trimers

as has been performed for other coiled-coil proteins[5,6]; cloning of the genes responsible for coding these proteins and making recombinant proteins that can be used to create films, fibers, or other materials; fully characterizing thermal properties of the egg capsule materials via such methods as differential scanning calorimetry; determining the permeability of the capsules to determine functionality as a biomedical encapsulant.

In the end, there are too many potential future directions to list here in this dissertation. It seems that whereas each experiment may provide the answer to one question, it also raises three more in turn. One of the struggles in working on a project such as this was to learn when to finally start to tuck the loose ends in rather than pulling on them. It will be up to the next group of scientists working on this project to address all of these remaining questions. There are certainly many more publications and potential dissertations that can come from this model system.

D. Materials and Methods for Preliminary Studies

Non-viable *Busycotypus canaliculatus* egg capsules were purchased from Marine Biological Laboratories (Woods Hole, MA). Capsules were cut open and the embryonic materials drained out and were then washed repeatedly in Milli-Q water with physical agitation. Afterwards the capsule material was ground with a stone mortar and pestle under liquid nitrogen to

produce a powdery particulate which was smaller than 0.5 mm in individual grain size.

This particulate was then treated with $NaBH_4$ (5mg/ml) in phosphate buffer (pH 7.0) for 30 min to reduce/protect any potentially unstable lysine derived crosslinks. The reaction was terminated by the addition of several drops of glacial acetic acid, and was then washed repeatedly with Milli-Q water.

Reduced egg capsule samples were hydrolyzed in 6N HCl, in vacuo at 105°C for 24 hours. The HCl was flash evaporated off and the hydrolysate was washed several times each with water and methanol to remove all traces of acid. The hydrolysate was then subjected to Bio-Gel P2 (Bio-Rad) size exclusion chromatography on a 100 X 2 cm column eluted with 5% acetic acid. After the void volume passed through, 100 3ml fractions were collected for analysis.

Aliquots of fractions were flash evaporated once again, resuspended in NaS buffer, and analyzed on a Beckman Coulter 6300 Amino Acid Analyzer as described in the materials and methods section of Chapter 2 of this dissertation.

The remaining volume of the fractions was analyzed by positive ion mode TOF ESI-MS as described elsewhere[7]. Molecules with masses significantly greater than single amino acids were deemed to be potential crosslinks and were further analyzed by MS/MS using argon gas and a

collision voltage of 30 V for collision-induced decomposition on the same instrument. Structure was deduced from decomposition-induced fragment ion masses.

E. Preliminary results

As mentioned previously in this chapter as well as in Chapter 2 of this dissertation, the egg capsule material adds covalent crosslinks to the material as one of the final processing steps. Although the structure and location of these crosslinks in the primary protein sequence is unknown, there has been evidence dating back to the 60's that these crosslinks are borohydride reducible compounds, suggesting the potential for lysine derived molecules[8]. The goal of the experimentation listed above is to isolate these crosslinks from the mature material as well as determine molecular structure.

Bio-Gel P2 effectively separates biological molecules in the range of 100-1800 daltons, very much within the range of divalent and multivalent protein crosslinks, with the larger molecules eluting first. As such, it is expected that the crosslinks would elute in the first fractions collected from this column whereas the single amino acids would come off later.

This proved to be the case as the amino acid analysis profile of the first 10 or so fractions (~30ml total) collected indicated a very high proportion of non-standard residues eluting in the slightly basic region of the curve, the

area around histidine and lysine, where crosslinked amino acids are known to elute (Fig 6.1). The later fractions began to include larger molecular weight amino acids such as arginine and phenylalanine, and then, later, smaller molecular weight amino acids.

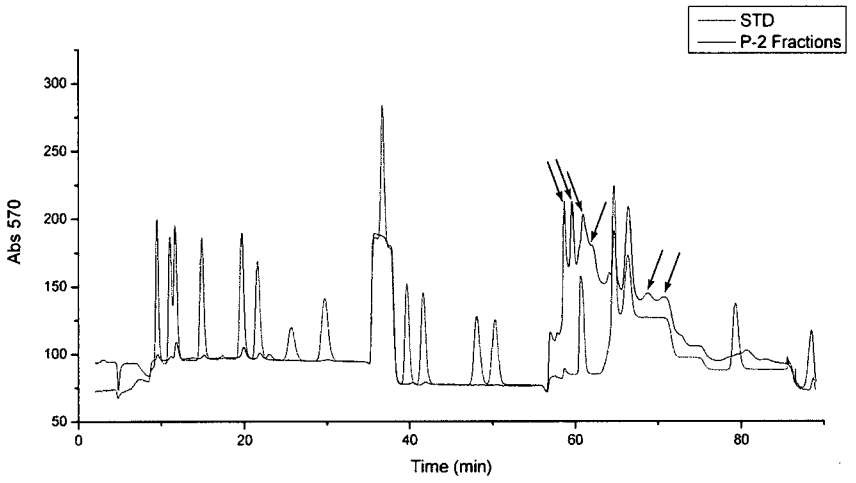

Figure 6.1. Amino acid elution profile of a 17 residue standard, red trace, and of the fastest eluting P2 fractions, blue trace. The P2 fractions contain numerous unidentified peaks (marked by arrows) eluting around the 60 minute mark, which is approximately where crosslinks commonly elute.

The TOF ESI-MS profile of the fractions indicated a variety of high molecular weight candidates for potential crosslinks (Table 6.1). These candidates were subjected to MS/MS with CID and the mass spectra were analyzed to deduce structure. It soon became apparent that although many of

Masses (m/z) of potential crosslink targets
259.2, 275.1, 289.2, 358.2, 373.3, 388.2, 516.3

Table 6.1. List of crosslink target masses

the candidates in Table 6.1 have different masses, their fractionation patterns are similar. Some, such as the 289.2 m/z candidate and the 516.2 m/z candidate had the not only the parent ion of the smaller molecule as a fractionation ion in the larger molecule's spectrum , but also had the same degradation ions (Fig 6.2). This suggests not only that the two are related, but that the smaller molecule in it's entirety might be incorporated into a much larger, multivalent system.

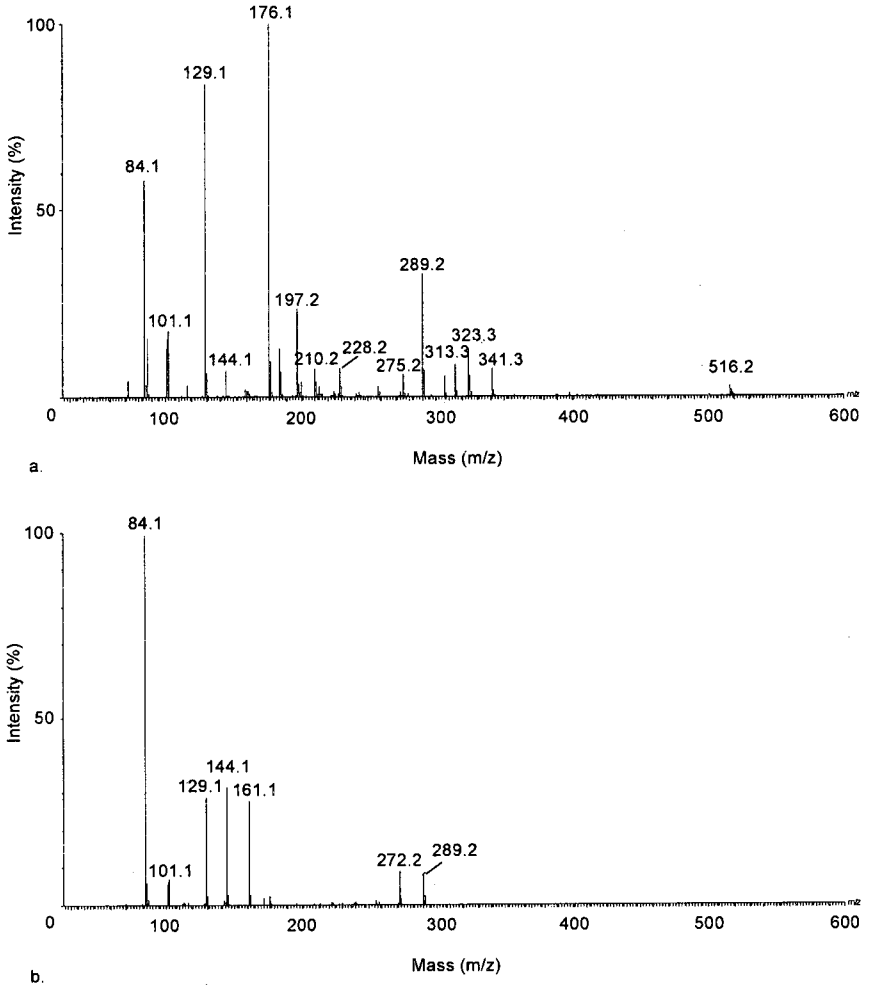

Figure 6.2. Mass spectra of a) 516.2 dalton crosslink target and b) 289.2 dalton crosslink target. Not only is the 289.2 dalton parent ion present in the 516.2 dalton fractionation patern, but the fractionation ions are similar in both suggesting a relation between the two parent ions.

One fractionation pattern that almost all of the crosslink candidates shared was a strong peak at 84.1 m/z and a weaker peak at 101.1 m/z. This is indicative of an amino acid with an epsilon amine group, such as lysine. During collision induced dissociation, when the carboxyl group is cleaved off, the molecule preferentially cyclizes and loses an amino group. This causes

a distinct mass spectra pattern with a very strong peak at 84.1 m/z (the cyclized, stable molecule) and a weaker peak at 101.1 m/z (the linear, unstable molecule) (Fig 6.3)[9]. That most of the crosslink candidate molecules have this pattern in their MS/MS spectra strongly suggests that these molecules are lysine derivatives with an epsilon amine group.

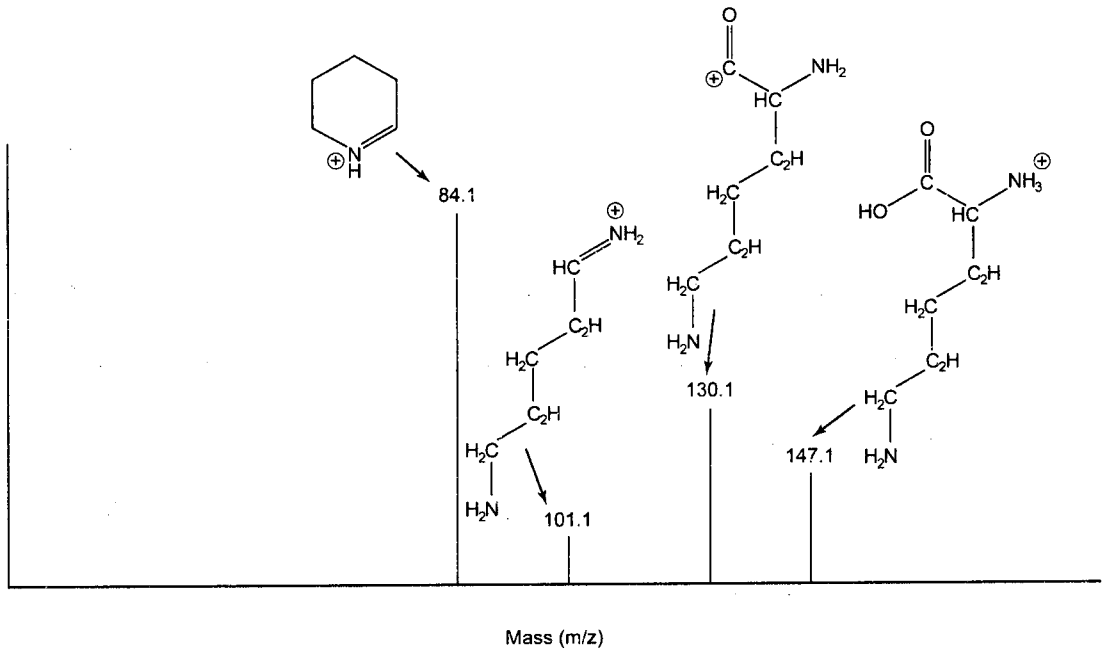

Figure 6.3. MS/MS spectra of L-Lysine. Derived from References [9] and [10]

Complete analysis of one of the candidates, the 289.2 m/z peak, was performed and the structure derived (Fig 6.4). In this model, the structure is a divalent crosslink between lysine and citrulline, a derivative of arginine.

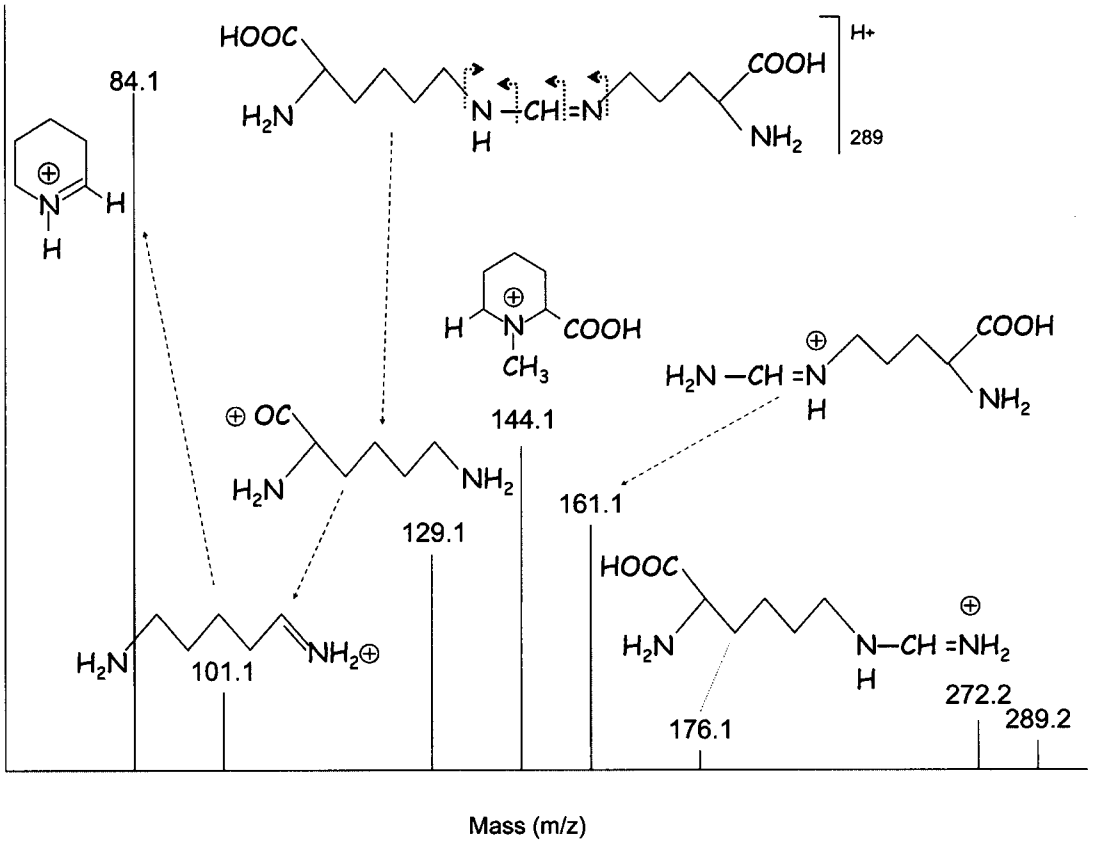

Figure 6.4. Derived mass spectra of 289.2 dalton crosslink target. Fragmentation patterns suggest lysine-citrulline divalent crosslinks.

Although the proposed structure is consistent with the mass spectra from the tandem MS, other questions need to be addressed before stating that this is a definitive crosslink. First of all, in order for lysine to form spontaneous crosslinks, it must be converted to the active aldehyde allysine by lysyl oxidase. Preliminary studies into the presence of lysyl oxidase in egg capsule material, although not exhaustive, has come up negative. Similarly, arginine must be converted to citrulline enzymatically by the nitric

oxide synthase pathway or urea cycle. No studies have explored the presence of those enzymes in the egg capsule materials. Furthermore, work going into detecting free citrulline in egg capsules has indicated that there is none. However, this may prove inconclusive since ornithine (the hydrolysis product of citrulline) elutes very closely to lysine and the large lysine peak may be blocking the smaller ornithine peak. Also, it could be that there is no free citrulline in the material, and that all citrulline residues are tied up in crosslinks. Lastly, as mentioned before, the 289.2 m/z structure appears in its entirety in the fractionation spectra of the 516.2 m/z candidate. It is entirely possible that the above structure is merely a small part of a multivalent crosslink, and that the 289.2 peak is observed in the TOF ESI-MS spectra due to unexpected degradation in the source region.

Further analysis is necessary to verify the structure of any crosslinks in this material.

F. Acknowledgements

Thanks are due to J. Pavlovich (Chemistry Department, UCSB) for assistance with the tandem mass spectrometry data collection and particularly to H. Waite (BMSE Program, UCSB) for insightful analysis of said data into meaningful structures. S.W. was financially supported by a California Sea Grant # R/MP-97B and UC BREP GREAT traineeship #2007-02.

G. References

1. Rawlings, T.A., Adaptations to physical stresses in the intertidal zone: The egg capsules of neogastropod molluscs. *American Zoologist* **39**, 230-243 (1999).
2. Rapoport, H. S., *Biomechanics, Biochemistry, and Molecular Biology of a Molluscan Scleroprotein Elastomer: Whelk Egg Capsule Biopolymer*, in *Marine Biology*. PhD thesis. University of California San Diego (2003).
3. Feughelman, M. Mechanical *Properties and Structure of Alpha-Keratin Fibres: Wool, Human Hair, and Related Fibres*, UNSW Press: Sydney, Australia, 1997.
4. Price, N. R. & Hunt, S. *Occurrence of Reducible Compounds in an Invertebrate Protein of Buccinum-Undatum (L). Cell. Mol. Life* **32**, 557- 558 (1976).
5. Brown, A. E. X., Litvinov, R. I., Discher, D. E., & Weisel, J. W. Forced unfolding of coiled-coils in fibrinogen by single-molecule AFM. *Biophysical J.* **92**, L39-L41 (2007).
6. Lim, B. B. C., Lee, E. H., Sotomayor, M., & Schulten, K. Molecular basis of fibrin clot elasticity. *Structure* **16**, 449-59 (2008).
7. Zhao, H., & Waite, J. H. Coating Proteins: Structure and Cross-Linking in fp-1 from the Green Shell Mussel *Perna canaliculus. Biochemistry* **44**, 5915-15923 (2005)
8. Hunt, S., Carbohydrate and amino-acid composition of egg capsule of whelk *Buccinum undatum* L. *Nature* **210**, 436-437 (1966).
9. Biemann, K., Seibl, J., & Gapp, F. Mass spectra of organic molecules I. ethyl esters of amino acids. *J. Am. Chem. Soc.* **83**, 3795–3804 (1961).
10. http://www.massbank.jp